DEGRADATION OF MECHANICAL PROPERTIES OF VINYLESTER AND CARBON FIBER/VINYLESTER COMPOSITES DUE TO ENVIRONMENTAL EXPOSURE

by

Alexander M. Figliolini

A Thesis Submitted to the Faculty of

The College of Engineering and Computer Science

in Partial Fulfillment of the Requirements for the Degree of

Master of Science

Florida Atlantic University

Boca Raton, Florida

December 2011

DEGRADATION OF MECHANICAL PROPERTIES OF VINYLESTER AND CARBON FIBER/VINYLESTER COMPOSITES DUE TO ENVIRONMENTAL EXPOSURE

by

Alexander M. Figliolini

This thesis was prepared under the direction of the candidate's thesis advisor, Dr. Leif A. Carlsson, Department of Ocean and Mechanical Engineering, and has been approved by the members of his supervisory committee. It was submitted to the faculty of the College of Engineering and Computer Science and was accepted in partial fulfillment of the requirements for the degree of Master of Science.

SUPERVISORY COMMITTEE:

Leif A. Carlsson, Ph.D.
Thesis Advisor

Gary Salivar, Ph.D.

Dr. Chi-Tay Tsai, Ph.D.

Dr. Richard Granata, Ph.D.

Javad Hashemi, Ph.D.
Chair, Department of Ocean and Mechanical Engineering

Mohammad Ilyas, Ph.D.
Interim Dean, College of Engineering and Computer Science

Barry T. Rosson, Ph.D.
Dean, Graduate College

November 23, 2011
Date

ACKNOWLEDGEMENTS

The author would like to take the time to acknowledge those who have aided in completion of this work. Without the guidance, dedication and support from my advising committee chair, Dr. Leif A. Carlsson, Department of Ocean and Mechanical Engineering, my sanity surely would have been lost long ago. The author would like to also give a special thanks to my advisory committee members: to Dr. Gary Salivar, Department of Ocean and Mechanical Engineering, for pushing me to higher standards; to Dr. Chi-Tay Tsai, Department of Ocean and Mechanical Engineering, for his continued support; to Dr. Richard Granata, Department of Ocean and Mechanical Engineering, for his support and guidance and for allowing the use of the research labs at SeaTech.

The author would also like to thank Dr. Yapa Rajapakse and the Office of Naval Research for support and sponsorship of my research project (contract No. N00014-05-1-0341). Furthermore, thanks go to Dr. Betiana A. Acha and Dr. Mahmoud Madani of Florida Atlantic University for their technical guidance and lab instruction. The author would like to also thank fellow graduate colleagues Elio E. Saenz, Bender H. Kutub, Michael A. Dale, Kyle R. Totten and Felicia Powell for their invaluable help throughout the project. A special thanks is extended to Patrick Boyle and General Sealants for supplying sealants for VARTM.

The author would also like to express appreciation to his family and friends for all the support and encouragement that has lead to this point.

ABSTRACT

Author: Alexander Figliolini

Title: Degradation of Mechanical Properties of Vinylester and Carbon Fiber/Vinylester Composites Due to Environmental Exposure

Institution: Florida Atlantic University

Thesis Advisor: Dr. Leif A. Carlsson

Degree: Master of Science

Year: 2011

An experimental investigation was undertaken to determine the effects of marine environmental exposure on the mechanical properties of vinylester resins (VE510A and VE8084) and carbon fiber/VE510A vinylester composites. The effect of carbon fiber sizing on the composite strengths was also examined. Neat resins were exposed to marine environments until moisture content reached a point of saturation after which they were tested in tension, compression and shear. Compared to the baseline dry specimens, specimens subjected to moisture showed overall increased ductility and a reduction in strength. Dry and moisture saturated composite specimens were tested in tension and compression in different orientations. Longitudinal specimens were tested in in-plane shear and interlaminar shear. Composites with F-sized carbon fibers displayed overall higher strength than those with G-sized fibers at both dry and moisture saturated conditions. An analysis of moisture absorption of the composites was performed which

shows that the moisture up-take is dominated by the fiber/matrix region which absorbs up to 90% of the moisture. The composites experienced reduced strength after moisture absorption. The results revealed that the fiber sizing has stronger effect on the fiber/matrix interface dominated strengths than moisture up-take.

DEGRADATION OF MECHANICAL PROPERTIES OF VINYLESTER AND CARBON FIBER/VINYLESTER COMPOSITES DUE TO ENVIRONMENTAL EXPOSURE

LIST OF FIGURES

LIST OF TABLES

NOMENCLATURE

γ	shear strain
γ_{xy}	global shear strain
γ_{12}	ply shear strain
ε_1	ply longitudinal strain
ε_2	ply transverse strain
ε_x	strain along the axis of loading
ε_y	strain transverse to the loading axis
ε_{ult}^{T}	tensile ultimate strain
$\Delta\varepsilon$	strain increment in the linear elastic region
θ	angle between the fiber axis and the loading axis
ρ_f	fiber density
ρ_m	matrix density
ρ_w	water density
σ_1	ply longitudinal tensile stress
σ_2	ply transverse tensile stress
σ_{ult}^{T}	tensile ultimate strength
σ_{ult}^{C}	compressive ultimate strength
σ_{ult}^{C}	compressive ultimate strength
σ_Y^C	compression yield strain

σ_{ult}^{T}	tensile ultimate strength
$\overline{\sigma}_{x}$	average laminate stress
$\Delta\sigma$	stress increment in the linear elastic region
τ	shear stress
τ_{ult}	ultimate shear strength
τ_{12}	in-plane shear stress
τ_{13}	interlaminar shear stress
τ_{ult}	ultimate shear strength
σ_{ult}^{T}	ultimate tensile strength
$[A]$	extensional stiffness matrix
$[a]$	inverse of the extensional stiffness matrix $[A]^{-1}$
A_{ij}	laminate stiffness elements
b	specimen width
BF	back-out factor for ply longitudinal compression strength
C(F)	carbon fiber with f-sizing
C(G)	carbon fiber with g-sizing
CoNap	cobalt naphthenate
DMA	dimethylaniline
E	Young's modulus
E_1	ply longitudinal Young's modulus
E_2	ply transverse Young's modulus
E^C	compressive modulus
E^T	tensile modulus

FRP	fiber reinforced composite
G	shear modulus
h	specimen thickness
ILSS	interlaminar shear strength (S_5)
ISS	interface shear strength
m	$\cos\theta$
MEKP	methylethylketone peroxide
M_C	composite moisture content
$M_{F/M}$	fiber/matrix moisture content
M_R	resin moisture content
n	$\sin\theta$
N_x	force applied per unit width
P	applied force
$\bar{Q}_{ij}$	elements of the off-axis reduced stiffness matrix
RH	relative humidity
RTM	resin transfer molding
S_5	interlaminar shear strength (ILSS)
S_6	in-plane shear strength
SBS	short beam shear
SFFT	single fiber fragmentation test
SW	seawater
VARTM	vacuum assisted resin transfer molding
V_f	fiber volume fraction

V_m	matrix volume fraction
V_V	void content volume fraction
VE	vinylester
W_i	specimen initial weight
W_t	specimen weight at time t
X_1^C	ply longitudinal compressive strength
X_2^C	ply transverse compressive strength
X_1^T	ply longitudinal tensile strength
X_2^T	ply transverse tensile strength
X_C	observed laminate strength
z_k & z_{k-1}	ply coordinates

1 INTRODUCTION AND OBJECTIVES OF THE STUDY

In general, a composite material can be considered any material that is formed from constituent materials of differing properties on the macro scale. The result is a material that has better properties than those of the constituent materials. Specific to the present work, fiber reinforced composites consist of a fiber and a polymer matrix. Fibers are used as structural reinforcement. However, fibers are discontinuous and act as individual strands. By themselves they have favorable properties in only tension. The matrix is much weaker than the fibers but is used to hold the fibers together. The matrix gives stability to fibers by allowing load transfer between fibers. The combination of the fibers and the matrix increase the overall mechanical properties [1].

Well designed composites are light weight, high strength, highly resistive to corrosion, fatigue, and environmental degradation. Due to their desirable properties fiber reinforced polymers have gained in popularity as a construction material for many high performance applications. Aerospace, automotive and marine industries have found great advantages to using these materials in place of other structural materials such as steel.

Use of man-made composite materials in naval applications can be seen as far back seventeenth century made by the Irish as wicker frame boats with skin shell [2]. Laminated composites made their first conceptual attempt in 1876 with paper rowing shells [2]. With development of glass and carbon in the 1960's and advances in thermoplastic and thermosetting resins and manufacturing processes the idea of cost

effective laminated composites began to take shape. Research continues to show the weight and cost reduction benefits by implementing composites in naval structures in place of other materials such as steel [3–5]. Fringe benefits have also appeared as composite materials are also multifunctional. For example, carbon fiber composite structures may be design with stealth properties desirable in naval and aerospace military applications [5].

Currently composite materials are used to replace monolithic construction materials such as aluminum and steel. Composites require less maintenance as they do not rot or rust in a marine environment [6]. However, polymer matrix composite materials do suffer from exposure to several environments such as water. It is understood that moisture absorption causes swelling and plasticization of the matrix, loss of fiber/matrix interface adhesion and possible fiber degradation all causing concerns about the structural durability. Of particular interest for naval structures is the degradation of material properties by seawater exposure. Though much research on water degradation of composites has been conducted [7–25], such studies have mostly been focused on aerospace composites. Vinylester resins have recently emerged as a promising alternative to epoxies and polyesters. A more thorough characterization of carbon fiber/vinylester composites is clearly demanded.

Of particular concern in this study is the effect of moisture absorption on composite properties governed by the fiber/matrix (F/M) interface. In the present work, an investigation is undertaken to immerse vinylester resins and composites in seawater and examine its effects on mechanical response. Specifically, several material strengths that are dominated both by the matrix and fiber/matrix interface, e.g., in-plane and

interlaminar shear response are examined. The mechanical behavior of vinylester resins and carbon fiber/vinylester composites is characterized in tension, compression and shear. The study includes two types of fiber sizings (F and G). Experimental data will be analyzed using micromechanics analysis and micromechanical and continuum failure theories.

The main objectives of this study are: (1) investigate the effects of marine environmental exposure on the mechanical response of vinylester resins (VE510A and VE8084); (2) investigate two types of carbon fiber sizing and their influence on the mechanical response of carbon fiber/vinylester composites; (3) investigate the effects of moisture exposure on the F/M interface of carbon fiber/vinylester composites.

The following points are included in the investigation:

- Mechanical characterization of neat vinylester resins in tension, compression and shear at dry conditions, and after exposure to 85% relative humidity (RH) at 50°C, and seawater at 40°C.
- Analysis of moisture absorption in the composites.
- Comprehensive mechanical characterization of carbon fiber/vinylester composites at dry, and seawater saturated conditions.
- Examination of the effects of moisture on mechanical response and failure modes of carbon fiber/vinylester composites at dry and seawater saturated conditions.
- Analyze experimental results using micromechanics and combined stress failure theories.

2 BACKGROUND

2.1 Matrix Materials for Naval Applications

Polymer matrix materials are divided into two classes, thermosets and thermoplastics. Common thermoplastics used in composites are polypropylene (PP), polyphenylene sulfide (PPS), polysulfone, and poly-ether-ether-ketone (PEEK). Thermoplastics must be heated to reach a liquid state before they can be formed. However, even at elevated temperatures thermoplastics maintain a high viscosity. The high viscosity makes thermoplastics more difficult to process and the fiber/matrix adhesion problematic. Properties of thermoplastics are also highly temperature dependent [1].

Thermosets are monomer based chemicals that undergo polymerization by a chemical reaction known as cure. During cure, monomers join to form long molecular chains. Covalent bonds connecting individual molecular chains develop that prevent flow of the material. A post cure is often required to insure full cross linking which improves strength and increases the glass transition temperature. Thermosets do not melt when heated although they soften. Initially, before polymerization, while in the liquid phase thermosets have a much lower viscosity than thermoplastic melts which makes impregnation of fibers and processing of composites much easier with thermosets. As a consequence of this and other favorable factors the most common type of matrix material is thermoset [1].

Common thermosets used for matrices in composite materials are epoxies, polyesters, polyimides, and vinylesters. Table 2.1 lists typical properties of some thermoset resins. Epoxies are used more than any other matrix material because they have great mechanical and thermal properties and adhere strongly to most fibers [1]. However, epoxies typically require cure at elevated temperatures and tend to degrade when exposed to moisture [26]. Polyesters cure quickly even at room temperature but tend to be sensitive to moderately elevated temperatures. Vinylester resins share aspects of both epoxies and polyesters. Vinylester cures at room temperature, are fire and heat resistant and have good mechanical properties. Vinylester resins absorb very little water which is an advantage over polyesters and epoxies in seawater environments [7–9, 18, 25]. Characterization of vinylester materials is as a major topic of this research.

Table 2.1: Typical properties of resins used in composite materials [1, 27, 28].

Resin	Density, g/cm^3	Tensile Modulus, GPa	Tensile Strength, MPa
Epoxy	1.17 - 1.28	3.4 - 4.3	69 - 90
Polyester	1.1 - 1.5	3.2 - 3.5	40 - 90
Vinylester	1.02 - 1.23	2.9 - 4.0	65 - 90

2.2 Fibers

Fibers are the primary structural component of composite materials which provide stiffness and strength. Table 2.2 lists typical properties of fibers used in composite materials. Attractive properties for fibers are high stiffness, high strength and low density. Fibers used in composites are glass, carbon, Kevlar and ceramics. Selection of fiber material is dependent on application of the composite since each fiber has different

strengths and weaknesses. Kevlar fibers have excellent properties in tension, but low compressive strength. Most common fibers are carbon and glass.

Table 2.2: Typical properties for fibers used in composites [1, 29].

Fiber	Density, g/cm^3	Tensile Modulus, GPa	Tensile Strength, MPa
E - Glass	2.54	73	3450
S - Glass	2.49	86	4500
AS-4 - Carbon	1.81	235	3700
T-300 - Carbon	1.76	230	3100
T-700 - Carbon	1.80	230	4900
IM7 - Carbon	1.80	290	5170
Kevlar 49	1.45	131	3800

2.2.1 Glass Fibers

Glass fibers are the most common fibers used in composite materials. Typically glass fibers are used in low to mid-performance applications. They appear in many products including sporting equipment, boats, piping. This is a result of favorable properties and low cost. E-glass is a general purpose fiber that comprises about 90% of all glass fiber applications. However, for more demanding applications, the higher stiffness and strength S-glass is favored [30–32].

2.2.2 Carbon Fibers

Development of carbon fibers began with Thomas Edison in 1879 in his pursuit of inventing the light bulb. Carbon fibers were first commercially produced in the 1960's by Union Carbide Corporation and have gained popularity as a structural material with a constant increase in demand for light weight high performance materials. Today carbon

fibers are used in high performance structures such as sporting goods, aerospace, automotive and naval applications. Carbon fibers are desirable as a reinforcement material because they exhibit high stiffness and strength and low density [1, 25, 33]. However, carbon fibers are anisotropic and have poor stiffness and strength transverse to the fiber axis. They can maintain properties at extreme temperatures which make carbon fibers suitable to combine with many types of matrix materials. Carbon fibers are corrosion resistant and inert to water.

2.2.3 Sizing and Surface Treatment of Fibers

Research has shown that the fiber/matrix interface has a strong effect on how well composites perform. Increasing the adhesion between the fiber and matrix materials is beneficial for the stiffness, strength and durability of the composite. Fibers with little surface roughness, such as carbon fibers, are prone for poor adhesion with the matrix. Furthermore, the carbon atom bonds in the graphite crystal are fully saturated which limits the opportunity for chemical bonds to develop between fiber and matrix. This is especially true for the combination of carbon fibers and vinylester. Composites with poor interfacial strength will exhibit low strength [34–37]. As a result much research has been done to develop methods to enhance fiber/matrix adhesion by roughening of the fiber surface, fiber wetting, chemical coatings, and mechanical interlocking. Typically, fiber surface treatments and coatings (sizings) are applied to fibers. It should be noted some researchers distinguish between a sizing and finish. Allred et al. [38] considers a finish "as an adhesion-promoting chemistry applied to the fiber" while sizing "is applied for handling aid". However, most of the time, and in this thesis, they are not distinguished.

There are two basic types of surface treatments: oxidative and non-oxidative methods [39, 40]. Oxidative methods increase surface roughness by removing material. These methods are usually caustic and tend to damage the fibers. Methods include gas-phase oxidation, liquid-phase oxidation, and catalytic oxidation [39]. Gas-phase oxidation is performed at extreme temperatures in the presence of air, oxygen, or gases that contain oxygen. The elevated temperature exposure, however, may degrade fibers. Liquid-phase oxidation tends to be less caustic and generates better materials properties by not degrading fibers. In this method of surface treatment fibers are immersed in an acid or alkaline solution to increase surface roughness [39].

Sizing is a thin coating applied to the fiber surface and may require a surface treatment prior to application. Sizings also serve to protect the fibers from corrosion and damage that occurs when fibers rub against each other during transportation. Sizings and the methods of application required are commonly proprietary to the fiber manufacturer [30, 39]. Sizings are also used to promote fiber/matrix interface strength and tend to be matrix specific for optimal bonding. For glass fibers, silane, a coupling agent, is used to promote adhesion for low-temperature cure resins [38]. The coupling agent increases adhesion at the interface by chemically bonding directly to the fiber surface and the matrix [38]. For carbon fibers, sizings suitable for epoxy matrices are available, but sizing chemistry research is still in progress to develop a suitable for vinylester [38].

2.2.4 Fiber/Matrix Interface

In determining mechanical properties of composite materials through testing it is essential to understand the function of the fiber/matrix (F/M) interface. In the most simplistic sense, the fiber matrix interface is a surface defined by the contact between the

fibers and the matrix of the composite. Drzal et al. [41] however, provides a more detailed view and describes the fiber/matrix interface as a three-dimensional transitional region, called “interphase”, that exists near the boundary where the fiber and the matrix come into contact, see Figure 2.1. The interphase has material properties that are different than both the bulk matrix and the fiber due to the gradual transition from bulk matrix to bulk fiber.

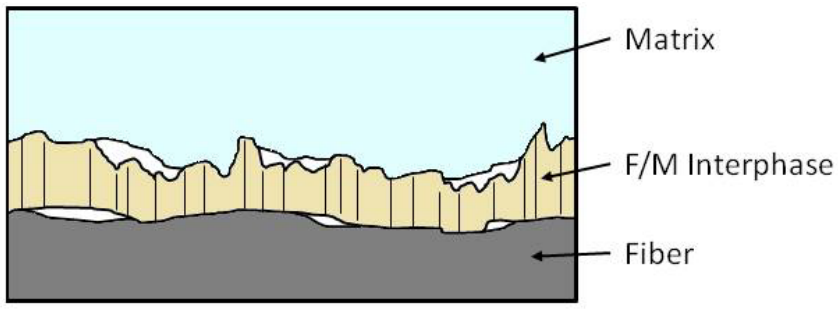

Figure 2.1: Fiber/matrix interface region.

The F/M interface is responsible for load transfer into the composite and within the composite through shear. There have been numerous investigations on the effects of F/M interface strength on composite material properties [34–37, 42–45]. The F/M interface adhesion is typically quantified by the interface shear strength (ISS), which may be determined by highly specialized test methods, such as the single-fiber pull-out test, single fiber fragmentation and other test methods [34]. The quality of the F/M interface dictates the types of failure mode that occur during testing. Such modes will be discussed later in section 3.2, which covers testing of composite specimens. The most drastic effect of the F/M interface on the composite are in transverse and off-axis failure modes where

the failures are governed by the F/M interface in case if it is weak. The F/M interface, however, has a small effect on small strain elastic properties like modulus [41].

Through mechanical testing and scanning electron microscopy, Madhukar and Drzal [34–37] have examined the influence of fiber/matrix adhesion on the tensile, compressive and shear failure strengths of carbon/epoxy composites. The matrix is a diglycidyl ether of Bisphenol-A epoxy resin with a meta-phenylene diamine (mPDA) curing agent. Specifically, they examined untreated and specially sized fibers denoted by AU-4/mPDA, AS-4/mPDA and AS-4C/mPDA composites. AU-4 are untreated carbon fibers, AS-4 fibers were surface treated for an epoxy matrix, and AS-4C was surface treated for an epoxy matrix plus an additional thin layer of epoxy.

Madhukar and Drzal [34] conducted an extensive experimental study to determine how interfacial shear strength and quality of adhesion affect in-plane and interlaminar shear properties of unidirectional carbon/epoxy composites. For in-plane shear, it was found that composites with low interface shear strength (ISS) fail at the F/M interface. Cracks initiate at a flaw at the interface and propagate along the F/M interface. In specimens with intermediate ISS, failure was a combination of F/M interface failure and matrix failure mode. In such cases Madhukar and Drzal [34] detected matrix debris on the exposed carbon fibers on the failure surface. Specimens with high ISS failed in the matrix. For such cases, Madhukar and Drzal [34] reported clean fracture surfaces with no evidence of interfacial failure.

Table 2.3 lists ISS, in-plane shear (S_6) and interlaminar shear (S_5) strengths determined by Madhukar and Drzal [34]. Madhukar and Drzal [34] found from

intermediate ISS to high ISS there was no significant change in the apparent in-plane shear strength.

Table 2.3: ISS and composite shear strengths for carbon/epoxy [34].

Adhesion	ISS (MPa)	S_6 (MPa)	S_5 (MPa)
Low	37.2	55.0 ± 3.0	47.5 ± 5.4
Intermediate	68.3	95.6 ± 5.1	84.0 ± 7.0
High	81.4	93.8 ± 3.3	93.2 ± 3.8

In general, it is accepted that fiber properties govern the longitudinal properties of a composite. But the F/M interface strength influences also the longitudinal tensile strength. Table 2.4 lists the ISS, longitudinal tensile and transverse tensile strengths. The increased longitudinal strength was highest for composites with the strongest fiber/matrix interface. The benefits of increasing ISS were most evident when improving a poor interface. There was little gain in longitudinal tensile strength by improving the quality of the interface of composites from intermediate to high ISS [35].

Table 2.4: ISS and lamina tensile strengths of carbon/epoxy [35].

Adhesion	ISS (MPa)	X_1^T (MPa)	X_2^T (MPa)
Low	37.2	1403 ± 107	18.0 ± 3.9
Intermediate	68.3	1890 ± 143	34.2 ± 6.2
High	81.4	2044 ± 256	41.2 ± 4.7

Madhukar and Drzal [35] explained the low longitudinal tensile strength for the composites with a weak interface as a result of poor load transfer between fibers. In such

cases the adhesion between the matrix and fiber is too weak to transfer load from broken fibers to the neighboring fibers. Madhukar and Drzal [35] observed that composite specimens with high interface strength cracked in small sections perpendicular to the fiber.

Significant increase in transverse tensile strengths were observed with the increase of ISS [35], see Table 2.4. This shows that the transverse tensile strength is highly dependent on fiber/matrix interface adhesion. SEM investigation by Madhukar and Drzal [35] of low ISS specimens after testing revealed bare fibers and matrix failure. Bare fibers are an indication fiber/matrix interface failure, which resulted in unbroken fibers liberated from the matrix. Specimens with intermediate ISS failed at a much higher applied stress than low ISS specimens [35]. Microscopic investigation of tested specimens revealed bare and some broken fibers [35]. This is also an indication of fiber/matrix interface and matrix failure. Highest tensile strength was observed in the high ISS specimen [35]. Fracture surfaces revealed few bare fibers, matrix coated fibers and increased fiber breakage [35]. An increase in broken fibers and matrix coated fibers is an indication the dominant failure is due to the matrix with minimal failure at the fiber/matrix interface. It should also be noted that increased ISS had an insignificant effect on the transverse modulus E_2 [35].

There are five typical failure modes of a composite material in compression. Failure modes include (a) global buckling (b) delamination buckling (axial splitting), (c) shear failure, (d) microbuckling and (e) kink zone, see Figure 2.2. Global buckling is a geometric failure and can be avoided by proper fixturing and specimen design. Delamination buckling may occur when the fiber/matrix interface adhesion is weak,

leading to ply separation. Shear failure occurs commonly in transversely loaded specimens and is a result of matrix failure. Microbuckling of the fibers occurs due to elastic support by the matrix. Kink bands may follow after microbuckling, causing localized bending of the fibers so great that the fiber snaps at the boundaries of the kink band.

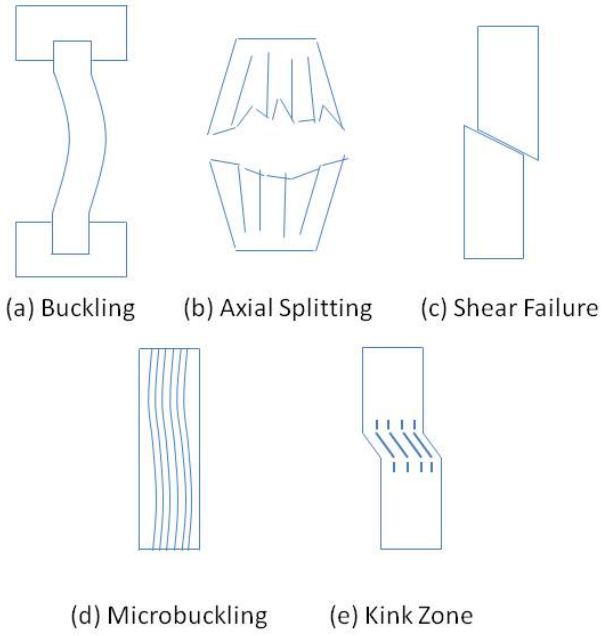

Figure 2.2: Compression failure modes.

Madhukar and Drzal [36] measured the longitudinal compressive strength and examined failure modes of unidirectional compression specimens with various quality of adhesion at the F/M interface. Table 2.5 lists ISS and compression strengths.

Table 2.5: ISS and longitudinal compressive strength [36].

Adhesion	ISS (MPa)	X_1^C (MPa)	Failure Mode
Low	37.2	679 ± 116	Delam. Buckling
Intermediate	68.3	911 ± 180	Kink Band
High	81.4	1174 ± 207	Kink Band

Madhukar and Drzal [36] found that composites with poor adhesion at the F/M interface failed by delamination buckling. In-plane compression causes fibers to separate laterally by overcoming the interfacial adhesion. Kink bands were observed in composites with intermediate fiber/matrix interface strength. This failure mode involves local fiber/matrix interface failure in the kink zone. The highest compressive strengths observed by Madhukar and Drzal [36] were in composite specimens with high fiber/matrix interface strengths. Such specimens, probably failed by kink band formation, but the fiber/matrix adhesion is strong and is able to better supports the intense shear stress in the kink zone.

Based on this review it is clear that the F/M is a critical link for durability and strength of the composite [1, 30, 46]. Testing of the composites in the current work will indirectly assess the quality of the F/M interface. In particular, tests that directly promote loading of the F/M interface, such as off-axis and transverse tension tests, as well as shear tests will help to determine the importance of the F/M interface. The experimental program will also examine the effects of the F/M interface on the longitudinal, off-axis and transverse compression strengths.

2.3 Degradation of Composite Materials by Water Exposure

The durability of composite materials in marine environments is of prime importance to the naval industry. As mentioned previously, currently composite materials replace monolithic materials such as steel and aluminum. Composites require less maintenance as they do not rot or rust in a marine environment [6]. However, polymer composite materials degrade after exposure to moisture.

Absorption of moisture by a polymer depends on the type of polymer and the degree of cure [47–49]. In general, water absorption results in swelling and plasticization of the polymer and a reduction of the elastic modulus and glass transition temperature (T_g). T_g is an important limit and defines the temperature where a polymer transitions from glassy, brittle material towards a more rubbery state [50].

For a composite there are three mechanisms for moisture transport; diffusion through the matrix, transport through the F/M interface, and transport through cracks and voids. Diffusion is the random motion of water molecules through the matrix driven by a concentration gradient. This phenomenon may be modeled using the Fickian diffusion model [24]. The diffusion process depends on the temperature and water concentration. Much work has been done on modeling of moisture diffusion through polymers and composite materials [16, 22, 24, 25, 51, 52].

Moisture absorption at the fiber/matrix interface (wicking) occurs by capillary action. Wicking is the fastest method of moisture transport through a composite and is highly dependent on the quality of adhesion at the F/M interface [53]. Analysis of wicking in carbon/vinylester and carbon/epoxy composites was conducted by Ramirez et al. [18]. In this analysis a few assumptions must be considered. The total moisture

absorbed by the composites must be the sum of moisture absorption by the fibers, matrix and F/M interface. However, carbon fibers are inert to water. The matrix can only absorb moisture until saturation is reached. Hence, the remaining moisture content must be attributed to voids and wicking. Ramirez et al. [18] analyzed the total moisture content in a void-free composite in terms of the volume fraction of the fiber and matrix (V_f and V_m) and derived the following equations to determine moisture contents of the resin (M_R) and fiber/matrix interface ($M_{F/M}$),

$$M_R = \frac{\rho_w V_m}{\rho_f V_f + \rho_m V_m} M_m \tag{2.1a}$$

$$M_{F/M} = M_c - \frac{\rho_w V_m}{\rho_f V_f + \rho_m V_m} M_m \tag{2.1b}$$

where ρ_w, ρ_f and ρ_m are the densities of water, fiber and the matrix respectively. M_m and M_c are the saturation moisture contents for the matrix and the composite.

Some work has been done on the relation between void content and moisture content. Costa et al. [54] have shown that high void contents (V_V > 2.0%) in a composite can promote the moisture up-take. But the effects of voids are highly dependent on the shape, size and distribution of the voids. For a well manufactured composite the void content is less than 1% and as a result voids should have minimal effect on the moisture content.

The swelling and plasticization of the matrix due to water absorption can reduce the interface adhesion by reduction of the residual pressure on the fiber/matrix interface left after cure of the resin [11]. The residual compressive stress state is due to shrinkage of the matrix onto the fiber.

Moisture effects on mechanical properties of composite materials has predominantly been focused on glass/epoxy and carbon fiber/epoxy based composites [9, 17, 18, 55–57]. Shen and Springer [55, 56] reported negligible change in strength for carbon fiber/epoxy longitudinal and 45° off-axis tensile specimens having moisture content less than 1%. Similarly, the moduli remained unaffected by the amount of moisture content. However, many researchers have found that fiber/matrix dominated strengths, e.g. the transverse strength and interface shear strength, are greatly affected by moisture content [17, 18, 21, 55, 56]. Ramirez et al. [18] reported an 82% reduction of interface shear strength in carbon/epoxy specimens after exposure to moisture using the single fiber fragmentation test (SFFT). Since carbon fibers are inert to water, this reduction must be attributed to debonding at the fiber/matrix interface. Weitsman [57] relates debonding at the fiber/matrix interface to induced residual stresses caused by moisture expansion mismatch between the fibers and the matrix. As discussed previously, vinylester resins absorb less moisture and expand less than epoxies. Thus, vinylester should be more resistant to debonding at the fiber/matrix interface. This is of great interest to the present work.

3 MATRIX AND COMPOSITE SPECIMENS AND TEST METHODS

3.1 Matrix Testing Methods

Because of the visocelastic behavior of polymers, it should be pointed out that results from mechanical testing of the vinylester resins are only relevant to load-time scale and environment in which they are tested [58, 59]. The vinylester resins will be considered homogenous and isotropic materials.

3.1.1 Tensile Testing

Tensile testing of polymers is discussed in many texts [59–62]. Tensile testing and preparation of vinylester neat resin specimens in the present work are in accordance to ASTM D638 [58]. Details will be presented in Chapter 4.

Tensile testing will determine modulus and tensile strength of vinylester resins. Young's modulus E is defined by,

$$E = \frac{\Delta\sigma}{\Delta\varepsilon} \tag{3.1}$$

where $\Delta\sigma$ and $\Delta\varepsilon$ are the increments of stress and strain in the linear elastic region.

Tensile strength σ_{ult}^{T} is defined as the highest observed stress before failure [59].

3.1.2 Compression Testing

Compression testing and preparation of vinylester neat resin specimens was conducted in accordance to ASTM D695 [63]. This test is conducted on short unsupported specimens between parallel loading platens. Special care must be taken in preparing compression specimens to insure that load faces are parallel to one another. Specimens are loaded in compression by displacing the platens at a constant cross head rate until failure.

Compression testing will determine modulus and compressive strength of vinylester resins. Compressive Young's modulus E is determined by the same equation as for the tensile test, Equation (3.1). Compressive strength σ_{ult}^{C} is defined as the highest observed magnitude of stress before failure [59].

3.1.3 Shear Testing

Currently there is no accepted standardized test for characterizing the shear response of polymers. However there has been extensive work performed in this area that utilizes the Iosipescu test fixture developed by Walrath and Adams [64]. The test method and specimen geometry were developed by Nicolae Iosipescu [65] for determining shear properties of metals. This test method was later applied to composites and developed into an ASTM standard [66].

A common fixture used for Iosipescu shear testing shown in Figure 3.1 is known as "the Adams and Walrath (A&W)" fixture.

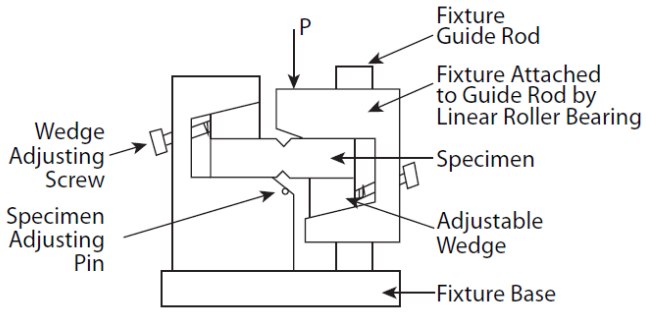

Figure 3.1: Iosipescu shear specimen and fixture [67].

The importance of this test relies on the fact that in the gage section the specimen is loaded purely in shear. A loading diagram of the specimen is shown in Figure 3.2. Notice in the loading diagram that the gage section of the specimen is loaded in shear; the bending moment is zero. This loading diagram infers that failure of the specimen in this region will be due to shear stress [66]. Failure of a ductile material in shear would occur by yielding in the gage section of the specimen from notch root to notch root, see research by Kwon et al. [66] on ABS specimen. Testing of a brittle polymer by Sullivan et al. [68], however, revealed brittle failure due to resolved tension in the section.

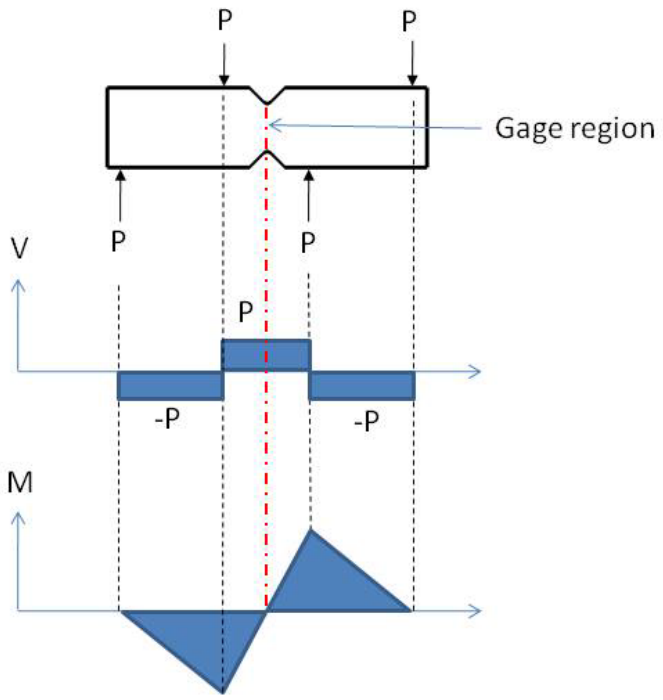

Figure 3.2 Iosipescu loading shear/moment diagram [66].

Shear stress (τ) is shear force (P) over the shear area (area between the notches),

$$\tau = \frac{P}{A} \tag{3.2}$$

Shear strength (τ_{ult}) is defined as the highest observed shear stress during testing.

Shear strain (γ) is monitored by strain gages oriented at ±45° to the horizontal in the test section and is defined as the sum of the absolute values of the strain gage readings.

$$\gamma = |\varepsilon_{45°}| + |\varepsilon_{-45°}| \tag{3.3}$$

3.2 Composite Test Methods

For a full characterization of mechanical properties of a composite, tensile, compression and shear tests are performed. Tensile testing is conducted according to ASTM D3039 and includes testing of unidirectional 0°, 45° off-axis and 90° (transverse) specimens. Compression testing is conducted per ASTM D6641, using the combined loading compression test method, and includes a cross-ply laminate for determining longitudinal (0°) strength, and 45° off-axis and transverse specimens. Shear testing of unidirectional 0° specimens is done to determine in-plane shear modulus and strength and interlaminar shear strength per ASTM D5379 and ASTM D2344.

3.2.1 Tensile Testing

Three properties can be determined from the longitudinal tensile test, modulus (E_1), Poisson's ratio (ν_{12}) and strength (X_1^T). Determination of E_1 typically involves linear regression of the stress-strain curve to determine the slope [69]. However, the highly linear response allowed a simplified evaluation of E_1 based on the longitudinal and transverse strains (ε_1 and ε_2) recorded using strain gages. Stress, σ_1, is calculated from the measured load,

$$\sigma_1 = \frac{P}{A} \tag{3.4a}$$

$$E_1 = \frac{\Delta\sigma_1}{\Delta\varepsilon_1} \tag{3.4b}$$

$$\nu_{12} = -\frac{\Delta\varepsilon_2}{\Delta\varepsilon_1} \tag{3.4c}$$

where $\Delta\sigma_1$ is an increment of stress within the linear elastic region of the stress-strain curve, and $\Delta\varepsilon_1$ and $\Delta\varepsilon_2$ are the corresponding increments in axial and transverse strains [67].

The longitudinal tensile strength X_1^T is defined by,

$$X_1^T = \sigma_1^{ult} \tag{3.4d}$$

where σ_1^{ult} is the maximum value of the longitudinal stress.

Testing of transverse tensile specimens is done to determine transverse modulus E_2 and strength, X_2^T. The transverse modulus E_2 is defined by,

$$E_2 = \frac{\Delta\sigma_2}{\Delta\varepsilon_2} \tag{3.5a}$$

where $\Delta\sigma_2$ is an increment of stress in the linear-elastic region of the stress strain curve and $\Delta\varepsilon_2$ is the corresponding strain increment.

Transverse tensile strength X_2^T is defined as the maximum stress observed during testing.

$$X_2^T = \sigma_2^{ult} \tag{3.5b}$$

The present work also includes tensile testing of 45° off-axis specimens. The term off-axis refers to a specimen with the orientation of the fibers off-set an angle θ to the loading axis. This test has become popular because it offers a simple method of

achieving a biaxial stress state, see Figure 3.3. Generally, off-axis specimens are not used to determine lamina properties alone but to verify properties determined by other testing methods [67], and examine strength under combined stress.

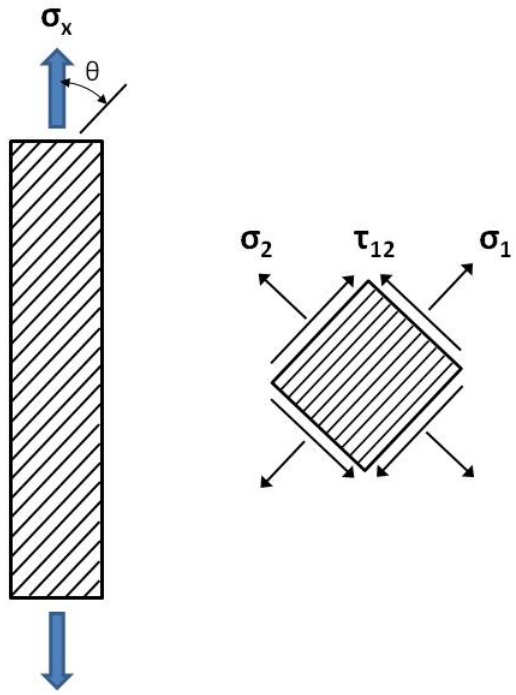

Figure 3.3: Biaxial stress state in off-axis tension specimen.

The longitudinal tensile (σ_1), transverse tensile (σ_2) and shear (τ_{12}) stresses can be calculated by,

$$\sigma_1 = m^2\sigma_x \tag{3.6a}$$

$$\sigma_2 = n^2\sigma_x \tag{3.6b}$$

$$\tau_{12} = -nm\sigma_x \tag{3.6c}$$

where $m = \cos\theta$, $n = \sin\theta$, and θ is the angle between the fiber direction and the loading axis.

3.2.2 Compression Testing

Compression testing in this project utilized the Combined Loading Compression (CLC) test method shown in Figure 3.4, ASTM D6641 [70]. This test fixture takes advantage of both shear-loading and end-loading. By clamping both ends of the specimen in the fixture load is transferred into the specimens by shear while the remaining load is applied through end loading. The CLC test method also prevents buckling by using a short (12.5 mm) unsupported span.

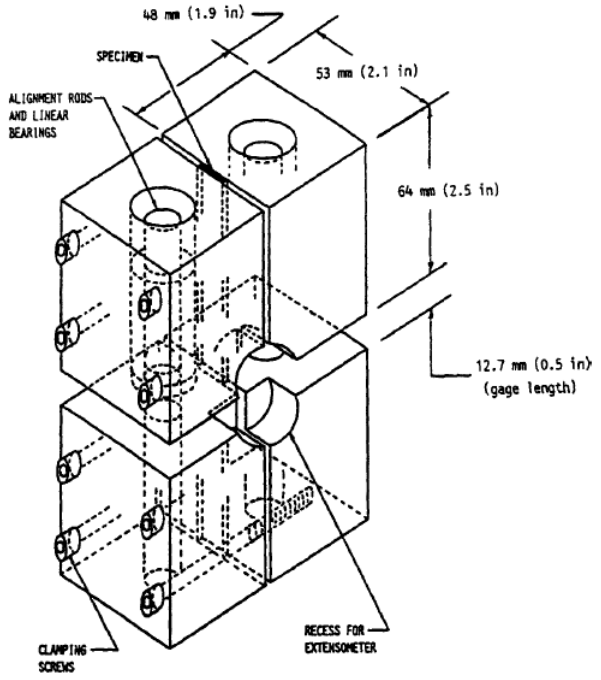

Figure 3.4: Combined loading compression (CLC) test fixture, ASTM D6641 [70].

Compression testing of unidirectional composites is typically conducted on longitudinal (0°) and transverse (90°) unidirectional test specimens. The longitudinal

and transverse compressive strengths X_1^C and X_2^C are defined as maximum magnitudes of the stresses σ_1 and σ_2,

$$X_1^C = \left|\sigma_1^{ult}\right| \tag{3.7a}$$

$$X_2^C = \left|\sigma_2^{ult}\right| \tag{3.7b}$$

It should be pointed out that testing of unidirectional 0° specimens problematic because they are extremely strong and tend to fail by other mechanisms than pure compression. As a result, cross-ply specimens are commonly tested. Cross-ply laminate specimens fail at lower stress, and it is possible to "back-out" the compressive strength of the unidirectional plies (X_1^C). The "back-out factor", BF, is multiplied by the observed laminate strength (X_C) to determine the 0° ply strength,

$$X_1^C = BFX_C \tag{3.8}$$

The "back-out" factor is calculated from the ply stiffnesses and lay-up of the laminate. Adams et al. [67] gives an expression for the back-out factor valid for a balanced and symmetric cross-ply laminate with even and equal number of alternating $[0/90]_{ns}$ plies.

$$BF = \frac{{}^1\!/_2\, E_1(E_1 + E_2) - (\upsilon_{12}E_2)^2}{{}^1\!/_4\,(E_1 + E_2)^2 - (\upsilon_{12}E_2)^2} \tag{3.9}$$

However, although the cross-ply specimens in the present work are balanced and symmetric, they contain a different number of 0° and 90° plies. Analysis of such a laminate under compressive load, Figure 3.5, is presented.

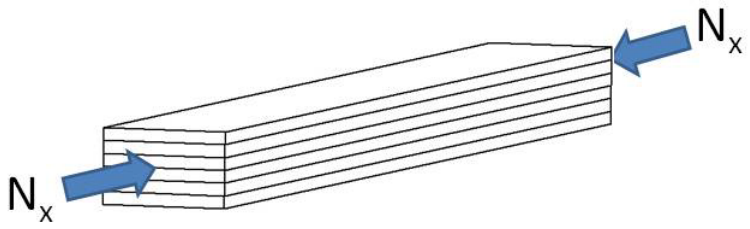

Figure 3.5: Symmetric cross-ply laminate under uniaxial compressive load.

The strain-force relationship is as follows [1, 30],

$$\begin{bmatrix} \varepsilon_x \\ \varepsilon_y \\ \gamma_{xy} \end{bmatrix} = \begin{bmatrix} a_{11} & a_{12} & 0 \\ a_{12} & a_{22} & 0 \\ 0 & 0 & a_{66} \end{bmatrix} \begin{bmatrix} N_x \\ 0 \\ 0 \end{bmatrix} \tag{3.10}$$

where $[a] = [A]^{-1}$, and $[A]$ is the extensional matrix, ε_x the axial strain, ε_y the transverse strain and, γ_{xy} the shear strain. N_x is the force applied per unit width. From Equation (3.10) we obtain,

$$\varepsilon_x = a_{11} N_x \tag{3.11a}$$

$$\varepsilon_y = a_{12} N_x \tag{3.11b}$$

$$\gamma_{xy} = 0 \tag{3.11c}$$

The ply stresses are given by,

$$\begin{bmatrix} \sigma_1 \\ \sigma_2 \\ \tau_{12} \end{bmatrix}_k = \begin{bmatrix} \bar{Q}_{11} & \bar{Q}_{12} & 0 \\ \bar{Q}_{12} & \bar{Q}_{22} & 0 \\ 0 & 0 & \bar{Q}_{66} \end{bmatrix}_k \begin{bmatrix} \varepsilon_x \\ \varepsilon_y \\ \gamma_{xy} \end{bmatrix} \tag{3.12}$$

where $\bar{Q}_{ij}$ are elements of the off-axis reduced stiffness.

The stiffness matrixes for the 0° and 90° plies are,

$$[\bar{\mathrm{Q}}]_{0^\circ} = [\mathrm{Q}] = \begin{bmatrix} Q_{11} & Q_{12} & 0 \\ Q_{12} & Q_{22} & 0 \\ 0 & 0 & Q_{66} \end{bmatrix}, \quad [\bar{\mathrm{Q}}]_{90^\circ} = \begin{bmatrix} Q_{22} & Q_{12} & 0 \\ Q_{12} & Q_{11} & 0 \\ 0 & 0 & Q_{66} \end{bmatrix} \tag{3.13}$$

The stiffness elements are defined in terms of the engineering stiffness constants as follows,

$$Q_{11} = \frac{E_1}{1 - v_{12}v_{21}} \tag{3.14a}$$

$$Q_{12} = \frac{v_{12}E_2}{1 - v_{12}v_{21}} = \frac{v_{21}E_1}{1 - v_{12}v_{21}} \tag{3.14b}$$

$$Q_{22} = \frac{E_2}{1 - v_{12}v_{21}} \tag{3.14c}$$

$$Q_{66} = G_{12} \tag{3.14d}$$

For the 0° plies, Equation (3.12) yields,

$$\sigma_1 = Q_{11}\varepsilon_x + Q_{12}\varepsilon_y \tag{3.15}$$

Combining equations (3.11a), (3.11b) and (3.15) results in the following,

$$\sigma_1 = (Q_{11}a_{11} + Q_{12}a_{12})N_x \tag{3.16}$$

The applied force per unit width N_x corresponds to an average laminate stress $\bar{\sigma}_x$,

$$\bar{\sigma}_x = \frac{N_x}{h} \tag{3.17}$$

where h is the total thickness of the laminate. Combining equations (3.16) and (3.17) yields

$$\sigma_1 = Q_{11}a_{11}\bar{\sigma}_x h + Q_{12}a_{12}\bar{\sigma}_x h \tag{3.18}$$

The back-out factor is defined as the ratio between the axial stress in the 0° plies and the average stress in the laminate. Eq. (3.18) yields,

$$BF = \frac{\sigma_1}{\bar{\sigma}_x} = (Q_{11}a_{11} + Q_{12}a_{12})\text{h} \tag{3.19}$$

It is often preferred to express the "back-out" factor in terms of the laminate stiffness elements, A_{ij}, given by,

$$A_{ij} = \sum_{k=1}^{N} (\bar{Q}_{ij})_k (z_k - z_{k-1}) \tag{3.20}$$

where $(\bar{Q}_{ij})_k$ are the reduced stiffness elements for to ply k. z_k and z_{k-1} are the so called ply coordinates defined in Figure 3.6.

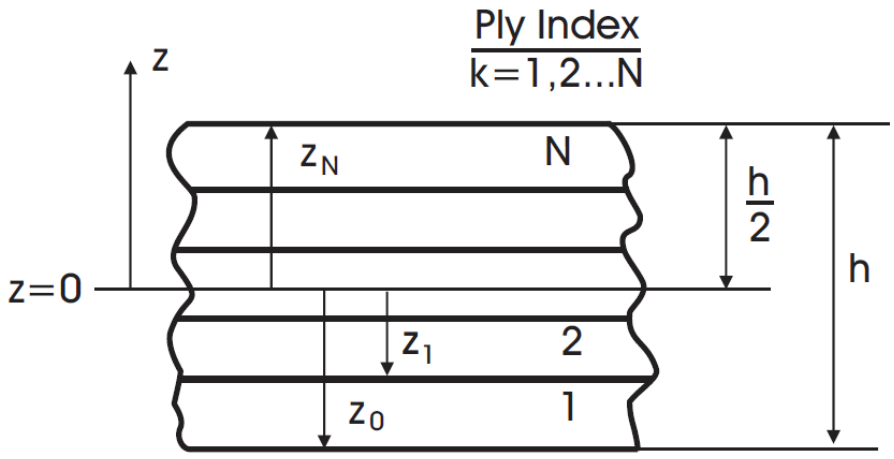

Figure 3.6: Coordinate location for individual plies.

The following relations between a_{11} and a_{12} and A_{11}, A_{22} and A_{12} applies to a symmetric and balanced laminate.

$$a_{11} = \frac{A_{22}}{A_{11}A_{22} - A_{12}^2} \tag{3.21a}$$

$$a_{12} = \frac{-A_{12}}{A_{11}A_{22} - A_{12}^2} \tag{3.21b}$$

With the expressions (3.21) for a_{11} and a_{22}, Equation (3.19) becomes,

$$BF = \frac{(Q_{11}A_{22} - Q_{12}A_{12})\mathrm{h}}{A_{11}A_{22} - A_{12}^2} \tag{3.22}$$

3.2.3 Short Beam Shear Testing

The short beam shear (SBS) [71] in commonly used to measure interlaminar shear strength. Interlaminar shear strength (ILSS) is used as a measure of F/M interface quality [34, 40, 42, 67, 72–74]. The SBS test method is a three-point bend test, see Figure 3.7, conducted at short span lengths to promote shear failures.

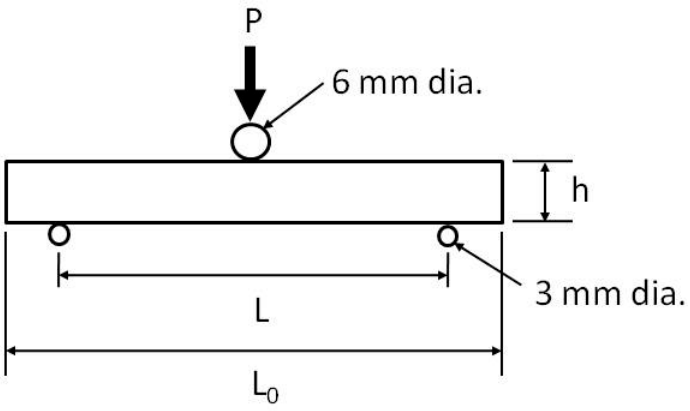

Figure 3.7: Short beam shear test principle.

When the SBS specimen is loaded at mid-span a combined bending and shear stress state is induced. The bending stress is compressive at the top half of the beam and progresses linearly to the bottom tension half of the specimen. At the center plane the bending stress is zero. The interlaminar shear stress, τ_{13}, is parabolic through the thickness of the specimen with maximum value at the central neutral axis. Hence, the shear stress is maximum at a location where the bending stress is zero, which is beneficial for determining interlaminar shear strength. However, care must be taken in choosing span and thickness of the specimens. If the span-to thickness ratio is too large, the specimens will fail in flexure. To achieve shear failure, span-to-thickness ratio less than 4:1 is recommended [71].

The maximum interlaminar shear stress (τ_{13}) is given by,

$$\tau_{13} = \frac{3P}{4bh} \tag{3.23}$$

where P is the load applied, b is the specimen width and h is the specimen thickness. The interlaminar shear strength (S_5) is defined as the interlaminar shear stress corresponding to failure of the specimens, $P = P_{max}$

Desired failure mode for SBS testing is interlaminar cracking at the neutral axis. However, researchers have found difficulty in producing this failure mode. Often failure is a result of compression near the central load introduction [34, 73]. The specimen may fail due to a combination of interlaminar shear and compression stress near the central loading pin.

4 TEST PROGRAM AND EXPERIMENTAL PROCEDURES

The primary objective of this research is to quantify degradation of the mechanical behavior of vinylester resins and carbon/vinylester composites from environmental exposure. Accurate failure modeling of the composite requires dry and moisture saturated (wet) material properties of the constituent matrix materials. Materials included in the characterization are 510A and 8084 vinyl ester resins, F and G sized carbon fibers and composites produced from these fibers and resins. The carbon fibers are not degraded by exposure to relative humidity and water. The resins will be exposed to dry, 85% relative humidity (RH) at 50°C and seawater at 40°C environmental conditions. The composite materials will be tested at dry conditions and after immersion in seawater at 40°C.

A full characterization of the constitutive mechanical behavior of a material requires tensile, compressive and shear tests. Hence, the vinylester 510A and 8084 resins are tested in tension, compression and shear. Composite materials consisting of F and G sizing carbon fibers in VE 510A resin were tested in tension, compression and various configurations of shear. The outline for materials characterization is shown in Figure 4.1.

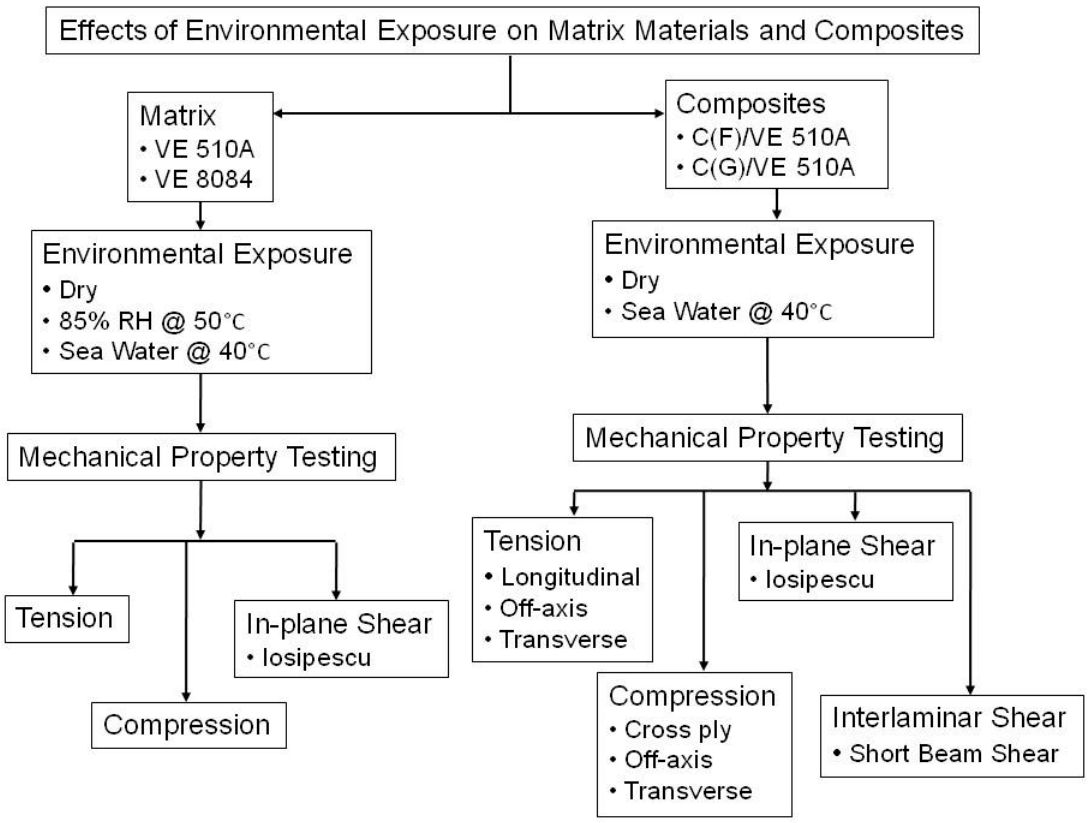

Figure 4.1: Outline of materials characterization research.

The neat resin specimens will be tested in tension according to ASTM D638 [58], compression, ASTM D695 [63], and shear, ASTM D5379 [66] ("V" notch specimen). Each specimen will be exposed to three environmental conditions, dry, sea water at 40°C, and 85% RH at 50°C. Each combination of test and environmental condition requires a minimum of 5 replicates.

Tensile tests will be conducted on unidirectional composites at 0°, 45° and 90° fiber directions, ASTM D3039 [75], compression tests on $[\bar{0}/90]_{9S}$ cross-ply, 45° off-axis and 90° specimens, ASTM D6641 [70]. Iosipescu shear tests on 0° composites, ASTM D5379 [66] and short beam shear (SBS) tests on 0° laminates, ASTM D2344 [71].

4.1 Materials and Specimens

The carbon fibers used in this research are T700S carbon fibers manufactured by Toray [29]. The fibers were coated with F and G sizings. The purpose of adding sizing to fibers is to improve the adhesion between the matrix and fiber. F sizing is specifically designed for compatibility with vinylester matrices. G sizing is a general purpose sizing. Fiber properties are listed in Table 4.1.

Table 4.1: Torayca T700S carbon fibers [29].

Fiber Properties	
Filament Diameter, μm	7
Density, g/cm^3	1.8
Tensile Modulus, GPa	230
Tensile Strength, MPa	4,900
Strain, %	2.1

Two types of matrix materials, Derakane vinylester 510A and 8084, manufactured by Ashland [27, 28] are examined. VE 510A-40 is derived from a brominated bisphenol-A resin. This resin is designed to promote fire and corrosion resistance. The resistance of this resin to caustic alkalis, hypochlorite bleaching chemicals and hot water is excellent. Applications of this resin include FRP ductwork, stacks and stack liners, handling mixtures of hot air and hot gases or potentially flammable liquids. VE 8084 resin is elastomer modified with favorable adhesive strength, abrasion resistance, and toughness. This resin is also fairly resistive to many acids, bases and organic chemicals. Both resins can be processed using resin transfer molding (RTM), hand-lay, spray-up, filament winding as well as other processing methods. The physical and mechanical

properties of the 510A and 8084 resins provided by the manufacturer are listed in Tables 4.2 and 4.3.

Table 4.2: Physical properties of vinylester 510 and 8084 resins [27, 28].

Physical Properties	**510**	**8084**
Density, g/cm^3	1.23	1.02
Dynamic Viscosity, (RT) mPas	400	360
Styrene Content, %	38	40
Shelf Life(2), Dark, RT, months	4	6

Table 4.3: Mechanical properties of vinylester 510 and 8084 resins [26–28].

Mechanical Properties	**510**	**8084**
Tensile Modulus, GPa	3.4	2.9
Tensile Strength, MPa	86	76
Tensile Elongation, %	4-5	8-10
Heat Distortion Temperature, °C	113	82
Glass Transition Temperature, °C	125	117

4.1.1 Processing of Resins

Mixing ratios are specified by the manufacturer "DERAKANE 510A-40 Epoxy Vinyl Ester Resin [27]." For the 510A resin specimens methylethylketone peroxide (MEKP) at 1.0% and Cobalt Naphthenate-6% (CoNap6%) at 0.20% by mass of resin were mixed. For the current work the 510A resin was prepared at 24°C using these mixture ratios which resulted in a gel time of 50 ±15 min. The promoter, Cobalt Napthenate-6%, is mixed with the vinylester resin for 15 min. The resin/promoter mixture is left for 60 minutes to allow the promoter to react with the resin. The catalyst,

MEKP, is then added to the resin and mixed for 3 minutes. To reduce the amount of bubbles the mixture was placed in a freezer for five minutes. By this procedure, the bubbles rise to the top and reduce the amount air trapped within the resin. The gel time is also increased.

Mixture ratios used for the 8084 resin specimens are 1.50% MEKP, 0.30% CoNap6%, and 0.025% Dimethylaniline (DMA) by mass of resin. Mixing ratios were acquired from manufacturer data sheet, "DERAKANE 8084 Epoxy Vinyl Ester Resin [28]." These mixture ratios resulted in 50 ±15 minute gel time at 30°C. The promoters, Cobalt Napthenate-6% and DMA, were mixed with the resin for 15 min. The promoters/resin mixture is left for 60 minutes to allow the promoters to react with the resin. The catalyst, MEKP, is then added to the resin and mixed for 3 minutes.

4.1.2 Neat Resin Specimen Preparation

Neat resin tensile, compression and shear specimens are needed for the materials characterization. Tensile properties including Young's modulus, ultimate tensile strength, and ultimate strain, were determined following the ASTM standard for tensile testing of polymer materials, ASTM D638 [58] with some minor deviations. Figure 4.2 shows the specimen geometry and dimensions. Due to unavailable tooling the radius of the dog bone specimen was reduced from the ASTM specification (76 mm) to 19.1 mm.

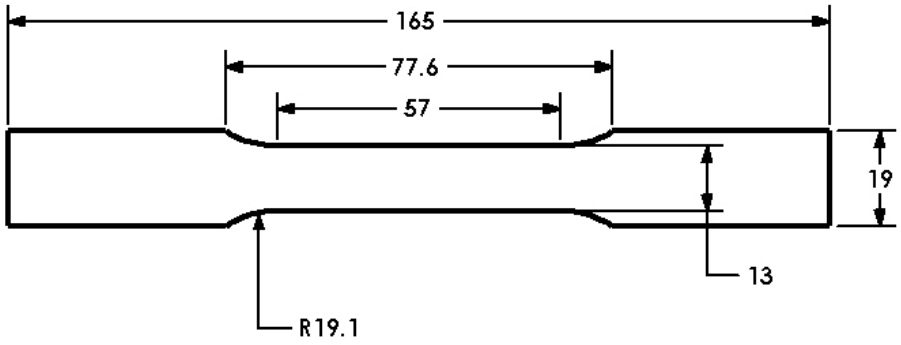

Figure 4.2: Neat resin tensile specimen dimensions (mm).

Various methods were used to manufacture neat resin specimen including: open faced silicon molds and specimen milled from flat sheets of resin; the latter being a more effective method. When casting neat resin specimens great care should be taken to avoid trapping air and gas bubbles within the specimen. Bubbles create stress concentrations within the specimen and induce premature failure.

One method used to directly prepare dog-bone shaped tensile specimens utilized an open faced RTV silicon mold. The first step in creating the mold is to make a rigid male mold. This was done by CNC cutting a 25.4 mm thick PVC plate with the same geometry as the dog bone tensile specimen. The CNC male mold can be filled with a two-part RTV silicon compound. Once the silicon cures the vinylester resin can be mixed and poured into the mold. Figure 4.3 shows a RTV silicon open faced mold for tensile specimens. Figure 4.4 shows an example of neat resin tensile test specimen created using an open faced mold.

Figure 4.3: Open face silicon mold for dog-bone tensile test specimens.

There are a number of difficulties that occur when using an open faced mold. Surface flaws, concave surfaces and bubbles are common with this type of mold. Surface flaws are transferred directly to the neat resin specimens. Such flaws can be seen in the lower tensile specimen in Figure 4.4; notice the lines oriented in the transverse direction that reoccur over the entire length of the specimen. Those lines are marks left from the cutting tool for the PVC mold. Care must be taken when machining the molds to avoid leaving imperfections in the tensile test specimens.

Figure 4.4: Tensile specimens from an open faced mold.

Surface concavity is another problem. Flat surfaces are needed for the grips of the tensile test machine. Furthermore, application of strain gages and accurate measurements of the cross-sectional area require flat surfaces. Figure 4.5 shows a cross-section of a molded neat resin tensile test specimens. The concavity of the top and sides is caused by shrinkage of the vinylester resin during cure.

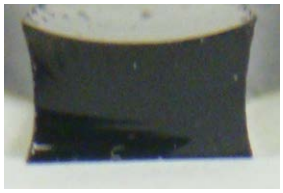

Figure 4.5: Cross-section of a tensile specimen from an open face mold.

As an alternative, specimen may be fabricated from flat neat resin sheets. The most effective method for making flat tensile neat resin specimens is by machining the specimens from a sheet of neat resin. Dimensions can be held tighter and surfaces from the cut specimen contain fewer imperfections than a molded specimen. The method where specimens are cut from a sheet is the simpler of the two methods. There are no concave surfaces, bubbles are reduced and surface flaws are avoided. To enable manufacture of such a sheet, a mold consisting of two vertical square glass plates of 9.5 mm thickness with a side length of 305 mm was prepared, Figure 4.6.

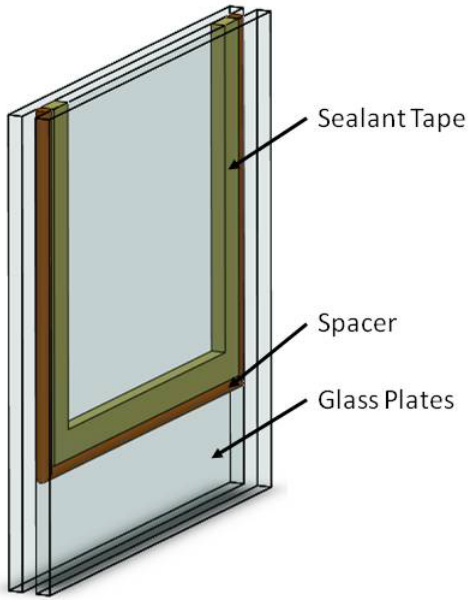

Figure 4.6: Glass mold for a sheet of neat resin.

An outline of a rectangle was created (254 mm by 279 mm) on the inner side of one glass panel using vacuum bag sealant tape. Sometimes the tape was doubled up to allow for a proper neat resin panel thickness between 4.57 and 6.35 mm. The top side of the rectangle was left open to allow for resin to be poured. Spacers should be placed on the three outer edges of the sealant tape to insure a uniform thickness of the sheet. The spacer should be thinner than the tape thickness to allow the tape to seal when the panels are clamped together. Release agent (Freekote 700) was applied to the bonding (inner) surface of each panel. The second glass panel was placed opposite the first panel with the release agent sides facing each other. The two panels were clamped together until both panels touched the spacers on all three edges. The resin was poured into the rectangular opening between the glass panels. With the glass panels arranged vertically

and using a mixture ratio with the long gel time will allow all the air bubbles within the resin to travel to the top. This will leave a resin sheet that is free of voids.

The resin sheets were cut into oversized strip using a tile saw (approximately 165 by 20 mm). A high precision surface grinder was used to insure that specimen edges were parallel and brought the width to 19 mm. Specimens were machined using a special fixture and a mill. A two fluted end mill was used as the cutting tool. The radii of the dog-bone specimen are based off of the diameter of the end mill. Figure 4.7 shows specimen machined from a sheet of resin.

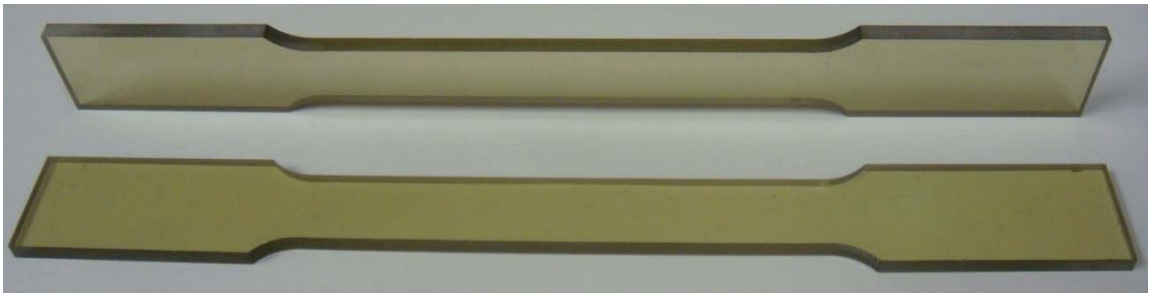

Figure 4.7: Tensile specimen from neat resin panel.

Compression testing utilized cylindrical specimens with a length of 25.4 mm and 12.7 mm diameter prepared according to ASTM D695 [63], see Figure 4.8. Care was taken in preparing the cylindrical specimen such that the ends are parallel to each other and perpendicular to the axis of the specimen. This will insure that loading will be uniaxial during testing.

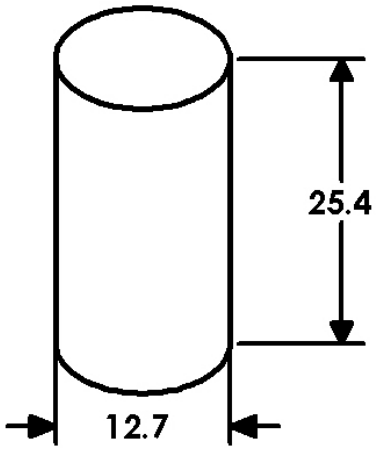

Figure 4.8: Neat resin compression specimen. All dimensions are in mm.

Compression specimens were molded in 12.7 mm internal diameter PVC pipes. The PVC pipes were cut to 25.4 mm lengths, rinsed with water, and dried. The internal surface was coated with Freekote 700 NC release agent to insure the cured resin would release from the pipe. The release agent was applied with a spray bottle then evenly distributed on the internal surfaces of the pipe by passing a pip brush through the PVC pipe several times. Once the release agent was applied, the pipe was closed by gluing a PVC slip cap to one end of the pipe using PVC plastic pipe cement. The pipe was placed vertically in a stand and the adhesive was left to dry for about 20 minutes. Resin was mixed with the hardener and poured into the PVC pipe. The PVC pipe mold arrangement is shown in Figure 4.9.

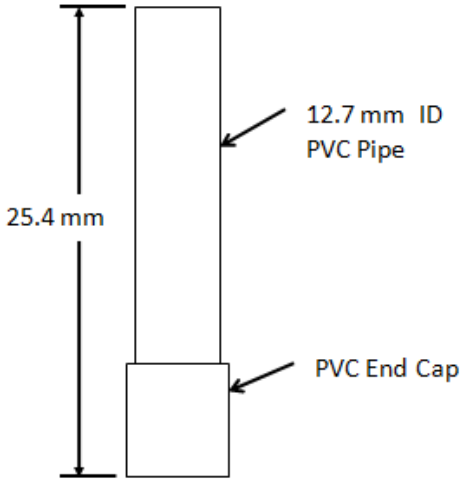

Figure 4.9: PVC pipe compression specimen mold.

To remove the molded resin from the pipe the end cap was cut off. The neat resin slid right out of the pipe. This is probably assisted by the cure shrinkage of the resin. The neat resin cylinder was rough cut to size using a band saw; the finishing cuts were done using a lathe. The finishing cuts on the lathe insure dimensions within ±0.0254 mm and that the end planes of the compression specimen are parallel. A neat resin compression specimen is shown in Figure 4.10. Specimens dimensions indicated in Figure 4.10 are as specified in the ASTM standard D 695 [63].

Figure 4.10: Neat resin compression specimen.

Currently there is no ASTM standard for shear testing of polymers. However, there has been extensive development work on a test method that can determine the shear response. In 1967 Nicolae Iosipescu proposed a double V-notched specimen loaded at four points; see Figure 4.11 for specimen geometry. Much of the work conducted by Nicolae Iosipescu was with metals and has been extended to composites by Adams and Walrath [64]. A comparative analysis of experimental testing and finite element modeling of Iosipescu specimens made of Derakane 470-36 (Dow Chemical) vinyl-ester resin was conducted by Sullivan et al. [68]. Specimens tested in this configuration seemed to fail in a tensile mode starting at the notch root and moving across the gage section at 45° to the shear plane.

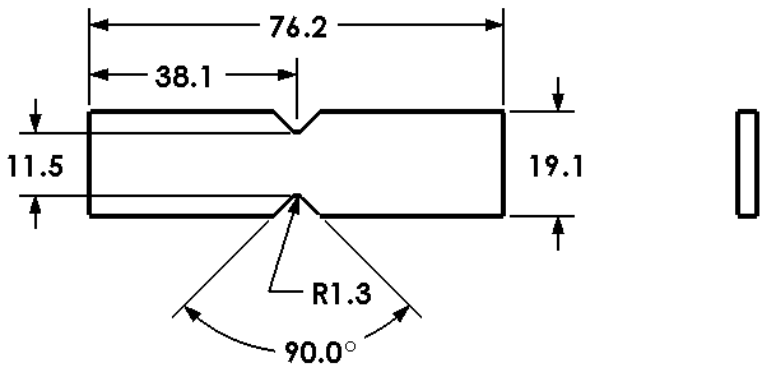

Figure 4.11: Double V-notched specimen dimensions (mm).

The Iosipescu shear specimens were cut to dimensions shown in Figure 4.11 from sheets of neat resin prepared as described in section 4.1.2. A high precision surface grinder was used to insure parallelism of the horizontal edges of the specimens. A surface grinder was used with a specially designed wheel to cut the 90° notch with the

proper radius (r = 1.30 ± 0.3 mm). Specimens were prepared according to standard ASTM D5379 [66].

All neat resin specimens cured at room temperature for 24 hours. After cure specimens were machined to final dimensions followed by a post cure according to the manufacturer's instructions. Vinylester 510A and 8084 were post cured at 120 and 99°C respectively for 2 hours.

4.1.3 Composite Panel and Specimen Preparation

Fiber reinforced composite specimen were prepared using F and G sized carbon fibers with vinylester 510A resin. Dispersion of the resin through the fibers was done by vacuum assisted resin transfer molding (VARTM) [1]. Panels were fabricated utilizing a partition of a 1.2 m by 2.4 m (4' by 8') flat glass table top as the mold surface. Figure 4.12 outlines the VARTM layup setup used during the manufacture of the composite laminates.

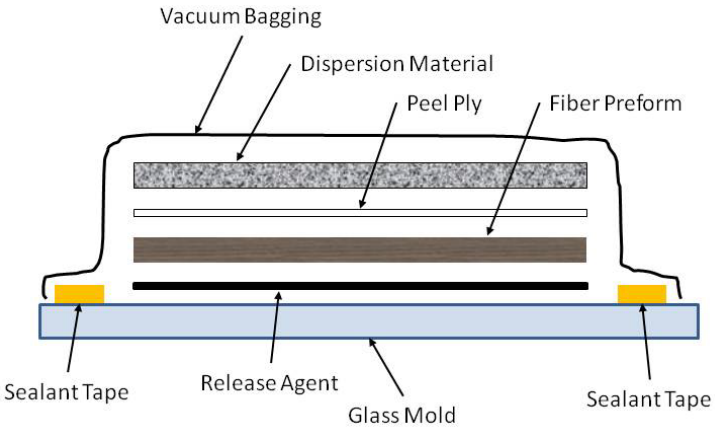

Figure 4.12: Layup configuration for VARTM.

Figure 4.13 shows the VARTM mold assembly. The basic steps for mold preparation are as follows:

i. Large debris was removed from the glass mold surface by razor blades and a final wipe down with acetone to remove any remaining contaminates.

ii. The mold perimeter was outlined with AT-200Y sealant tape courtesy of General Sealants.

iii. The glass surface within the perimeter was coated with a releasing agent, Freekote 700, and left to dry for 20 min.

iv. Fibers were layered in the desired layup orientation.

v. A Nylon non-stick peel ply sheet was laid on top of the fibers.

vi. Dispersion material was placed on top of the nylon sheet.

vii. Vacuum lines were setup around the perimeter of the mold. One 15.9 mm (5/8”) vacuum hose joining the mold and the vacuum and five 9.5 mm (3/8”) hose lines connecting the resin basin to the mold.

viii. The entire mold was sealed with vacuum bagging.

ix. The hoses are clamped closed and a vacuum is drawn to check sealing.

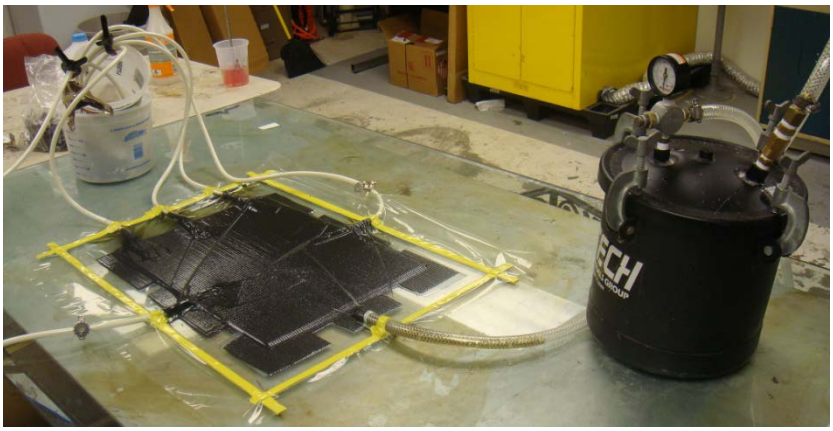

Figure 4.13: VARTM manufacturing configuration.

Laminate orientations are indicated in Table 4.4. Average ply thicknesses were 0.32 and 0.30 mm after cure for C(F)/VE 510A and C(G)/VE 510A, respectively.

Table 4.4: Composite laminate layups.

	Laminate Layup	
Test Specimen Type	C(F)/VE 510A	C(G)/VE 510A
Tensile - Longitudinal	$[0]_3$	Not Tested
Tensile - Off-axis 45°	$[45]_{11}$	$[45]_{11}$
Tensile - Transverse	$[90]_{11}$	$[90]_{11}$
Compression – Cross-ply	$[\bar{0}/90]_{9S}$	$[\bar{0}/90]_{9S}$
Compression - Off-axis 45°	$[45]_{11}$	$[45]_{11}$
Compression - Transverse	$[90]_{11}$	$[90]_{11}$
Iosipescu Shear	$[0]_{12}$	$[0]_{12}$
Short Beam Shear	$[0]_{13}$	$[0]_{11}$

* The over-score for the cross ply indicates the ply about which the laminate is symmetric.

4.1.4 Composite Tensile Test Specimens

Tensile test specimens were prepared according to ASTM D3039 [75]. Unidirectional composite specimens were prepared with 0°, 45°, and 90° ply orientations. Performing tensile tests on 0° and 90° specimens allows determination of Young's moduli of the composite in the 1 and 2 directions along with Poisson's ratio. Off-axis tensile testing is commonly used determine off-axis properties and to verify material properties that have already been determined using tension, compression and shear testing.

Tensile test specimens with 45° and 90° orientations were prepared with 11 plies. Dimensions of the 0° orientation tensile test specimen conform to standard ASTM D3039 [75]; Figure 4.14 (a). Due to a shortage of materials, the 45° and 90° specimens were

smaller than specified in ASTM D3039 [75]; 25 x 175 (mm) i.e. 12.5 x 140 (mm), Figure 4.14 (b). Notice that there is no ASTM standard for the off-axis specimen.

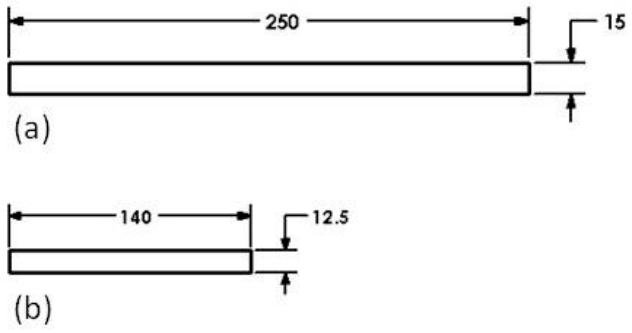

Figure 4.14: Tensile test specimens a) 0°, b) 45° and c) 90°. All dimensions are in mm.

Strain was measured by strain gages. Strain for the 0° specimens was measured in both 1 and 2 directions to determine Poisson's ratio, see Figure 4.15a. Transverse and off-axis unidirectional specimens had strain gages oriented along the loading axis only, see Figure 4.15b and c. 350 Ω strain gages were used.

For tensile testing of composite specimens loaded in the direction of the fiber specimen tabs are commonly used in testing. However, emery cloth can be used in place of tabs. Emery cloth requires less preparation and will not debond from the specimen during loading [67].

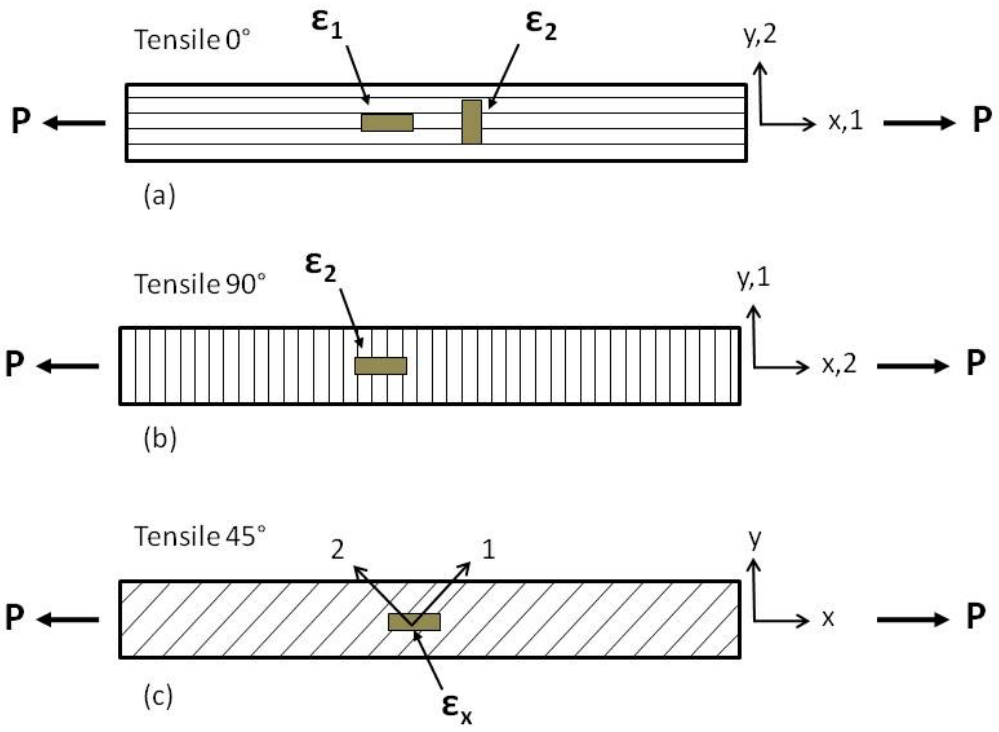

Figure 4.15: Strain gage instrumentation for tensile test specimens a) 0°, b) 90°, c) 45° off-axis.

4.1.5 Compression Test Specimens

The compression test was conducted according to ASTM D6641 [70], to be discussed further in section 4.4. Compressive test specimen dimensions are shown in Figure 4.16. Specimens are 140 mm long and 12 mm wide. The lay-ups were $[\bar{0}/90]_{9s}$, $[45]_{11}$, and $[90°]_{11}$. Specimen with $[\bar{0}/90]_{9s}$ are used to determine compressive strength of the 0° ply using a "backing-out procedure" explained in section 3.2.2.

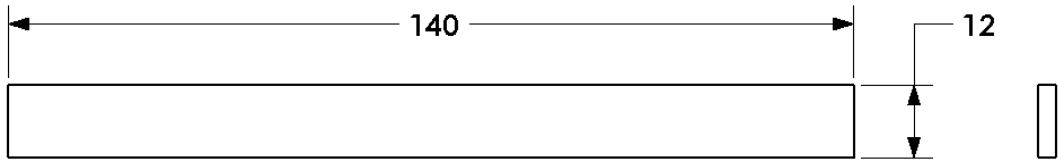

Figure 4.16: Compression test specimen geometry and dimension (mm).

Compression tests often utilize back-to-back strain gages in the test section of the specimen to measure strain and monitor buckling. However, in the present work strain gages were not used due to the short gage section.

4.1.6 Shear Test Specimens

Shear properties of the composite were determined using the previously discussed standard test method, ASTM D5379, also known as Iosipescu [66]. Double V-notched specimens of lay-up $[0]_{12}$ were prepared to dimensions shown in Figure 4.11.

The interlaminar shear strength was determined using the short beam shear test ASTM D2344 [71]. Because the specimens are small there is little room for strain gages. This test allows determination of shear strength only [67]. Span length-to-thickness ratio should be less than 4 to 1 with an overall specimen length-to-thickness ratio of 6 to 1 to achieve shear failure. Minimum thickness of the specimen is 2 mm. Specimen width should be at least twice the specimen thickness. These dimensions have been shown to promote failure at the mid-plane of the specimens which is loaded pure shear. The specimen dimensions are shown in Figure 4.17.

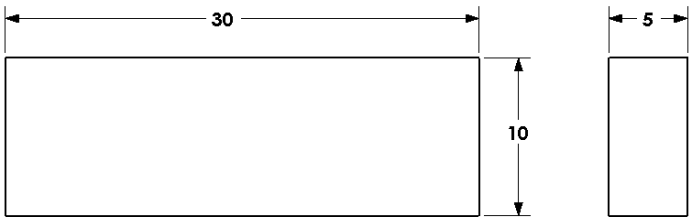

Figure 4.17: Short beam shear specimen dimensions (mm).

4.2 Environmental Exposure

Conditioning of specimens is required prior to testing. Dry specimens were tested shortly after post cure. Specimens exposed to sea water were immersed at 40±1°C controlled by an immersion heater. Sea water was obtained directly from the Atlantic Ocean, changed once a month. Specimens exposed to humidity were placed in an environmental chamber. Humidity and temperature within the chamber were controlled to 85±1% RH and 50±1°C. Specimens were left in environment until no change in weight was recorded. A minimum of five of specimen for each type of resin and composite material were prepared.

Specimens subjected to water and humid environments were periodically monitored for percent weight gain. Moisture content is calculated using Equation (4.1). M_C is the percentage moisture content. W_i is the initial weight of the specimen and W_t is the weight at time t.

$$M_C = \frac{W_t - W_i}{W_i} \times 100 \tag{4.1}$$

4.3 Test Procedure for Matrix Test Specimens

Tensile testing of neat resin specimens was conducted according to ASTM D638 [58]. See section 4.1.2 for specimen preparation and Figure 4.7 for specimen dimensions. Vinylester resins are brittle and for this reason and consistency with the composite tests, the cross head speed was reduced from the ASTM recommendation of 5 to 1 mm/min. An extensometer was used to measure strain in the gage section. Whiteout was applied to prevent the extensometer from slipping along the glossy specimen surface.

Compressive modulus, yield strength, and ultimate strength of the resins were determined according to ASTM D695 [63]. The test specimen, Figure 4.8, was placed between two parallel plates in the test machine. The upper plate was driven towards the stationary bottom plate at a constant displacement rate of 1.3 mm/min. The compression test setup can be seen in Figure 4.18. Due to the short length of the specimen, strain gages were not used. Displacement was measured from the movement of the cross head of the testing machine. The measured deformation was adjusted for compliance of the load cell and testing apparatus during data reduction.

Figure 4.18: Neat resin compression test set-up.

The shear response of the resins were determined using the double V-notched shear test ASTM D5379 [66] shown in Figure 3.1 in section 3.1.3. By this arrangement a pure state of shear is achieved in the gage section of the double V-notched specimen. Strains in the ±45° directions were recorded by strain gages, see Figure 4.19.

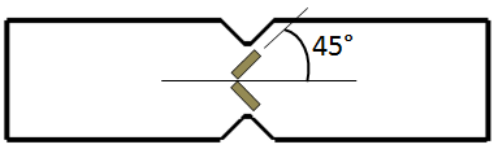

Figure 4.19: Composite V-notched shear specimen and strain gage orientation.

The specimen was loaded at a constant displacement at a rate of 2 mm/min. Table 4.5 summarizes the test program for the neat resin specimens.

Table 4.5: Neat resin specimen test matrix.

	VE 510A			VE 8084		
	Dry	85% RH 50°C	SW 40°C	Dry	85% RH 50°C	SW 40°C
Tensile	5	4	4	5	6	6
Compression	5	7	8	5	7	8
Shear	5	9	8	5	7	7

4.4 Test Procedure for Composite Test Specimens

Tensile testing was conducted in accordance with ASTM 3039 [75]. Specimens were mounted in wedge-action tensile clamps that tighten progressively with applied load. Emory cloth was placed between the specimens and the clamps to protect specimens from localized stress concentrations and damage caused by the surface clamp roughness. Specimens were aligned with the loading axis by an alignment fixture. Specimens were loaded at a constant displacement of 2 mm/min until failure.

Compression testing utilized the CLC fixture shown in Figure 3.4. Load is introduced into the specimen by a combination of end compression and shear. This test method will provide the compressive modulus, ultimate stress, and strain. However, due to the short gage section of the specimen, strain gages were not used and only ultimate stress was determined. Specimens were mounted into the fixture insuring the ends of the specimen are flush with the ends of the fixture. The fixture was loaded in compression at a 2 mm/min cross head rate.

The shear response of composite specimens was measured using the V-notched fixture shown in Figure 3.1 in section 3.1.3. To determine interlaminar shear strength of the composites a short beam shear fixture was used. Figure 4.20 shows the actual fixture used for the short beam shear test. The lower supports of the fixture were spaced to 4 times the thickness of the specimen. The load was applied at a constant displacement rate of 1.0 mm/min.

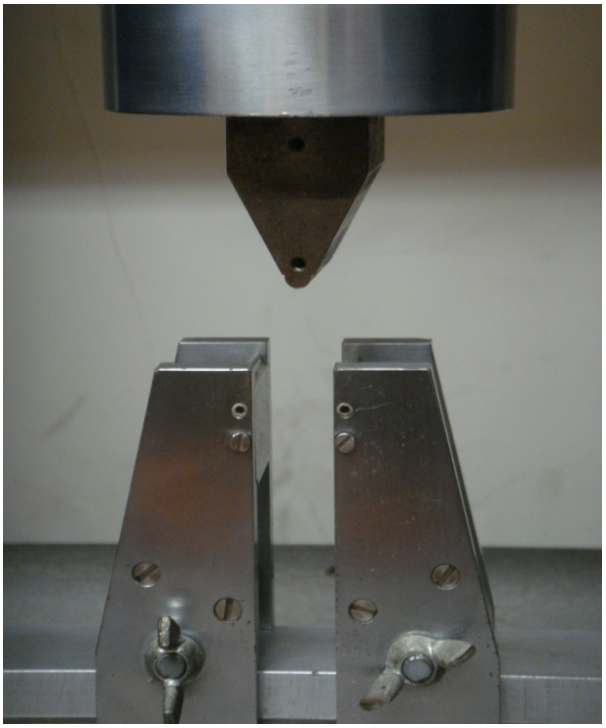

Figure 4.20: Short beam shear test fixture.

Table 4.6 is the test matrix for composite test specimens. Three types of instrumentation were used to measure displacement during testing; strain gages (SG), linear variable displacement transformers (LVDT) and an extensometer (Extens.).

Table 4.6: Test matrix for composite specimens.

	C(F)/VE 510A					C(G)/VE 510A				
	Dry		SW 40°C			Dry		SW 40°C		
	SG	LVDT	SG	LVDT	extens.	SG	LVDT	SG	LVDT	Extens.
Tensile - Longitudinal	2	3	3	4	-	-	-	-	-	-
Tensile - Off-axis 45°	2	5	-	-	9	3	4	-	-	7
Tensile - Transverse	2	3	-	-	8	2	5	-	-	7
Compression - Cross ply	-	7	-	9	-	-	7	-	8	-
Compression - Off-axis 45°	-	6	-	8	-	-	7	-	6	-
Compression - Transverse	-	6	-	9	-	-	6	-	7	-
Iosipescu - Shear	3	2	3	4	-	3	4	3	4	-
Short Beam Shear	-	8	-	9	-	-	8	-	5	-

5 EXPERIMENTAL TEST RESULTS

5.1 Moisture Absorption

Vinylester 510A and 8084 neat resin tension, compression, and Iosipescu specimens of dimensions specified in 4.1.2 were placed in 85% relative humidity at 50°C (85% RH 50°C) and seawater at 40°C (SW 40°C) environments for 92 days. Figures 5.1 through 5.3 show the moisture content (Eq. (4.1)) versus square root of time (days) for the neat resin specimens. The plots show the specimen immersed in sea water reached saturation. However there were problems with the relative humidity cabinet. The relative humidity cabinet intermittently lost power over the period of four weeks causing a reduction in temperature and relative humidity. As a result, specimens lost moisture.

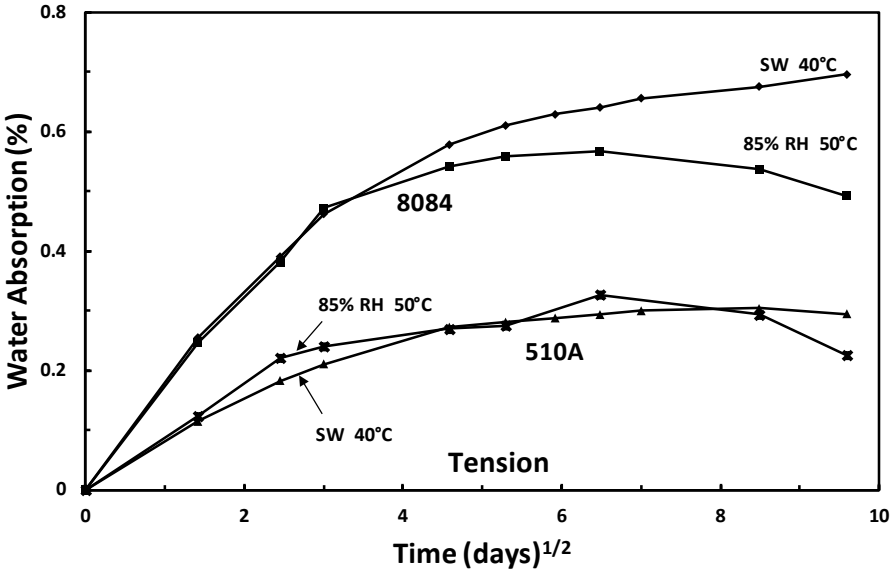

Figure 5.1: Moisture absorption of neat resin tension specimens.

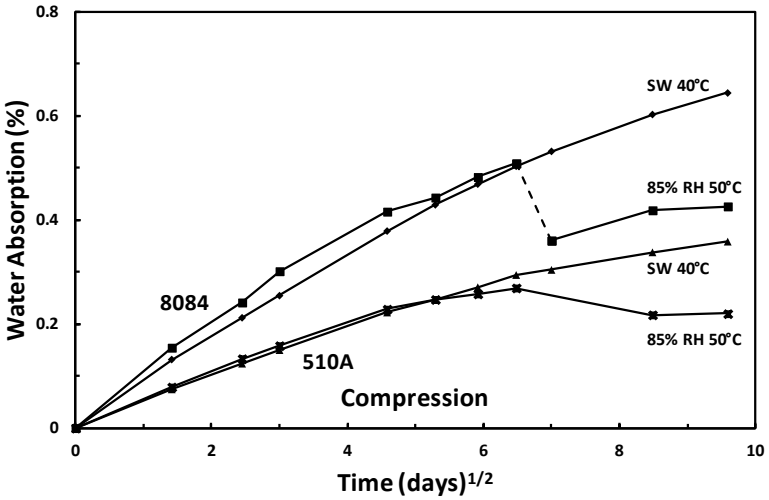

Figure 5.2: Moisture absorption of neat resin compression specimens.

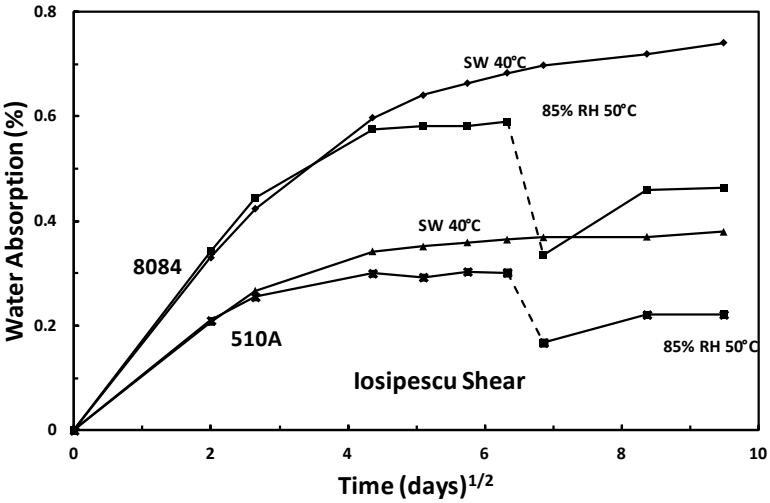

Figure 5.3: Moisture absorption of neat resin Iosipescu specimens.

Moisture contents at saturation of VE 510A and VE 8084 specimens are listed in Tables 5.1 and 5.2. The saturation moisture contents for exposure to 85% RH at 50°C are not reliable due to equipment malfunction. The saturation moisture content for the seawater exposed VE 510A ranges from about 0.30 to 0.38%. The corresponding range for VE 8084 is about 0.65 to 0.74%. The moisture absorption results for VE 8084 match closely with the findings of Ramírez [26]. The results in Tables 5.1 and 5.2 reveal that

VE 8084 absorbs about twice as much seawater as VE 510A. The manufacturer, Ashland, claims that VE 510A is designed to be water resistant. A comparison of the gathered data for the two resins and other resins (e.g. epoxy, polyester, and other vinylesters) [8, 14, 15, 26], supports the claim made by Ashland.

Table 5.1: Moisture content (%) of VE 510A at saturated conditions.

Specimen	RH @ 50°C*	SW @ 40°C
Tension	0.226 ± 0.021	0.295 ± 0.019
Compression	0.220 ± 0.007	0.358 ± 0.006
Iosipescu Shear	0.221 ± 0.019	0.379 ± 0.009

* not accurate due to equipment failure

Table 5.2: Moisture content (%) of VE 8084 at saturated conditions.

Specimen	RH @ 50°C*	SW @ 40°C
Tension	0.492 ± 0.083	0.695 ± 0.018
Compression	0.426 ± 0.006	0.644 ± 0.017
Iosipescu Shear	0.463 ± 0.006	0.741 ± 0.008

* not accurate due to equipment failure

Moisture absorption by carbon/VE 510A composites is considered next. The carbon fibers were G and F sized as explained earlier. Figure 5.4 shows the moisture absorption of C(F)/VE 510A longitudinal tension specimen exposed to sea water at 40°C. Figures 5.5 through 5.11 show moisture absorption for various C(F)/VE510A and C(G)/VE510A composite specimens exposed to seawater at 40°C until saturation. Saturation of moisture content for specimens is indicated by a horizontal asymptote.

Longitudinal, 45° off-axis and transverse tensile specimens (Figures 5.4 through 5.6) and transverse compression, Iosipescu and SBS specimens (Figures 5.9 through 5.11) display such behavior. However, thicker specimens such as cross-ply and 45° off-axis compression specimens require longer immersion periods to reach full saturation, see Figures 5.7 and 5.8.

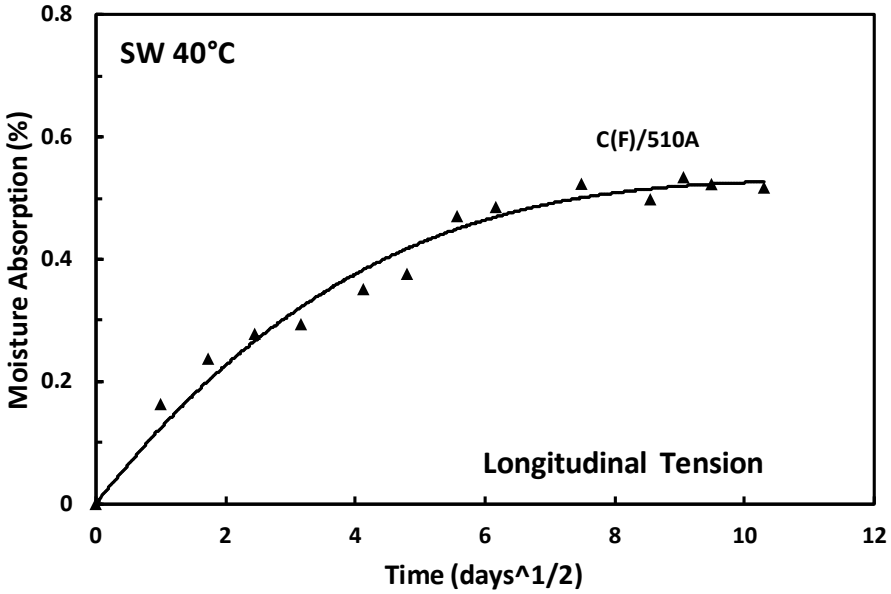

Figure 5.4: Moisture absorption for C(F)/VE 510A longitudinal tension specimens immersed in seawater at 40° C.

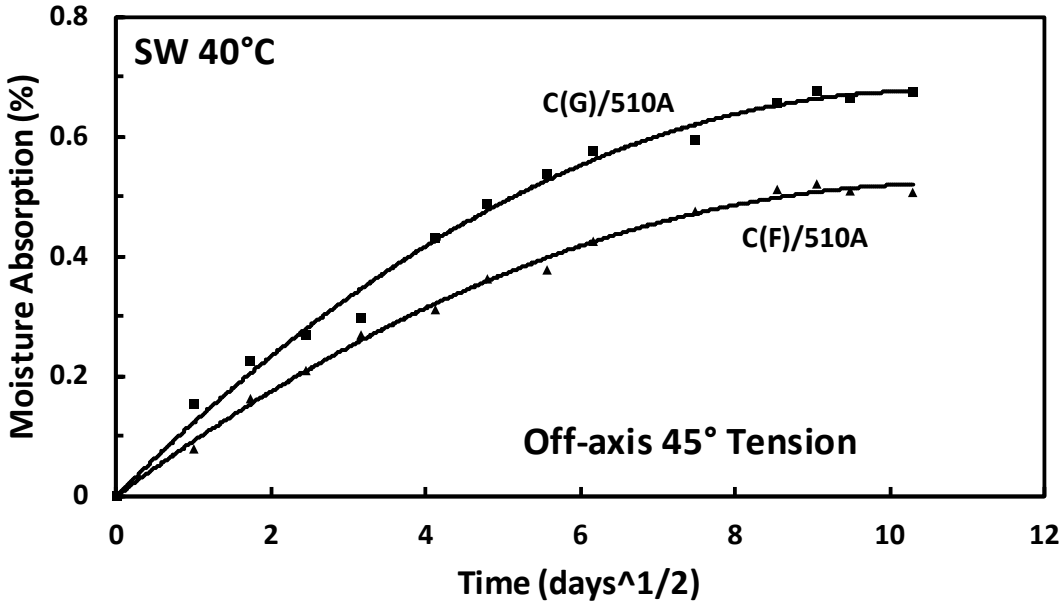

Figure 5.5: Moisture absorption for C(F)/VE 510A and C(G)/VE 510A off-axis 45° tension specimens immersed in seawater at 40° C.

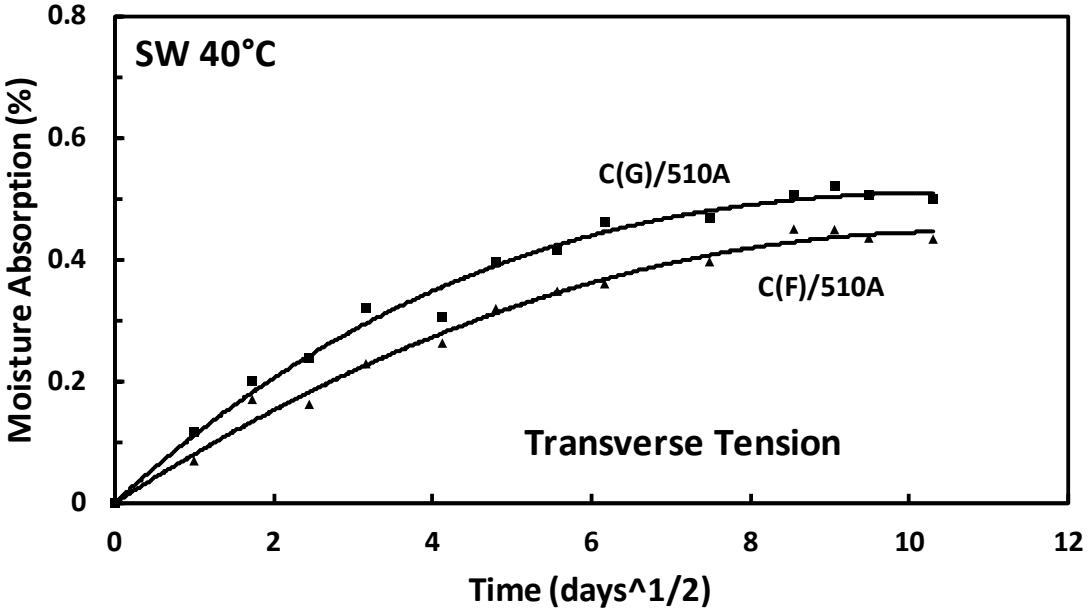

Figure 5.6: Moisture absorption for C(F)/VE 510A and C(G)/VE 510A transverse tension specimens immersed in seawater at 40° C.

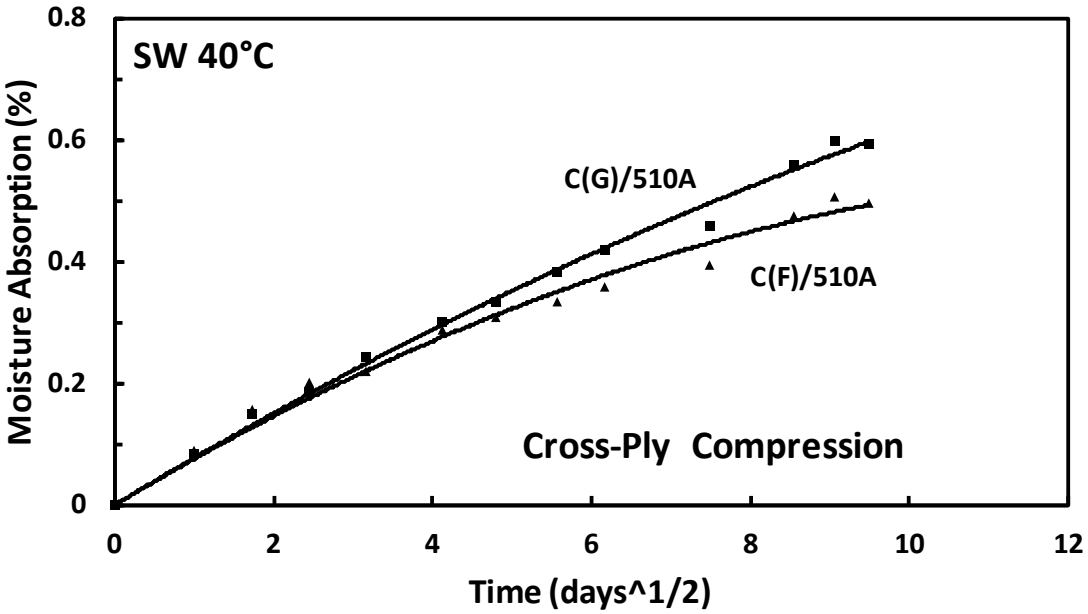

Figure 5.7: Moisture absorption for C(F)/VE 510A and C(G)/VE 510A cross-ply compression specimens immersed in seawater at 40° C.

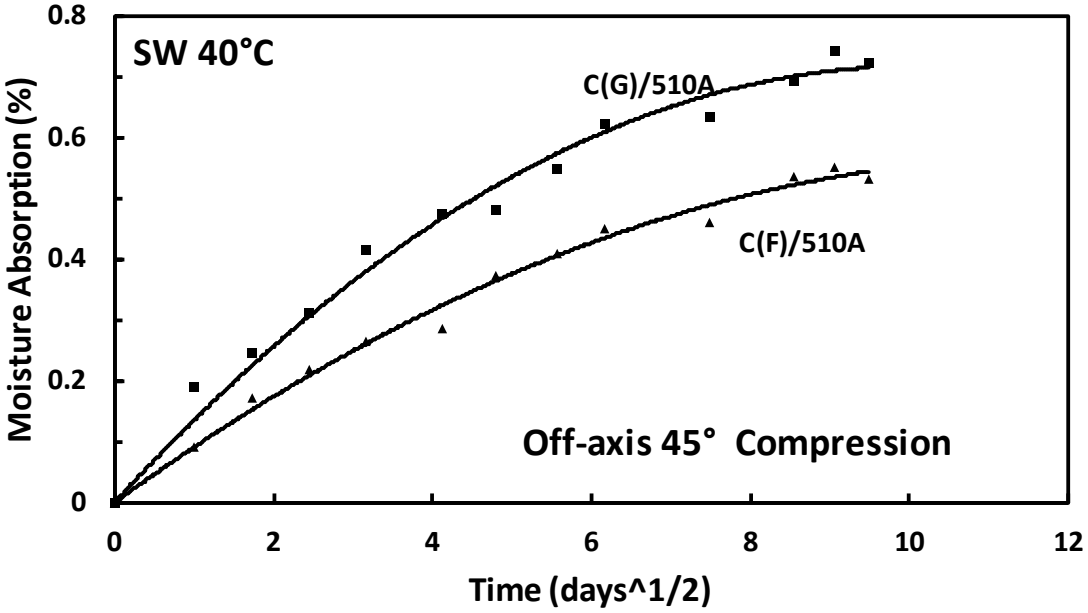

Figure 5.8: Moisture absorption for C(F)/VE 510A and C(G)/VE 510A off-axis 45° compression specimens immersed in seawater at 40° C.

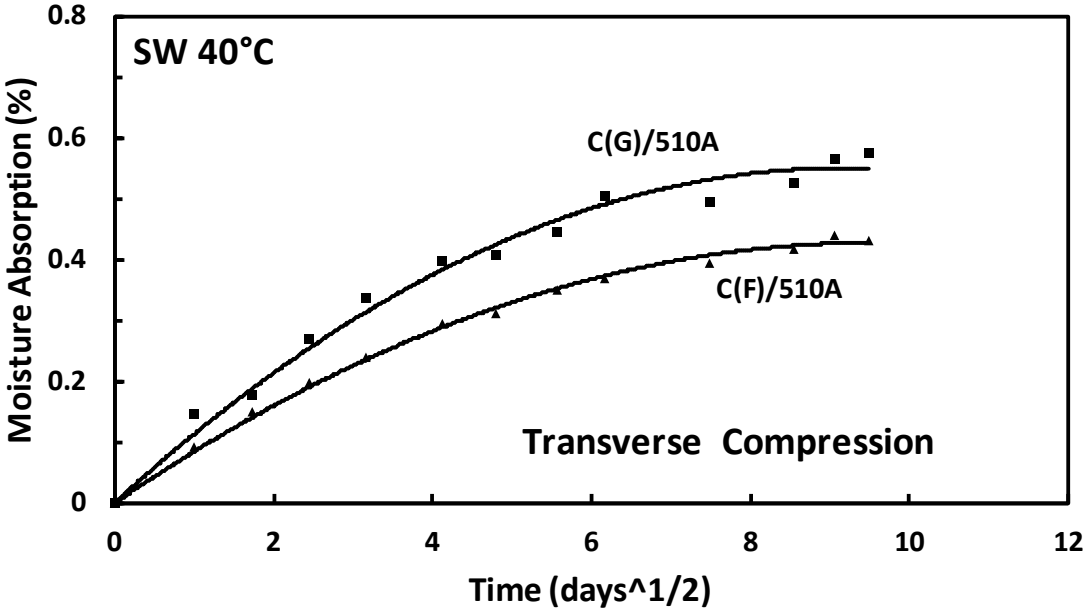

Figure 5.9: Moisture absorption for C(F)/VE 510A and C(G)/VE 510A transverse compression specimens immersed in seawater at 40° C.

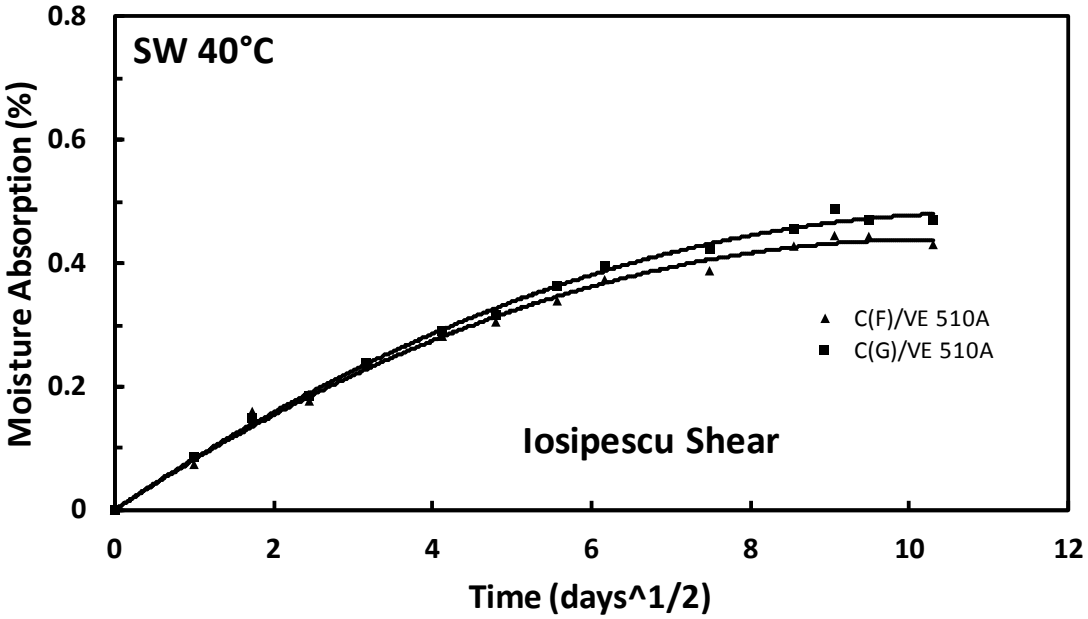

Figure 5.10: Moisture absorption for C(F)/VE 510A and C(G)/VE 510A Iosipescu shear specimens immersed in seawater at 40° C.

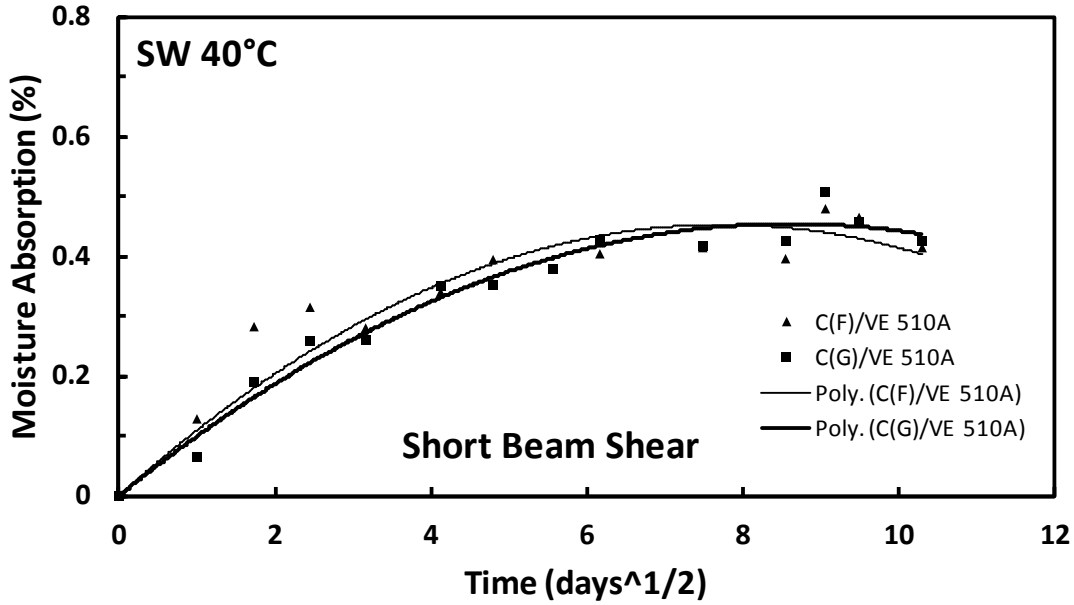

Figure 5.11: Moisture absorption for C(F)/VE 510A and C(G)/VE 510A short beam shear specimens immersed in seawater at 40° C.

Table 5.3 summarizes the saturation moisture contents for C(F)/VE510A and C(G)/VE510A composites after exposure to seawater at 40°C. The C(G)/VE510A specimens consistently absorb more seawater than the corresponding C(F)/VE510A specimens.

The saturation moisture content for each composite system depends slightly on the specimen geometry, and fiber orientation. The thin longitudinal C(F)/VE510A reach very high moisture contents despite minimum area of exposed cut fibers. The small thickness, however, promotes more rapid saturation of the moisture content [24]. The SBS and Iosipescu specimens absorbed somewhat less moisture than the others.

Table 5.3: Moisture contents (%) for C(F)/510A and C(G)/510A exposed to sea water at 40°C.

	C(F)/510A		C(G)/510A	
Specimen	h (mm)	M(%)	h (mm)	M(%)
Longitudinal Tension	1.058	0.517 ± 0.057		N/A
Off-axis 45° Tension	3.642	0.507 ± 0.045	3.226	0.674 ± 0.059
Transverse Tension	4.020	0.434 ± 0.039	3.506	0.499 ± 0.125
Cross-Ply Compression*	5.271	0.496 ± 0.105	4.980	0.594 ± 0.125
Off-axis 45° Compression	3.570	0.532 ± 0.071	3.386	0.723 ± 0.028
Transverse Compression	3.920	0.431 ± 0.039	3.088	0.575 ± 0.059
Iosipescu Shear	4.524	0.431 ± 0.105	3.681	0.470 ± 0.125
Short Beam Shear	4.101	0.415 ± 0.030	3.254	0.425 ± 0.046

* not fully saturated

Moisture contents for the seawater exposed specimens can give an indication of the quality of the fiber/matrix interface bonding. The only difference between any given tensile, compression and shear specimen is the fiber sizing. Specimens with G-sized carbon fibers consistently absorb more seawater than those with F-sizing, see Table 5.3. This is an indication that fiber/matrix interface bonding is better for C(F)/VE510A than for C(G)/VE510A.

As discussed in the introduction, composite materials can absorb moisture by diffusion in the matrix, the fiber and by wicking at the F/M interface. However, carbon fibers do not absorb moisture. This leaves moisture absorption at the matrix and the F/M interface as the only option. Absorption of water at the interface is called “wicking”. Wicking is the phenomenon of moisture transport by capillary action along the fiber/matrix interface due to voids and unbonded regions between the fibers and the matrix. Wicking begins by moisture transport at the exposed end of the fiber and the water moves inward toward the center of the specimen.

An analysis of the moisture absorption, and partitioning of the moisture absorbed into matrix (M_R) and F/M interface contributions ($M_{F/M}$) is presented. The basic analysis is presented in section 2.3. Equations (2.1a) and (2.1b), presented in section 2.3, are employed here,

$$M_R = \frac{\rho_w V_m}{\rho_f V_f + \rho_m V_m} M_m \tag{5.1}$$

$$M_{F/M} = M_c - \frac{\rho_w V_m}{\rho_f V_f + \rho_m V_m} M_m \tag{5.2}$$

where ρ_w, ρ_f and ρ_m are the densities of water, fiber and matrix. The volume fractions for the fiber and matrix are denoted as V_f and V_m. M_c and M_m are the saturation moisture contents for the composite and matrix. Data is listed in Table 5.4.

Table 5.4: Moisture content analysis parameters

	C(F)/VE510A	C(G)/VE510A
Fiber volume fraction V_f	0.66	0.63
Matrix volume fraction V_m	0.34	0.37
Fiber density ρ_f, g/cm^3	1.8	1.8
Matrix density ρ_m, g/cm^3	1.23	1.23
Water density ρ_w, g/cm^3	0.997	0.997
Matrix moisture content M_m, (%)	0.344	0.344

Table 5.5 presents the moisture contents for the two types of composites (M_C) and the moisture content associated with the fiber/matrix interface ($M_{F/M}$). It should be

pointed out that the moisture content of the matrix (M_R) is constant assuming the fiber volume fraction for each type of sizing is constant. Table 5.5 reveals that the absorption by the fiber/matrix interface (wicking) dominates the water uptake. The composite specimens with G-sized fibers display more wicking than those with F-sized fibers. The moisture contents for the composite specimens with F-sized fibers in Table 5.5 agree closely with results reported by Ramirez et al. [18] for similar composites immersed in seawater.

Table 5.5: Moisture content of composite (C) and fiber/matrix (F/M) interface. As reference, the saturation moisture contents for the matrix in C/VE510A are 0.073 and 0.080% for F and G sizings, respectively.

	C(F)/VE510A		C(G)/VE510A	
	C	F/M	C	F/M
Specimen	(%)	(%)	(%)	(%)
Tensile - Longitudinal	0.517	0.445	-	-
Tensile - Off-axis 45°	0.507	0.434	0.674	0.594
Tensile - Transverse	0.434	0.361	0.499	0.419
Compression - Crossply	0.496	0.424	0.594	0.514
Compression - Off-axis 45°	0.532	0.459	0.723	0.643
Compression - Transverse	0.431	0.359	0.575	0.495
Iosipescu	0.431	0.358	0.470	0.390
Short Beam Shear	0.415	0.342	0.425	0.346

Average moisture contents for the neat resin and C(F)/VE510A and C(G)/VE510A composites are shown in Figure 5.12a. Figure 5.12a shows that the composite absorbs more moisture than the neat resin, although the resin content is only about 35%. The excess moisture must be contained at the F/M interface. Figure 5.12b graphically shows the partitioning of the moisture contents of the composite, into

moisture contents of the matrix and F/M interface. Notice the G-sized fibers retain a higher amount of moisture at the interface than the F-sized fibers. This is indicative of a lesser quality fiber/matrix interface.

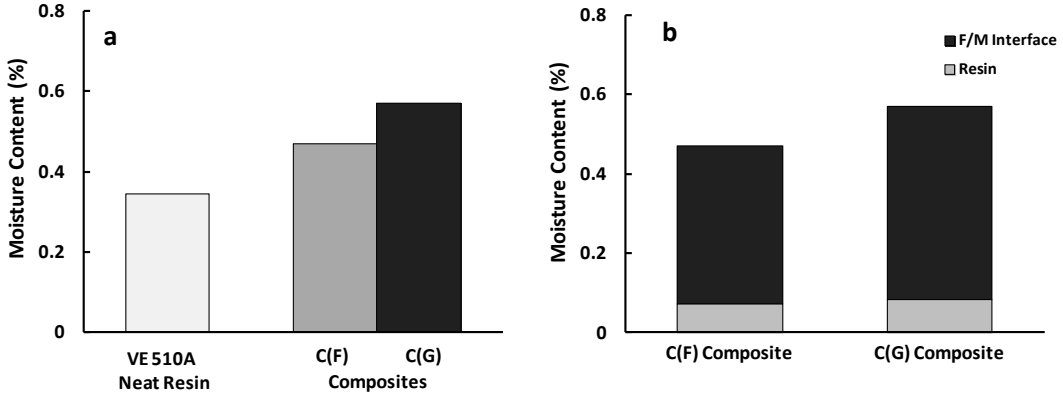

Figure 5.12: Moisture contents for resins and composites. a) neat resin and composite moisture content, b) partition of moisture content into resin and F/M interface.

5.2 Mechanical Test Results for VE 510A and VE 8084 Matrix Materials

Neat resin tensile testing utilized an extensometer to measure strain for all specimens. This test program involved five dry specimens, four specimens conditioned at 85% RH at 50°C and four seawater exposed VE510 specimens. Testing of dry VE8084 included five dry specimens, six specimens conditioned at 85% RH at 50°C and six seawater exposed specimens. Tensile stress-strain curves for all VE 510A and VE 8084 specimens are shown in Figures 5.13 and 5.14. For dry VE 510A, some specimens displayed a nonlinear softening response while others failed shortly after the end of the linear elastic region. Materials that are brittle tend to be susceptible to failure due to imperfections within the material, such as voids, and contaminants, which cause high

stress concentrations. The results for VE8084, shown in Figure 5.14, show that this resin is more ductile than the VE510A resin at dry and water saturated conditions. Ductile materials tend to deform plastically to redistribute high local stresses due to stress concentrations.

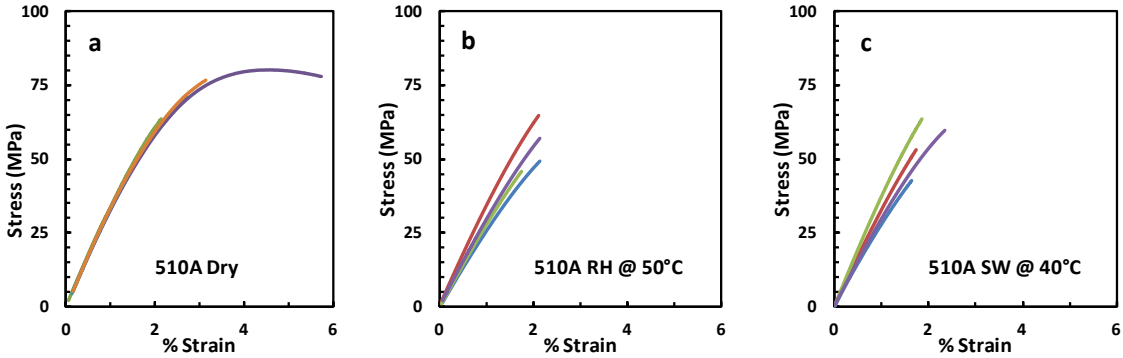

Figure 5.13: Tensile stress-strain curves for VE 510A specimens. a) Dry, b) 85% RH at 50°C and c) SW at 40°C.

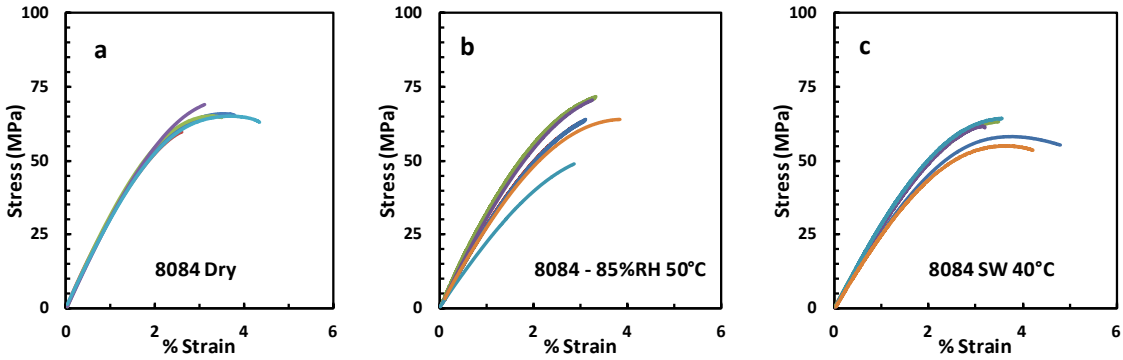

Figure 5.14: Tensile stress-strain curves for VE 8084 specimens. a) Dry, b) 85% RH at 50°C and c) SW at 40°C.

Fracture surfaces were overall planar and perpendicular to the loading axis. Macroscopic inspection of the failure surfaces showed that failure initiated at an imperfection within the resin such as a void, see Figure 5.15.

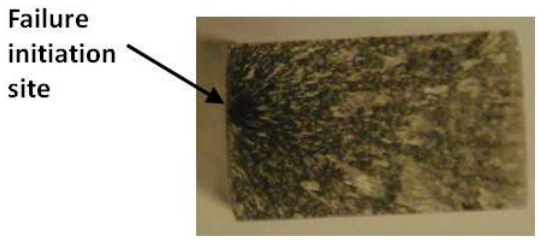

Figure 5.15: Fracture surface of a VE 510A tensile specimen.

Compression testing of neat resin specimen was done without strain gages. Five dry VE 510A specimens, seven specimens conditioned at 85% RH at 50°C and eight seawater exposed VE510A specimens were tested. For VE8084 specimens, five dry, seven specimens conditioned at 85% RH 50°C and eight seawater exposed VE8084 specimens were tested. To determine the actual specimen displacement from the measured cross head displacement, the compliance of the test equipment was measured. The compliance of the MTS 50 universal testing machine was determined by loading the test platens contacting each other to a 20 kN load while monitoring load and displacement. Figure 5.16 shows the resulting load-displacement curve. A 7^{th} order polynomial was used to fit the response curve. Using the curve fit the compliance of the test equipment was removed from the test data at all load levels encountered. In this manner a corrected load-displacement curve for the test specimen was generated, see Figure 5.17.

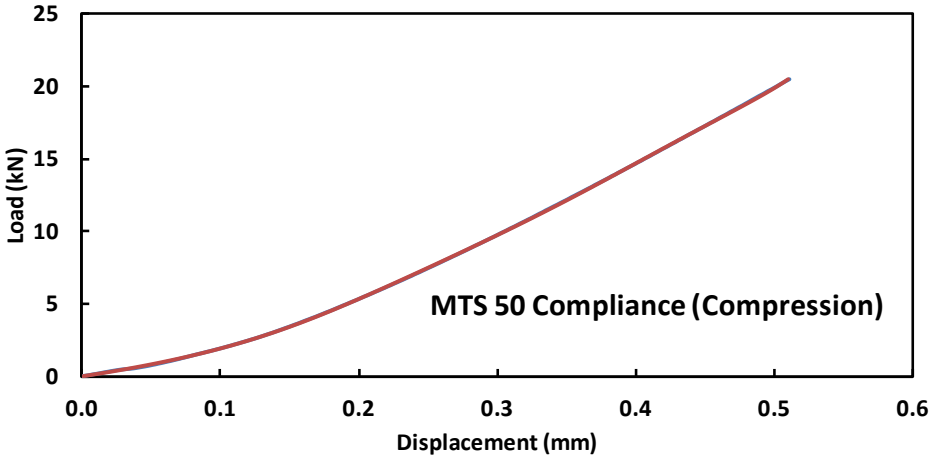

Figure 5.16: Load-displacement curve for determination of machine compliance for MTS 50 test machine.

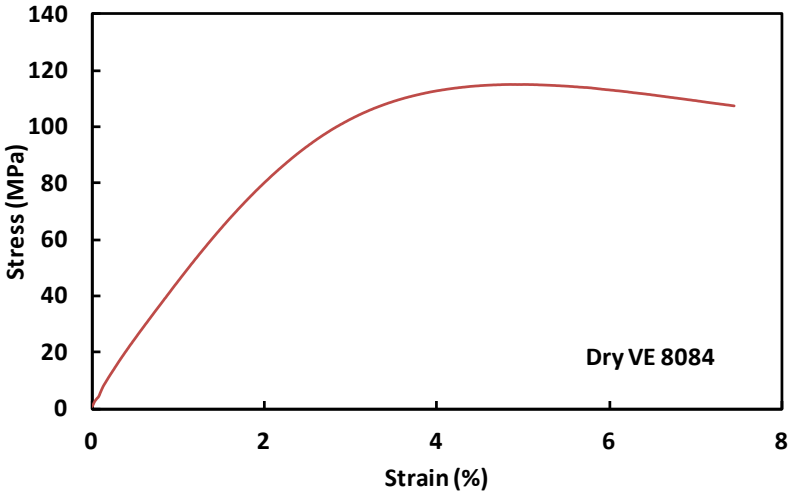

Figure 5.17: Compressive stress-strain curve for dry VE 8084 corrected for the machine compliance.

The compression stress-strain curves for VE 510A and VE 8084 are shown in Figures 5.18 and 5.19. The response curves for both resins are consisitent. For both resins exposure to moisture results in a slight reduction in ultimate strength and increased dispersion of the compressive strength. The compression strength of VE 510A was higher than that of VE 8084 in all environmental exposure conditions.

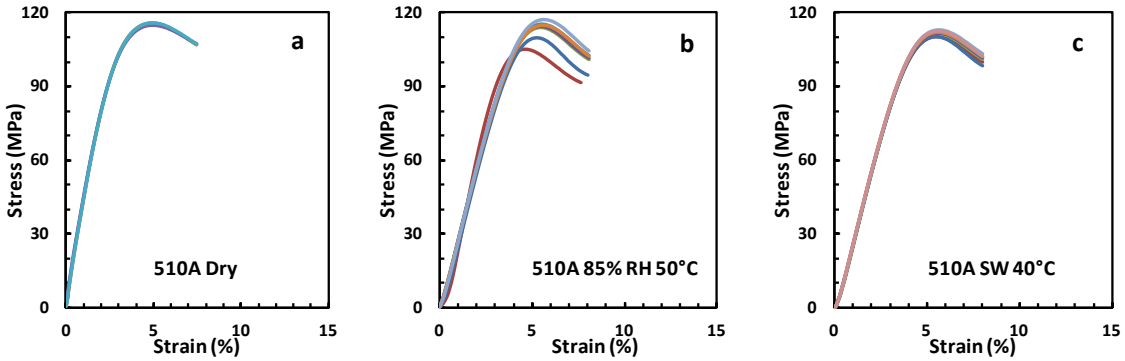

Figure 5.18: Compression stress-strain curves for VE 510A specimens. a) Dry, b) 85% RH at 50°C and c) SW at 40°C.

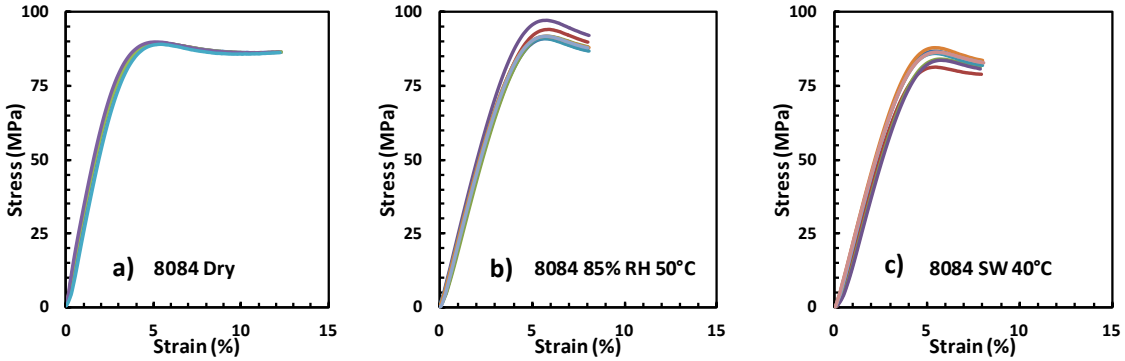

Figure 5.19: Compression stress-strain curves for VE 8084 specimens. a) Dry, b) 85% RH at 50°C and c) SW at 40°C.

The compressive specimens did not fail catastrophically. Rather, the specimens failed in a ductile manner; exhibiting substantial axial deformation while expanding radially. The largest radial expansion was at the mid-section of the specimens, see Figure 5.20. Because of lack of abrupt failure of the specimens, testing was stopped at 8% strain; suffciently after reaching the ultimate strength of the specimen.

Figure 5.20: Failed VE 510A compression specimen (85% RH at 50°C).

Neat VE510A resin shear testing involved five dry Iosipescu specimens, nine specimens conditioned at 85% RH at 50°C and eight seawater exposed specimens. For VE8084, five dry specimens, seven specimens conditioned at 85% RH at 50°C and seven seawater exposed specimens were tested. Three specimens for each environmental condition were instrumented with strain gages to determine strain. Shear stress-strain curves for the neat resin Iosipescu specimens are shown in Figures 5.21 and 5.22. The response at dry conditions is overall very brittle and scattered. The ductility and shear strength of the resins increase quite remarkably after exposure to moisture. It should be recalled that the specimens exposed to 85% RH at 50°C were partially dried due to malfunction of the humidity cabinet, and the results may not be reliable.

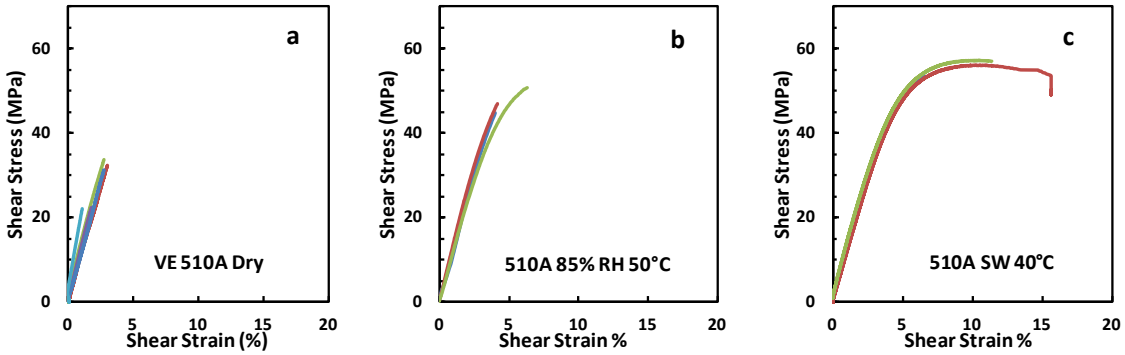

Figure 5.21: Iosipescu shear stress-strain curves for VE 510A specimens. a) Dry, b) 85% RH at 50°C and c) SW at 40°C.

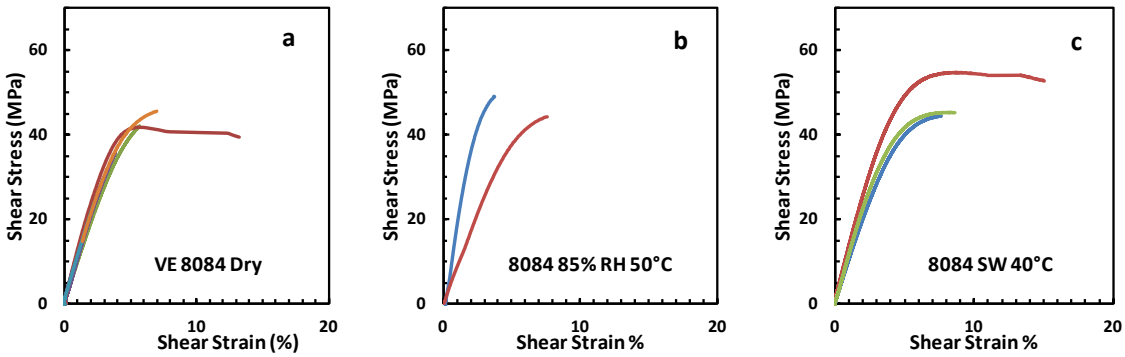

Figure 5.22: Iosipescu shear stress-strain curves for VE 8084 specimens. a) Dry, b) 85% RH at 50°C and c) SW at 40°C.

Inspection of the Iosipescu shear specimens during and after testing showed that specimens fractured abruptly. Figure 5.23 shows a failed Iosipescu shear specimen. Failure initiated at the notch root, as the result of a stress concentration. Furthermore, failure occurs in planes oriented approximately 45° to the pure shear planes, which indicates resolved tensile failure. Failure modes observed in the present work are similar to those observed in Derakane 470-30 vinylester Iosipescu specimens by Sullivan et al. [68].

Figure 5.23: Failed VE 510A Iosipescu shear specimen.

The mechanical properties determined from the experimental stress-strain curves for VE 510A are summarized in Table 5.6. The results show that the tensile and compressive properties such as moduli (E^T and E^C) are different, but the difference could be due to the different test geometries and test method. The moduli (E) and ultimate tensile strengths (σ^T_{ult}) of this resin tend to decrease after environmental exposure. Compressive yield and ultimate strengths (σ^C_y and σ^C_{ult}) are quite unaffected by exposure to moisture. The shear modulus (G) decreased slightly after moisture absorption; while the shear strength (τ_{ult}) increased. Seawater and humidity exposures influence the properties similarly, except for the tensile failure strain. The large scatter of this property, however, makes a comparison difficult.

Table 5.6: Mechanical properties of VE 510A.

	RT dry	RH @ 50°C*	SW @ 40°C
E^T, GPa	3.31 ± 0.04	2.88 ± 0.41	3.14 ± 0.52
σ^T_{ult}, MPa	70.3 ± 8.7	54.2 ± 8.5	54.8 ± 9.0
ε^T_{ult}, %	3.36 ± 2.0	2.03 ± 0.20	1.08 ± 0.75
E^C, GPa	4.02 ± 0.02	2.45 ± 0.03	2.39 ± 0.02
σ^C_y, MPa	92.1 ± 3.6	112 ± 2	110 ± 1
σ^C_{ult}, MPa	116 ± 1	114 ± 2	112 ± 1
G, GPa	1.31 ± 0.29	1.24 ± 0.09	1.25 ± 0.11
τ_{ult}, MPa	28.4 ± 5.7	48.9 ± 7.6	56.4 ± 1.2

* Results may not be reliable due to malfunction of the humidity chamber.

A summary of the mechanical properties of VE 8084 is provided in Table 5.7. The tensile and compressive moduli (E^T and E^C) and ultimate tensile strengths (σ^T_{ult}) tend to decrease after environmental exposure. Compressive yield and ultimate strengths (σ^C_y and σ^C_{ult}) were not substantially affected by moisture. This was also the case for the shear modulus. The shear strength increased after exposure to moisture.

Table 5.7: Mechanical properties of VE 8084.

	RT dry	RH @ 50°C*	SW @ 40°C
E^T, GPa	2.99 ± 0.07	2.71 ± 0.41	2.44 ± 0.25
σ^T_{ult}, MPa	65.0 ± 3.3	63.6 ± 9.1	60.9 ± 3.6
ε^T_{ult}, %	3.47 ± 0.67	3.11 ± 0.18	3.95 ± 0.59
E^C, GPa	3.00 ± 0.05	2.24 ± 0.03	2.15 ± 0.13
σ^C_y, MPa	68.2 ± 6.7	77.1 ± 6.7	73.3 ± 2.0
σ^C_{ult}, MPa	89.6 ± 0.4	92.8 ± 2.3	85.4 ± 2.2
G, GPa	1.08 ± 0.11	1.17 ± 0.48	1.17 ± 0.14
τ_{ult}, MPa	36.8 ± 8.1	48.9 ± 3.6	53.2 ± 7.2

* Results may not be reliable due to malfunction of the humidity chamber.

5.3 Test Results for C(F)/VE 510A and C(G)/VE 510 Composites

As pointed out earlier, only C(F) and C(G) fibers were combined with the VE510A resin were tested. For longitudinal tensile testing only C(F)/VE510A specimens were tested. The longitudinal stiffness and strength are dominated by the fibers and depend less on the matrix and fiber/matrix interface. At dry conditions two replicate strain gaged specimens were tested to determine modulus and Poisson's ratio. A total of

five specimens were tested for determination of longitudinal strength. Similarly for the seawater condition there was a total of seven specimens tested, three with strain gages.

Stress-strain curves for two dry and three seawater exposed C(F)/VE 510A composite specimens are shown in Figure 5.24. The discontinuities in the curves are indicative of non-catastrophic fiber breakages, and longitudinal splitting of the specimens parallel to the fibers. Herakovich [46] describes this splitting as a result of transverse tensile loading of the specimen induced by the Poisson shrinkage and end constraints. This type of failure mechanism is very common in tensile loading of highly orthotropic materials such as unidirectional [0°] composites. Partial failures resulted in emission of a sound similar to a vibrating string, such behaviors were also observed by Madhukar and Drzal [35]. The data of specimens displaying substantial damage prior to ultimate failure was not used to determine strength. However, the evaluation of modulus and Poisson's ratio at small strains is not affected by such damage. Propagation of spitting/cracking due to end constraints can be reduced by using cross-ply laminate test specimens [76].

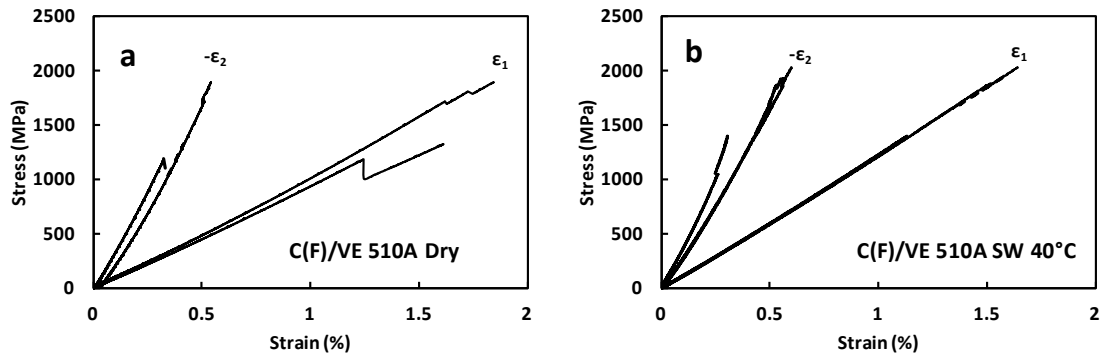

Figure 5.24: Tensile stress-strain curves for longitudinal C(F)/VE 510A specimens. a) Dry, b) SW 40°C.

The longitudinal tensile mechanical properties of C(F)/VE 510A are listed in Table 5.8. The data indicated no change in modulus, Poisson's ratio and strength after exposure to seawater. Thus, exposure to seawater has minor effect on the longitudinal properties of this composite, which confirms that the longitudinal properties are dominated by the properties of the fibers.

Table 5.8: Tensile properties of longitudinal C(F)/VE510 specimens.

	Dry		SW 40°C	
Property	avg.	Std	avg.	Std
Tensile Modulus E_1, GPa	120	± 7.4	124	± 0.3
Tensile Strength X^T_1, MPa	1910	± 159	1940	± 104
Poisson's ratio ν_{12}	0.37	± 0.07	0.37	± 0.04

For 45° off-axis tensile testing of dry C(F)/VE 510A two specimens were tested with strain gages and five with a LVDT. Similarly three dry C(G)/VE 510A specimens were tested with strain gages and four with a LVDT. All seawater exposed specimens were tested with an extensometer. Stress-strain curves determined for the off-axis 45° specimens are shown in Figures 5.25 and 5.26. The curves display no drastic change after seawater exposure. The 45° off-axis specimens failed in a brittle manner within the gage section of the specimens. The failure plane was 45° off of the loading axis in line with the fibers, see Figure 5.27. This is evidence for matrix failure since the carbon fibers remained intact. Complete separation of the specimen was prevented by carbon fibers that bridged both ends of the failed specimen, see Figure 5.27. Hart-Smith [76] describes a "fuzzy" fracture surface as a result of fiber misorientation and can occur even at slight misalignments. Prepreg tape unidirectional composites tend to have the fibers

highly collimated and fail cleaner during transverse and off-axis tensile loading than VARTM laminates [46].

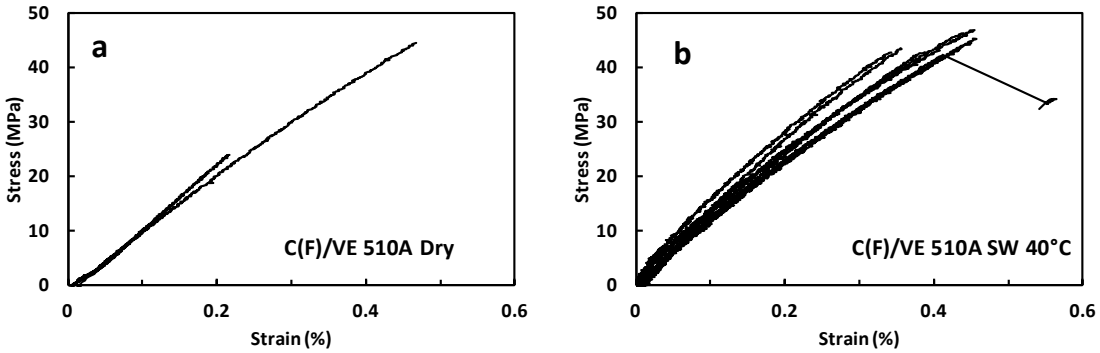

Figure 5.25: Tensile stress-strain curves for off-axis 45° C(F)/VE 510A specimens. a) Dry, b) SW 40°C.

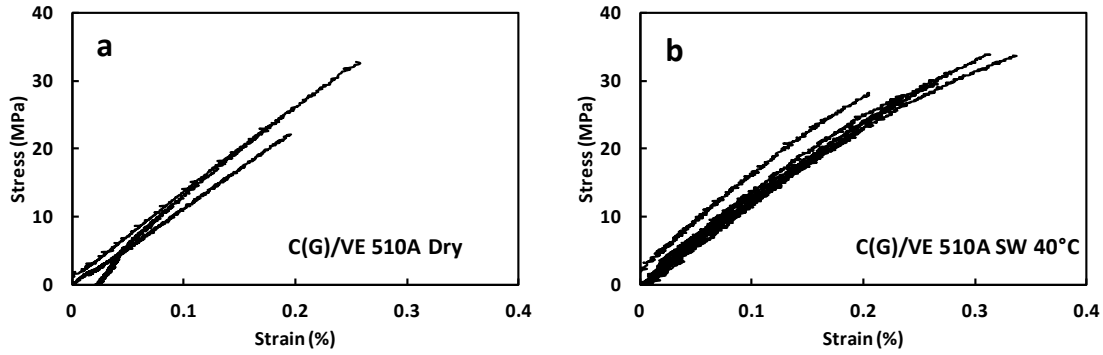

Figure 5.26: Tensile stress-strain curves for 45° off-axis C(G)/VE 510A specimens. a) Dry, b) SW 40°C.

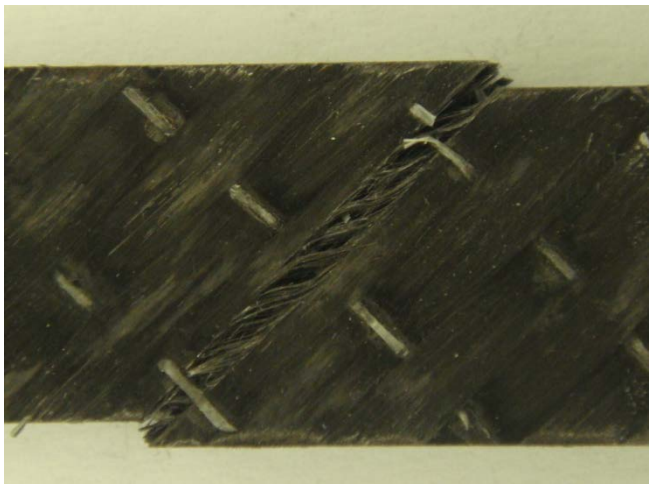

Figure 5.27: Tension failure mode observed for 45° off-axis C(F)/VE510A specimens.

Table 5.9 summarizes modulus and strength for the 45° off-axis specimens with F and G sized fibers. The C(F)/VE510A specimens are stronger than the C(G)/VE510A specimens. 45° off-axis tensile failure is attributed to tensile/shear debonding at the fiber/matrix interface. This suggests that the interface strength is greater for C(F)/E510A than C(G)/VE510A. The modulus is not very much affected by the type of fiber sizing and exposure to seawater. Seawater exposure has little effect on strength of off-axis specimens with F-sized fibers. However, there seems to be a strengthening effect due to moisture absorption for the off-axis specimens with G-sized fibers. Because of the scatter in strength, however, this effect may not be significant.

Table 5.9: Mechanical properties of 45° off-axis C(F)/VE 510A and C(G)/VE 510A tensile specimens.

	C (F)/VE 510A				C (G)/VE 510A			
	Dry		SW 40°C		Dry		SW 40°C	
Property	avg.	Std	avg.	Std	avg.	std	avg.	std
Tensile Modulus, GPa	11.1	± 1.4	10.6	± 1.1	12.7	± 1.0	11.3	± 0.6
Tensile Strength, MPa	41.3	± 4.7	41.2	± 2.0	25.3	± 5.0	30.8	± 2.6

Tensile testing of transverse (90°) specimens utilized two strain gaged specimens from each composite system while all seawater exposed specimens were tested with an extensometer. A total of 5 dry and 7 seawater at 40°C specimens were tested for C(F)/VE510A and 7 dry and 7 seawater at 40°C specimens for C(G)/VE510A. Stress-strain curves for transverse tensile specimens are shown in Figures 5.35 and 5.36. The linear response and sharp load drop at failure are evidence for a brittle failure behavior.

Failure occurred in the gage section parallel to the fibers. This is a sign of matrix failure and possibly fiber/matrix interface failure since the fibers remained intact. Similar to the off-axis specimens there were only partial separation of the failed specimens. Complete separation was prevented by fibers that bridged the failure plane, similar to the 45° off-axis specimen shown in Figure 5.27.

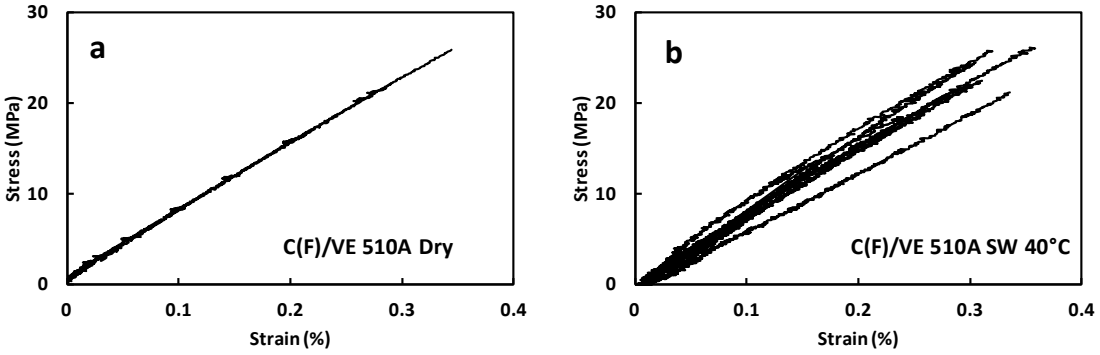

Figure 5.28: Tensile stress-strain curves for transverse C(F)/VE 510A specimens. a) Dry, b) SW 40°C.

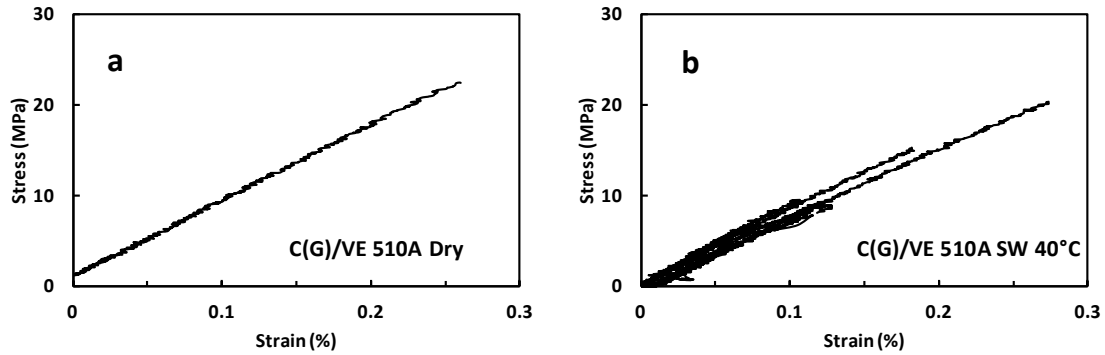

Figure 5.29: Tensile stress-strain curves for transverse C(G)/VE 510A specimens. a) Dry, b) SW 40°C.

Transverse tensile mechanical properties are listed in Table 5.10. The modulus is very little affected by the carbon fiber surface sizing and water exposure. The transverse tensile strengths of the composites depends on the type of fiber sizing but less on water absorption. The transverse strengths of the C(F)/VE510A and C(G)/VE510A composites are very different. C(F)/VE 510A is approximately twice as strong as C(G)/VE 510A. The transverse tensile strength is highly dominated by the fiber/matrix interface. The higher strength of the F-size fiber composite is attributed to better fiber/matrix adhesion.

Table 5.10: Tensile properties of transverse C(F)/VE 510A and C(G)/VE 510A specimens.

	C (F)/VE 510A				C (G)/VE 510A			
	Dry		SW 40°C		Dry		SW 40°C	
Property	avg.	Std	avg.	Std	avg.	std	avg.	std
Tensile Modulus E_2, GPa	7.49	± 0.02	7.69	± 0.67	8.54	± -	8.27	± 0.38
Tensile Strength X^T_2, MPa	24.5	± 2.0	23.0	± 2.5	12.8	± 4.0	11.8	± 5.0

Compression testing utilized cross-ply specimens without strain gages. Displacement of the cross-head was measured with a LVDT. Figure 5.30 shows an

example of a stress versus cross head displacement plot for a dry C(F)/VE 510A specimen. The saw tooth ridges in the stress versus displacements plots indicate end failure of the specimen or slipping within the CLC fixture. The compressive strength was determined as maximum stress encountered.

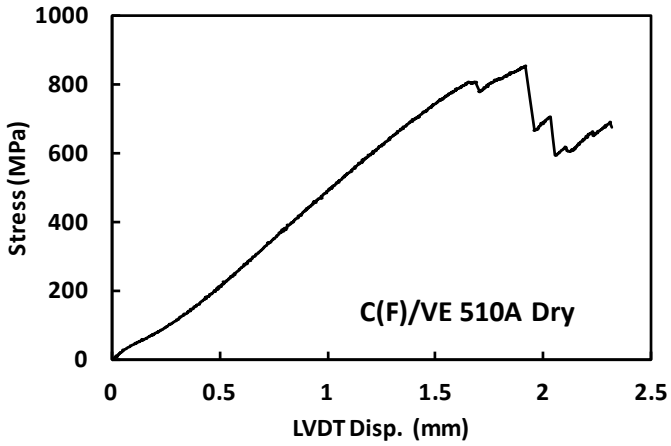

Figure 5.30: Compressive stress–displacement curves for a dry C(F)/VE 510A cross-ply specimen.

The compression specimens failed violently by axial splitting in the gage section, see Figure 5.31a. Some specimens failed both at one end and in the gage section, see Figure 5.31. Per ASTM standard D6641 [70] the results are still valid if the final failure of the specimen occurs within the gage section. Only the results for specimens that failed within the gage section in axial splitting were used to determine strength.

Figure 5.31: Failure modes of cross-ply compression specimens. a) axial splitting b) end failure.

The back-out factor approach discussed in section 3.2.2 is applied to determine the longitudinal compressive strength ($X^C{}_1$) from the compressive strength (X_C) of a cross-ply laminates. The back-out factor, BF, is defined by,

$$X_1^C = BFX_C \tag{5.3}$$

where X_C is the measured strength of the cross-ply laminate and X_1^C is the (backed-out) unidirectional longitudinal compression strength. The following expression for BF is derived in section 3.2.2,

$$BF = \frac{(Q_{11}A_{22} - Q_{12}A_{12})\mathrm{h}}{A_{11}A_{22} - A_{12}^2} \tag{5.4}$$

where Q_{ij} are the reduced stiffness elements for the plies, and A_{ij} are elements of the extensional stiffness matrix for the laminate, both defined in section 3.2.2.

Measured compression strengths, X_C, back-out factors and X_1^C for the C(F)/VE 510A and C(G)/VE 510A cross-ply specimens are listed in Table 5.11. At dry conditions, the C(F)/VE 510A specimens exhibit 22% higher compression strength (X_1^C) than C(G)/VE510A. As mentioned previously, the only difference between the two composite systems is the fiber sizing. The improved adhesion between fiber and matrix provided by the F-sizing evidently leads to higher compressive strength. This agrees with the findings of Madhukar and Drzal [36]. They found that compressive strength is improved with increased fiber/matrix interface strength.

Table 5.11: Compression strength (X^C_1) of C(F)/VE 510A and C(G)/VE 510A.

	C (F)/VE 510A				C (G)/VE 510A			
	Dry		SW 40°C		Dry		SW 40°C	
Property	avg.	Std	avg.	Std	avg.	std	avg.	std
Cross-ply Comp. Strength X_C, MPa	439	± 38	432	± 41	368	± 39	355	± 25
Longitudinal Comp. Strength X^C_1, MPa	787	± 69	773	± 73	644	± 69	622	± 44
Back-out factor	1.791		1.791		1.752		1.752	

The influence of environmental exposure on the compressive strength of these composites is minor. After exposure to seawater, the C(F)/VE 510A and C(G)/VE 510A experienced only 2 and 4% reductions in average strength values, both being within the scatter range.

The 45° off-axis compression testing utilized specimen without strain gages. An LVDT was used to monitor cross-head displacement. This test program involved six dry and eight seawater exposed C(F)/VE510 specimens and seven dry and six seawater exposed C(G)/VE510A specimens. Compressive stress-displacement curves for the 45° off-axis specimens tested under dry and moisture saturated conditions are shown in

Figures 5.32 and 5.33. The stress-displacement curves show that the specimens reach maximum stress asymptotically but fail suddenly. The displacement reading includes deformation of the load cell and possible slipping of the specimen within the grips. Hence only the compressive strength was determined from this testing. Examination of the stress-displacement curves reveals that the specimens with F-sized fibers endured larger axial deformations than those with the G-sized fibers at both dry and water saturated conditions.

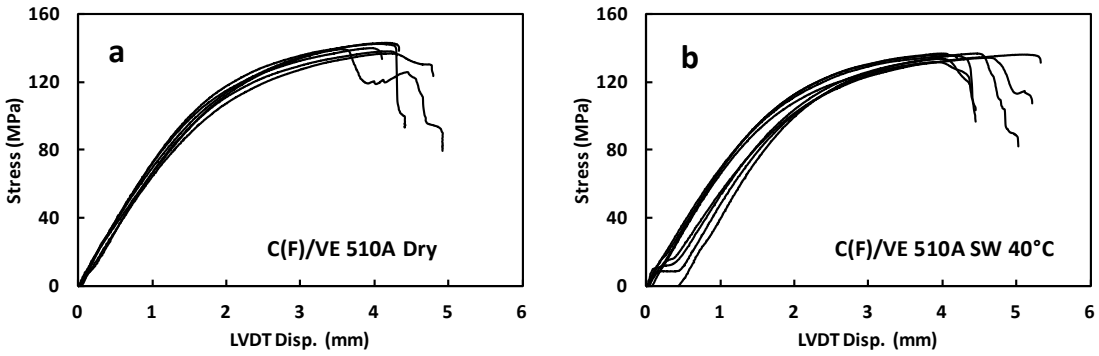

Figure 5.32: Compressive stress vs. displacement curves for 45° off-axis C(F)/VE 510A specimens. a) Dry, b) SW 40°C.

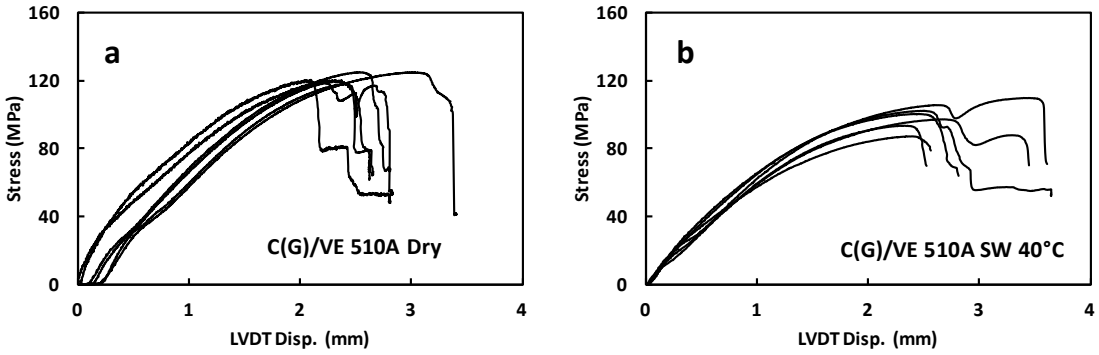

Figure 5.33: Compressive stress vs. displacement curves for 45°off-axis C(G)/VE 510A specimens. a) Dry b) SW 40°C.

The 45° off-axis compression specimens failed catastrophically within the gage section of the specimen. Figure 5.34 shows typical failed sea water exposed off-axis C(F)/VE 510A and C(G)/VE 510A specimens. Dry specimens failed similarly. Specimens tended to fail in planes 45° to the specimens axis, i.e. parallel to the fibers, Figure 5.34a. The failure plane was "wedge-shaped", with a wedge angle approximately 20-45° off the 1-2 plane, intersecting at the mid-plane of the specimen, see Figure 5.34b. The inclined failure plane indicates a resolved shear failure mechanism.

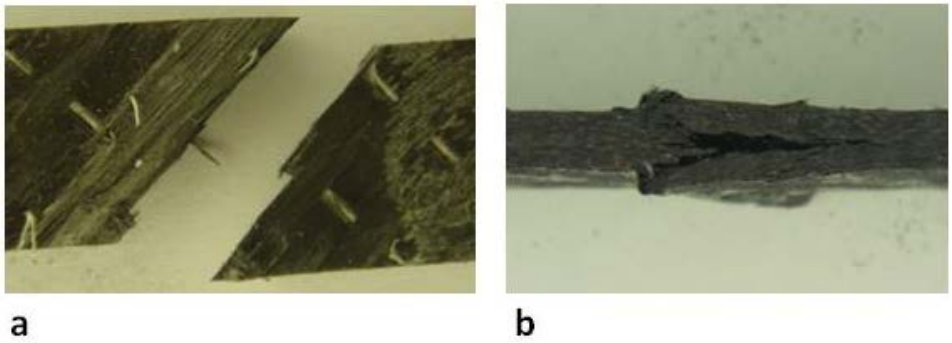

Figure 5.34: Failed compressive off-axis specimens. a) C(G)/VE 510A, b) C(F)/VE 510A (both exposed to SW/40°C).

Compression strengths of the 45° off-axis specimens are listed in Table 5.12. A comparison of the dry strengths of C(F)/VE 510A and C(G)/VE 510A reveals that the F sizing results in higher compressive strength both at dry and water saturated conditions. This suggests that off-axis compressive strength is dominated by the fiber/matrix interface strength.

Table 5.12: Off-axis compression strengths for C(F)/VE 510A and C(G)/VE 510A.

	C (F)/VE 510A				C (G)/VE 510A			
	Dry		SW 40°C		Dry		SW 40°C	
Property	avg.	Std	avg.	Std	avg.	std	avg.	std
Comp. Strength Off-axis 45°, MPa	140 ± 3		135 ± 2		122 ± 3		98 ± 8	

For the C(F)/VE 510A composite, moisture absorption has a small effect on the off-axis compression strength. For C(G)/VE 510A, however, moisture absorption results in a substantial reduction (20%) of the compressive strength. This suggests that the G-sized fiber/matrix interface is more susceptible to degradation by exposure to moisture.

The transverse compression testing utilized specimen without strain gages. An LVDT was used to monitor cross-head displacement. This test program involved six dry and nine seawater exposed C(F)/VE510 specimens and six dry and seven seawater exposed C(G)/VE510A specimens. Compressive stress-displacement curves for transverse specimens tested under dry and moisture saturated conditions are shown in Figures 5.35 and 5.36. For the dry and seawater saturated states both composites display a linear response and sudden failure typical for a brittle material.

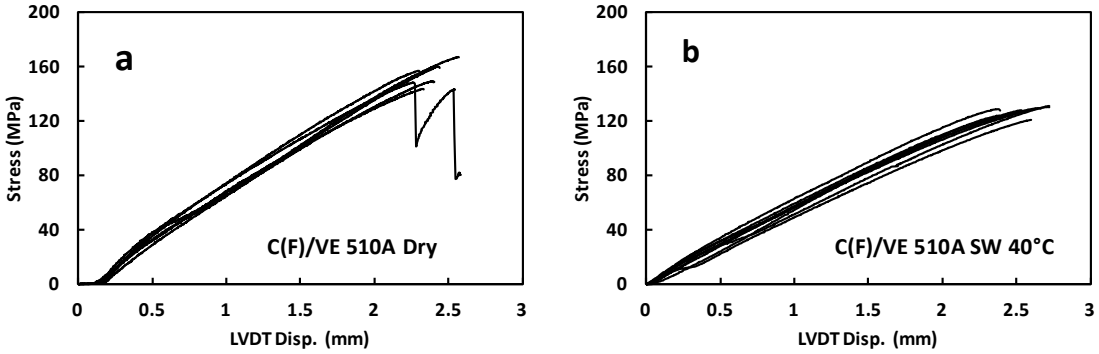

Figure 5.35: Compressive stress–displacement curves for transverse C(F)/VE 510A specimens. a) Dry, b) SW 40°C.

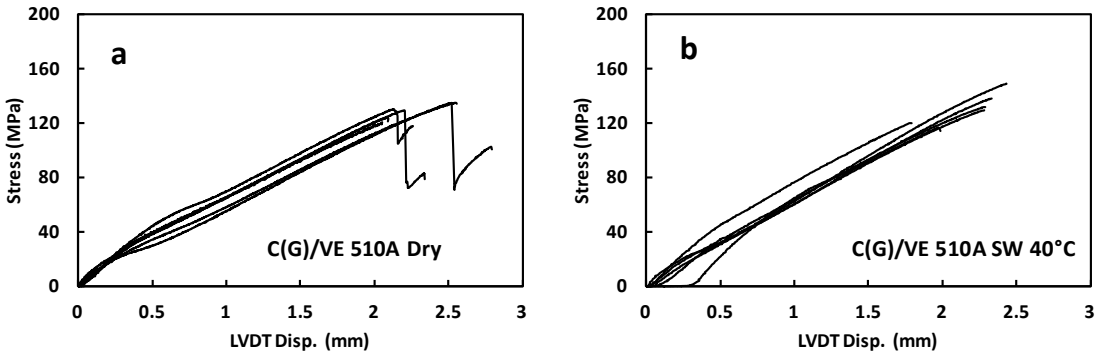

Figure 5.36: Compressive stress–displacement curves for transverse C(G)/VE 510A specimens. a) Dry, b) SW 40°C.

The transverse 90° compression specimens failed catastrophically within the specimen gage section. The specimens consistently failed at an angle perpendicular to the loading axis, see Figure 5.37a. Such a failure involves only the matrix and fiber/matrix interface. Figure 5.37b shows the compressive failure from the edge. The 45° angle is a result of shear failure caused by a combination of interface and matrix failure. Less common failures are shown in Figure 5.37c. Two failure planes oriented approximately 45° to the loading axis are observed, similar to those observed in failed 45° off-axis compression specimens.

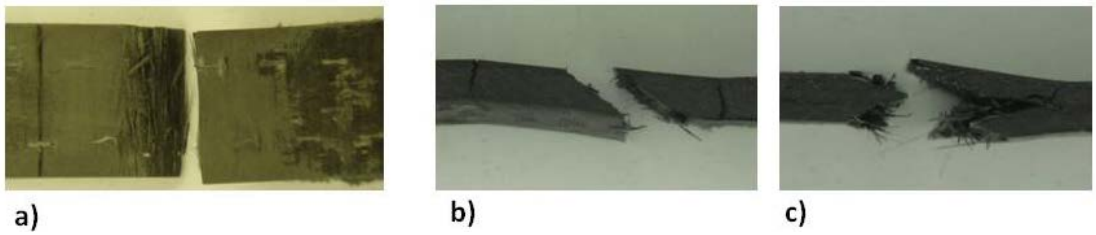

Figure 5.37: Compression failure modes observed for transverse (90°) C(F)/VE510A specimens. a) shear mode (surface) b) shear mode (edge) c) shear mode (edge).

The transverse compression strengths are listed in Table 5.13. Moisture absorption reduces the transverse compression strength of C(F)/VE 510A, but does not reduce the strength of C(G)/VE 510A. The compressive strength of C(F)/VE510A exceeds that of C(G)/VE510A. Evidently, the F fiber sizing improves the transverse compressive strength.

Table 5.13: Transverse compressive strength (X_2^C) for C(F)/VE 510A and C(G)/VE 510A.

	C (F)/VE 510A				C (G)/VE 510A			
	Dry		SW 40°C		Dry		SW 40°C	
Property	avg.	Std	avg.	Std	avg.	std	avg.	std
Transverse Comp. Strength X_2^C, MPa	154 ± 9		124 ± 8		129 ± 6		131 ± 12	

In-plane shear testing of the composites utilized the Iosipescu test specimen, see Figure 4.11. A total of 5 dry and 7 seawater exposed specimens were tested for C(F)/VE510A and 7 dry and 7 seawater for C(G)/VE510A. Three of each specimen were tested with a strain gage rosette arranged in the ±45° orientation.

In-plane shear stress-strain plots for dry and water saturated C(F)/VE 510A and C(G)/VE 510A specimens are shown in Figures 5.38 and 5.39. It is observed that the stress-strain response is linear initially followed by large non-linear plastic deformation. Specimens continued to experience increasing stress well into the plastic region. The ends of the stress-strain curves strain also indicate that the strain has stopped increasing. This is due to debonding of the strain gages from the specimens at large deformations.

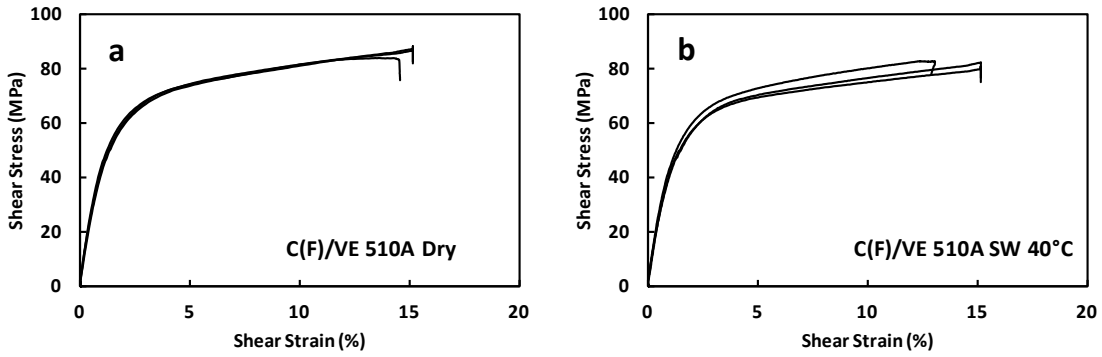

Figure 5.38: Iosipescu shear stress-strain curves for C(F)/VE 510A specimens. a) Dry, b) SW 40°C.

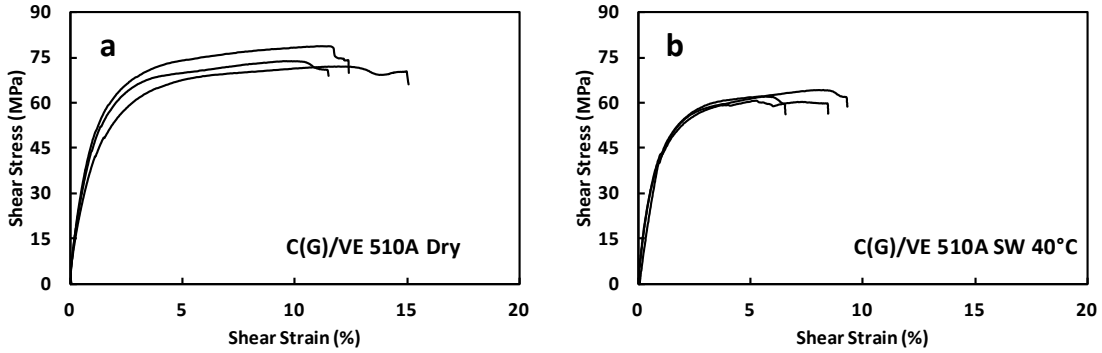

Figure 5.39: Iosipescu shear stress-strain curves for C(G)/VE 510A specimens. a) Dry, b) SW 40°C.

Failure modes encounted during Iosipescu shear testing were axial splitting starting at the notch root of the specimen and axial intralaminar cracking in the gage section, see Figure 5.40. These failure modes are typical in-plane shear failure modes of 0° composites. At large shear strains the specimens tended to fail by edge crushing at the fixture loading blocks. To prevent such and other failure modes not related to in-plane shear, testing was stopped at approximately 8 to 15% strain. As a result, for a more appropriate shear strength definition, ASTM D5379 [66] suggests that shear strength is defined as the shear stress at 5% strain.

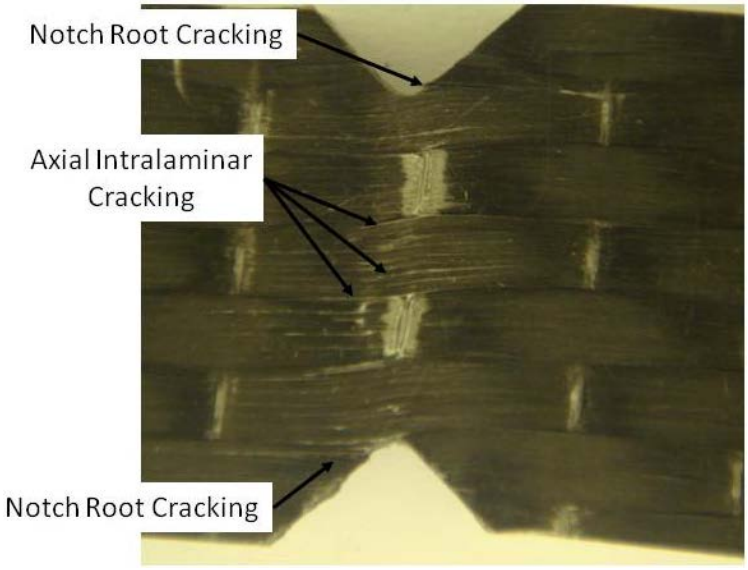

Figure 5.40: Failed Iosipescu dry C(G)/VE 510A specimen showing notch root cracking and axial intralaminar cracking.

Table 5.14 lists the in-plane shear mechanical properties of the composites at dry and saturated conditions. At dry conditions C(F)/VE510A and C(G)/510A have similar shear moduli, but the ultimate shear strength (S_6) and shear stress at 5% are less for the composite with G sized fibers, which shows that the in-plane longitudinal shear strength is F/M interface dependent. This is in general agreement with Madhukar and Drzal [34].

Moisture exposure reduces the shear strength for the G sized system, but the influence is minor for C(F)/VE 510A. The reduction in the shear strength of C(G)/510A after exposure to seawater suggests the fiber/matrix interface is susceptible to moisture attack.

Table 5.14: In-plane shear properties of C(F)/VE 510A and C(G)/VE 510A.

	C (F)/VE 510A				C (G)/VE 510A			
	Dry		SW 40°C		Dry		SW 40°C	
Property	avg.	Std	avg.	Std	avg.	std	avg.	std
Shear Modulus G_{12}, GPa	5.45	± 0.50	5.25	± 0.32	5.43	± 0.80	5.80	± 0.61
Shear Strength S_6, MPa	85.1	± 2.8	81.7	± 1.4	73.8	± 3.2	64.5	± 3.2
Shear Stress @ 5% Strain, MPa	74.2	± 0.5	56.9	± 1.7	70.4	± 3.2	53.4	± 1.0

Interlaminar shear testing utilized the short-beam shear (SBS) specimens. The test progeam involved eight dry and nine seawater saturated C(F)/VE510A specimens, and eight dry and five seawater saturated C(G)/VE510A specimens. As mentioned previously, the SBS test is commonly performed to evaluate the integrity of the F/M interface by measuring the interlaminar shear strength using equation (3.23) presented in section 3.2.3.

$$S_5 = \frac{3P}{4bh} \tag{5.5}$$

where P_m is the failure load, b is the specimen width and h is the specimen thickness.

The SBS specimens did not fail catastrophically, see the stress-deflection curves in Figures 5.41 and 5.42. Once maximum stress was reached the stress gradually decreased. Testing was stopped at approximately 1 mm to prevent damage from occuring due to failure modes other than interlaminar shear.

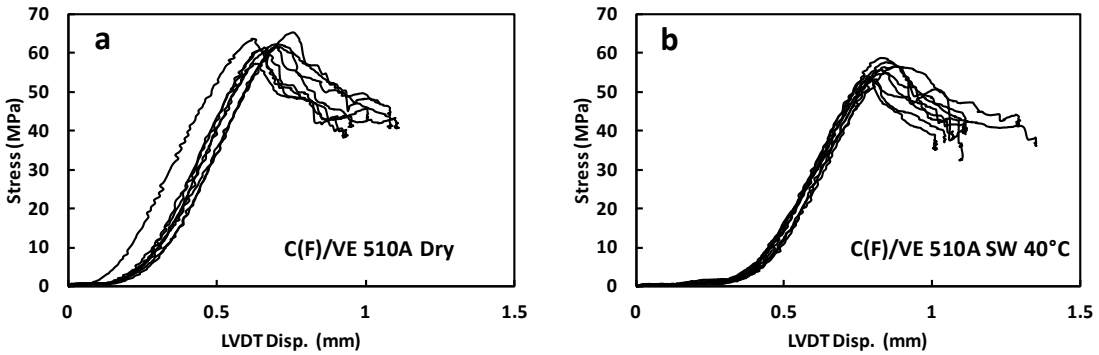

Figure 5.41: Shear stress-deflection curves for C(F)/VE 510A SBS specimens. a) Dry b) SW 40°C.

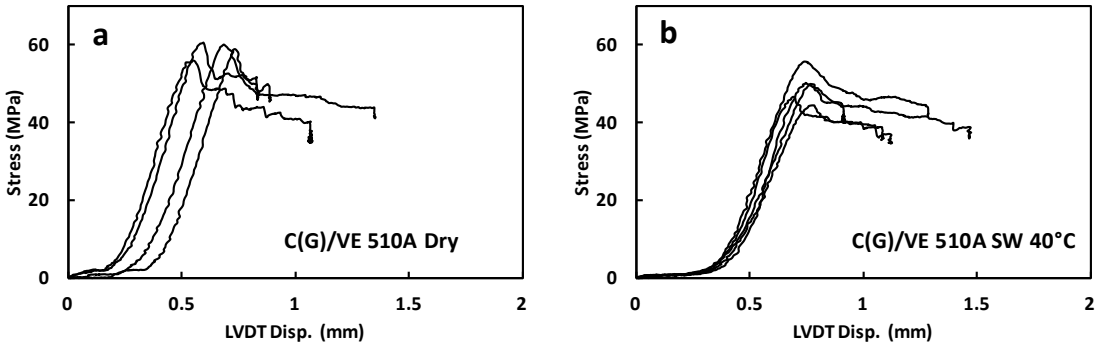

Figure 5.42: Shear stress-deflection curves for C(G)/VE 510A SBS specimens. a) Dry b) SW 40°C.

During testing cracking was noted along the mid-plane of some specimen. This is a clear indication of interlaminar shear failure. The loading applied to the specimen results in shear and bending stresses. The bending stress, however is zero at the mid-plane, where the shear stress is maximum. Hence, the shear stress remains the only cause of failure at the mid-plane. Microscopic investigation of a failed SBS specimen, see Figure 5.43, reveals multiple modes of failure. Specimens show longitudinal cracking at the mid-plane Figure 5.43a, but also evidence of compressive failure in the form of a kink band near the load nose, Figure 5.43b. This type of failure mechanism is known to cause errors in the apperent interlaminar shear strength determination [73].

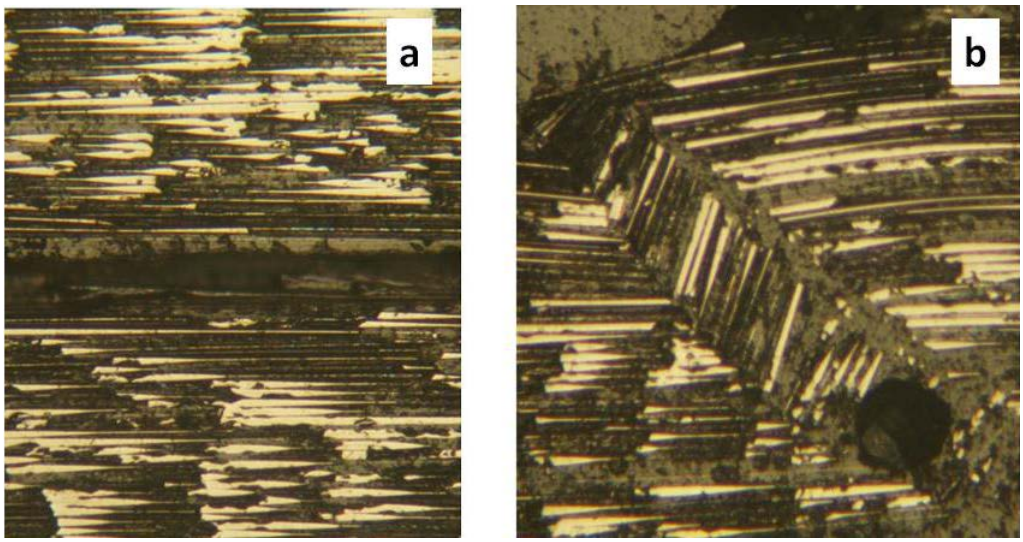

Figure 5.43: Photomicrographs of a failed dry C(G)/VE 510A SBS specimen. a) interlaminar cracking, b) compression failure near central load introduction.

From the shear strengths listed in Table 5.15, it is noted that dry C(F)/VE 510A has slightly higher interlaminar shear strength than dry C(G)/VE 510A. This suggests a stronger F/M interface for C(F)/VE 510A than C(G)/VE 510A at dry conditions. Madhukar and Drzal [34] found that a strong F/M interface directly enhances the SBS strength of carbon fiber/epoxy composites. The interlaminar shear strength is reduced after moisture exposure. The reduction for C(F)/VE 510A was 10%. For C(G)/VE 510A the corresponding reduction was approximately 16%. Furthermore, Herrera-Franco and Drzal [77] did an extensive comparison on methods for measuring F/M interface adhesion and found agreement between short beam shear testing and single-fiber fragmentation test for measuring interfacial shear strength.

Table 5.15: Interlaminar shear strengths of C(F)/VE 510A and C(G)/VE 510A.

	C (F)/VE 510A				C (G)/VE 510A			
	Dry		SW 40°C		Dry		SW 40°C	
Property	avg.	Std	avg.	Std	avg.	std	avg.	std
Interlaminar Shear Stength S_5, MPa	61.7	± 2.3	55.7	± 1.9	58.9	± 2.0	49.4	± 4.2

A summary of the mechanical properties of C(F)/VE 510A and C(G)/VE 510A composites at dry and saturated conditions is given in Table 5.16.

Table 5.16: Composite mechanical properties.

		C (F)/VE510A				C (G)/VE510A			
		Dry		SW 40°C		Dry		SW 40°C	
Property		avg.	Std	avg.	Std	avg.	std	avg.	std
Tensile Modulus Longitudinal, GPa	E_1	120.0	± 7.4	124.0	± 0.3	-	-	-	-
Tensile Modulus Transverse, GPa	E_2	7.49	± 0.02	7.69	± 0.67	8.54	± - *	8.27	± 0.38
Tensile Modulus off-axis 45°, GPa		11.1	± 1.4	10.6	± 1.1	12.7	± 1.0	11.3	± 0.6
Poisson's ratio	v_{12}	0.37	± 0.07	0.37	± 0.04	-	-	-	-
Tensile Strength Longitudinal, MPa	X^T_1	1910	± 159	1940	± 104	-	-	-	-
Tensile Strength off-axis 45°, MPa		41.3	± 4.7	41.2	± 2.0	25.3	± 5.0	30.8	± 2.6
Tensile Strength Transverse, MPa	X^T_2	24.5	± 2.0	23.0	± 2.5	12.8	± 4.0	11.8	± 5.0
Comp. Strength Longitudinal, MPa	X^C_1	787	± 69	773	± 73	644	± 69	622	± 44
Comp. Strength Transverse, MPa	X^C_2	154	± 9	124	± 8	129	± 6	131	± 12
Comp. Strength off-axis 45°, MPa		140	± 3	135	± 2	122	± 3	98	± 8
Shear Modulus, GPa	G_{12}	5.45	± 0.50	5.25	± 0.32	5.43	± 0.80	5.80	± 0.61
In-plane Shear Strength, MPa	S_6	85.1	± 2.8	81.7	± 1.4	73.8	± 3.2	64.5	± 3.2
Shear Stress @ 5% Strain, MPa		74.2	± 0.5	56.9	± 1.7	70.4	± 3.2	53.4	± 1.0
Interlaminar Shear Strength, MPa	S_5	61.7	± 2.3	55.7	± 1.9	58.9	± 2.0	49.4	± 4.2

* Only one strain gaged specimen produced reliable data.

It should be noted that a common assumption is equality of the in-plane (S_6) and interlaminar shear strengths (S_5) of unidirectional composites. However, in the current work, in-plane shear strength exceeds the interlaminar shear strength. This is in agreement with to the findings of Herrera-Franco and Drzal [77].

The strength data from the fiber/matrix dominated transverse and off-axis tension and compression and shear test are displayed graphically in Figures 5.44 to 5.46. The results show overall that the composites with F-sized fibers are stronger than those with G-sized fibers at both dry and water saturated conditions. Somewhat surprising is the increase in off-axis tensile strength in C(G)/VE510A composite systems after environmental exposure, see Figure 5.44. This could possibly be explained by the extreme flaw sensitivity of these tests and that moisture absorption mitigates the sensitivity.

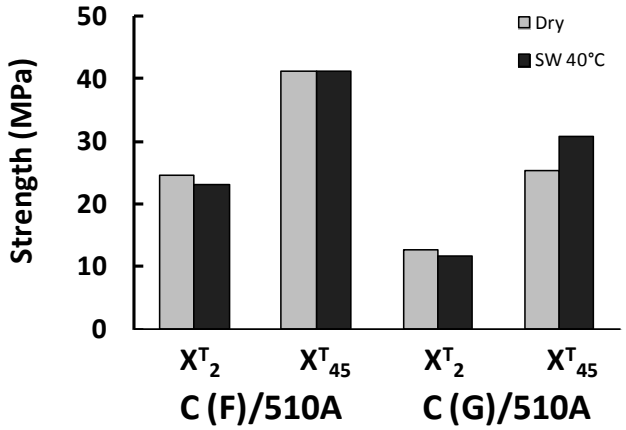

Figure 5.44: Tensile transverse and off-axis strengths.

Figure 5.45 shows the compressive transverse and off-axis strengths. The composite materials weaken in compression after environmental exposure to sea water. Figure 5.45 also shows that under compression, the composites are weaker in off-axis loading than in transverse loading.

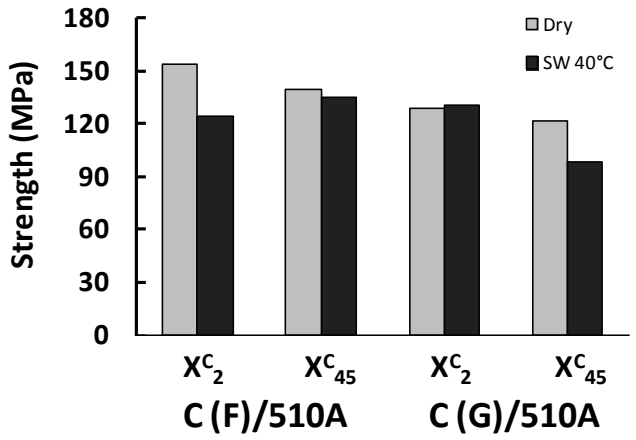

Figure 5.45: Compressive transverse and off-axis strengths.

Figure 5.46 shows the in-plane and interlaminar shear strengths. The results reveal that absorbed moisture reduces both the in-plane and interlaminar shear strengths. This suggests the fiber/matrix interface is weakened by environmental exposure.

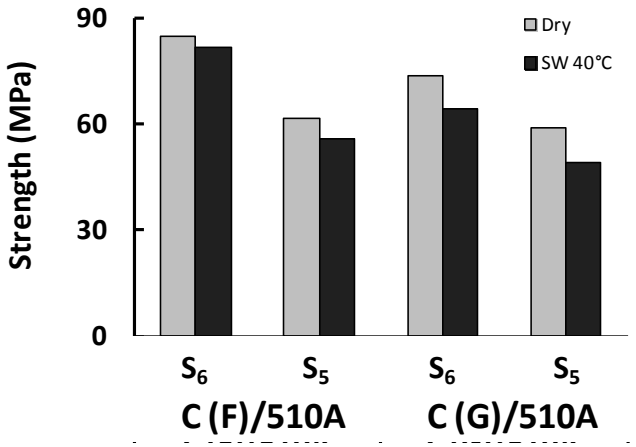

Figure 5.46: Interlaminar and in-plane shear strengths.

6 MODELING OF COMPOSITE STIFFNESSES AND FAILURE STRENGTHS

Stiffness properties of the carbon/vinylester composites are calculated using micromechanics and compared to experimental test data. Furthermore, simple micromechanical strength estimates are employed here and compared to experimental failure stresses for longitudinal tension (X_1^T), compression (X_1^C), and transverse tension (X_2^T). To determine the stiffness constants of the composites, the mechanics of materials (MoM) approach and Halpin-Tsai (H-T) equations were used, [1, 30].

$$E_1 = \mathrm{E_{1f}V_f} + \mathrm{E_m}(1 - \mathrm{V_f}) \qquad \text{(MoM)} \qquad (6.1)$$

$$E_2 = \frac{\mathrm{E_m}(1 + \eta_\mathrm{E}\xi\mathrm{V_f})}{1 - \eta_\mathrm{E}\mathrm{V_f}} \qquad \text{(H-T)} \qquad (6.2a)$$

$$\eta_E = \frac{E_{2f} - E_m}{E_{2f} + \xi E_m} \qquad (6.2b)$$

$$G_{12} = \frac{\mathrm{G_m}(1 + \eta_\mathrm{G}\xi\mathrm{V_f})}{1 - \eta_\mathrm{G}\mathrm{V_f}} \qquad \text{(H-T)} \qquad (6.2d)$$

$$\eta_G = \frac{G_{12f} - G_m}{G_{12f} + \xi G_m} \qquad (6.2e)$$

$$\nu_{12} = \mathrm{V_f}\nu_{12f} + \nu_{\mathrm{m}}(1 - \mathrm{V_f}) \qquad \text{(MoM)} \qquad (6.3)$$

where $\mathrm{E_m}$, $\mathrm{E_{1f}}$ and $\mathrm{E_{2f}}$ are the moduli for the matrix, and fiber in the longitudinal and transverse directions. $\mathrm{V_m}$ and $\mathrm{V_f}$ are the volume fractions for matrix and the fiber. $\mathrm{G_m}$ and $\mathrm{G_{12f}}$ are the shear moduli for the matrix and fiber in the axial direction. The Poisson ratios for the fiber and matrix are denoted as ν_{12f} and ν_{m}. For carbon fibers the parameter ξ = 1 in Equation is suitable [1].

The longitudinal tensile strength (X_1^T) of a ply may be estimated from the rule of mixtures. This estimation assumes that the fiber has much higher strengths than the matrix [1].

$$X_1^T \cong \sigma_{\mathrm{fl}}^{\mathrm{ult}}\mathrm{V_f} \qquad (6.4)$$

where $\sigma_{\mathrm{fl}}^{\mathrm{ult}}$ is the tensile strength of the fiber.

The longitudinal compression strength of the composite may be calculated based on a formulation derived for microbuckling.

$$X_1^C = \frac{\mathrm{G_{12}}}{1 + \frac{\bar{\emptyset}}{\gamma_{12}^{\mathrm{Y}}}} \qquad (6.5a)$$

where G_{12} is the shear modulus of the composite. γ_{12}^{Y} is the yield strain of the matrix. $\bar{\emptyset}$ is the average fiber misalignment angle (in radians).

Hyer [30] proposed using a range of $\frac{\bar{\emptyset}}{\gamma_{12}^{Y}}$ when calculating the compressive strength,

$$3 \leq \frac{\bar{\emptyset}}{\gamma_{12}^{Y}} \leq 6 \tag{6.5b}$$

This in Equation (6.5a) yields,

$$\frac{G_{12}}{7} \leq X_1^C \leq \frac{G_{12}}{4} \tag{6.5c}$$

Cooper and Kelly [78] developed a simple model (CKM) for the transverse strength (X_2^T). The CKM involves a parameter that quantifies the effectiveness of the fiber/matrix interface in terms of interface tensile strength (σ_i').

$$X_2^T = \sigma_m \left(1 - \sqrt{4\frac{V_f}{\pi}}\right) + \sigma_i' \sqrt{4\frac{V_f}{\pi}} \tag{6.6a}$$

where σ_m is the matrix tensile strength, V_f is the fiber volume fraction and σ_i' is the stress required to separate fibers from the matrix.

As mentioned previously, the model assumes regular fiber packing geometry and neglects residual stresses calculation [17]. Equation (6.6a) offers a range estimate for transverse tensile strength (X_2^T). The lower bound assumes there is no adhesion at the

fiber/matrix interface ($\sigma_i' = 0$) and assumes that fibers act as voids within the matrix reducing the overall transverse strength. The upper bound assumes that there is complete adhesion between the fiber/matrix interface and that the transverse tensile strength of the fiber is greater than the tensile strength of the matrix (σ_m) [17].

$$\sigma_m\left(1-\sqrt{4\frac{V_f}{\pi}}\right) \leq X_2^T \leq \sigma_m \tag{6.6b}$$

Table 6.1 lists the experimentally determined input properties for mechanical property estimates.

Table 6.1: Input properties for composite material property estimates.

Property		Property		
Matrix Tensile Strength (Dry) (σ_m), MPa	70.3	Fiber Tensile Strength (σ_{ft}^{ult}), MPa	4900	
Matrix Tensile Strength (SW 40°) (σ_m), MPa	54.8	Fiber Long. Modulus (E_{1f}), GPa	230	*
Matrix Modulus (dry) (E_m), GPa	3.31	Fiber Trans. Modulus (E_{2f}), GPa	15	**
Matrix Modulus (SW 40°C) (E_m), GPa	3.14	Fiber Shear Modulus, (G_{12f}), GPa	27	**
Matrix Shear Modulus (dry) (G_m), GPa	1.31	Fiber Poisson's Ratio (ν_{12f})	0.2	**
Matrix Shear Modulus (SW 40°C) (G_m), Gpa	1.25	Matrix Poisson's Ratio (ν_m)	0.35	**
Fiber Volume Fraction (F-sized) (V_f)	0.63	Fiber Volume Fraction (G-sized) (V_f)	0.66	

* Property from reference [29]
** Property from reference [1]

Tables 6.2 and 6.3 list the mechanical strengths and stiffnesses determined experimentally and through MoM and Haplin-Tsai calculations.

Table 6.2: Experimental mechanical property data for C(F)/VE510A composites and micromechanics estimates.

	Dry		SW 40°C	
	Experimental	Predicted	Experimental	Predicted
E_1, GPa	120 ± 7.4	146	124 ± 0.3	146
E_2, GPa	7.49 ± 0.02	7.77	7.69 ± 0.67	7.54
G_{12} , GPa	5.45 ± 0.50	4.81	5.25 ± 0.32	4.61
ν_{12}	0.37 ± 0.07	0.26	0.37 ± 0.04	0.26
X^T_1, MPa	1910 ± 159	3087	1940 ± 104	3087
X^C_1, MPa	787 ± 69	(779 , 1817)	773 ± 73	(750 , 1750)

Table 6.3: Experimental mechanical property data for C(G)/VE510A composites and micromechanics estimates.

	Dry		SW 40°C	
	Experimental	Predicted	Experimental	Predicted
E_2, GPa	8.54 ± -	8.13	8.27 ± 0.38	7.91
G_{12}, GPa	5.43 ± 0.80	5.23	5.80 ± 0.61	5.01
X^C_1, MPa	644 ± 69	(776 , 1810)	622 ± 44	(828 , 1933)

The micromechanics predictions of the longitudinal modulus (E_1) for C(F)/VE510A overestimates the actual modulus of the composites by 22%. This overestimation could be due to a difference in the fiber volume fraction. The actual test specimens could have a smaller fiber volume fraction than 0.63 (Table 6.1). The Haplin-Tsai equations provide reasonable estimates of the transverse and shear moduli. The longitudinal tensile strength (X_1^T) is grossly overestimated, and could be in part due to a lower fiber volume fraction. Longitudinal strength of unidirectional composites is among the hardest to experimentally characterize due to failure mechanisms that are not related to material properties (i.e. grip failure). The estimate of longitudinal compression

strength offers a rather large range. The longitudinal compression strength of C(F)/VE510A is close to the lower bound. For the C(G)/VE510A composite Table 6.3, the compression strength falls below the micromechanics lower estimate, probably due to poor interface or misaligned fibers.

The results from the CKM analysis are presented in Table 6.4.

Table 6.4: Cooper-Kelly fiber/matrix interface strength.

	C(F)/VE510A		C(G)/VE510A	
Property	Dry	SW 40°C	Dry	SW 40°C
X_2^T (Exp), MPa	24.5 ± 2.0	23.0 ± 2.5	12.8 ± 4.0	11.8 ± 5.0
X_2^T, MPa	7.34 *	5.72 *	5.86 *	4.57 *
σ'_i, MPa	19.2	19.3	7.6	7.9
σ'_i/σ_m, %	27.2	35.2	10.8	14.4

* $\sigma'_i = 0$.

The CKM estimate of transverse tensile strength with $\sigma'_i = 0$ provides the transverse tensile strength assuming no F/M adhesion. The fact $\sigma'_i \neq 0$ shows that there is adhesion present at the fiber/matrix interface. However, if fiber/matrix adhesion was perfect then σ'_i would equal σ_m. The relatively low ratios σ'_i/σ_m show that the fiber/matrix interface strength is far from ideal. The analysis also reveals that the F-sized carobn fibers have much better adhesion at the fiber/matrix interface than the G-sized fibers.

6.1 Failure Prediction using Phenomenological Approach

The Tsai-Wu failure analysis for a lamina of a fiber reinforced polymer composite was applied to calculate the failure stress of the 45° off-axis tensile and compressive test specimens. The Tsai-Wu failure envelope is three-dimensional, when plotted in terms of the in-plane normal stresses (σ_1 and σ_2) and the shear stress (τ_{12}). 2D Plots may be obtained if any stress σ_1, σ_2 or τ_{12} is constant. The expression for the Tsai-Wu failure criterion is [30],

$$F_1\sigma_1 + F_2\sigma_2 + F_{11}{\sigma_1}^2 + F_{22}{\sigma_2}^2 + F_{66}{\tau_{12}}^2 - \sqrt{F_{11}F_{22}}\sigma_1\sigma_2 = 1 \qquad (6.7)$$

The failure envelope is defined by any stress state (σ_1, σ_2, τ_{12}) where this polynomial is equal to/or greater than one. The strength parameters F_i and F_{ij} are given in terms of basic strengths,

$$F_1 = \frac{1}{{X_1}^T} + \frac{1}{{X_1}^C}, \qquad F_2 = \frac{1}{{X_2}^T} + \frac{1}{{X_2}^C} \qquad (6.8a, b)$$

$$F_{11} = -\frac{1}{{X_1}^T{X_1}^C}, \qquad F_{22} = -\frac{1}{{X_2}^T{X_2}^C} \qquad (6.8c, d)$$

$$F_{66} = \frac{1}{S_6^2} \qquad (6.8e)$$

The NU failure criterion is a fairly recent failure theory developed by Daniels et al. [79] at Northwestern University. The NU failure criterion was in agreement with experimental data determined by Daniel et al. [79]. This failure criterion characterizes failure of a composite under a combined stress state. The NU failure criterion also predicts a transition point where failure mode changes from compression to tension or compression to shear. The NU criterion is expressed by the following three equations for compression, shear and tension,

$$\left(\frac{\sigma_2}{{X_2}^C}\right)^2 + \left(\frac{\tau_{12}}{{X_2}^C}\right)^2 \left(\frac{E_2}{G_{12}}\right)^2 = 1 \qquad \text{(Compression)} \quad (6.9a)$$

$$\left(\frac{\tau_{12}}{S_6}\right)^2 + 2\frac{\sigma_2}{S_6}\frac{G_{12}}{2E_2} = 1 \qquad \text{(Shear)} \quad (6.9b)$$

$$\frac{\sigma_2}{{X_2}^T} + \left(\frac{\tau_{12}}{{X_2}^T}\right)^2 \left(\frac{E_2}{2G_{12}}\right)^2 = 1 \qquad \text{(Tension)} \quad (6.9c)$$

In order to analyze the off-axis strength the Tsai-Wu failure criterion in equation (6.7) is reduced to a simple quadratic form. The following expressions of σ_1, σ_2 and τ_{12} apply to the off-axis tensile and compression test specimens.

$$\sigma_1 = m^2\sigma_x \qquad (6.10a)$$

$$\sigma_2 = n^2\sigma_x \qquad (6.10b)$$

$$\tau_{12} = -nm\sigma_x \qquad (6.10c)$$

where $m = \cos\theta, n = \sin\theta$.

Substitution of these expressions and collecting like terms Equation (6.7) leads to the following quadratic equation in terms of σ_x,

$$A{\sigma_x}^2 + B\sigma_x + C = 0 \tag{6.11}$$

where the coefficients A, B, and C are given by,

$$A = F_{11}\cos^4\theta + F_{22}\sin^4\theta + F_{66}\cos^2\theta\sin^2\theta + 2F_{12}\cos^2\theta\sin^2\theta \tag{6.12a}$$

$$B = F_1\cos^2\theta + F_2\sin^2\theta \tag{6.12b}$$

$$C = -1 \tag{6.12c}$$

Solving Equation (6.11) will define the tensile and compressive off-axis strengths,

$$\sigma_x = \frac{-B}{2A} \pm \frac{\sqrt{B^2 - 4AC}}{2A} \tag{6.13}$$

Properties used to determine the parameters defined in Equation defined in Equation (6.8) are presented in Table 6.1.

Experimental data for 45° off-axis specimens and predictions from the Tsai-Wu criterion are listed in Table 6.5. The Tsai-Wu prediction are accurate for the 45° off-axis tensile strengths.

For compression, however, the Tsai-Wu criterion overestimates the strength for the 45° off-axis specimens by as much as a factor of 2. Hyer [30] has pointed out that this is a common observation caused by too strong stress interactions in the Tsai-Wu (T-W).

Table 6.5: Tsai-Wu failure predictions for 45° off-axis loading

	Carbon (F)/VE510A				Carbon (G)/VE510A			
	Dry		SW 40°C		Dry		SW 40°C	
Property	Exp.	T-W	Exp.	T-W	Exp.	T-W	Exp.	T-W
Tensile Strength (MPa)	41.3 ± 4.7	45.9	41.2 ± 2.0	41.6	25.3 ± 5.0	25.2	30.8 ± 2.6	22.9
Compression. Strength (MPa)	140 ± 3	201	135 ± 2	149	122 ± 3	202	98 ± 8	178

Tensile and Compressive Tsai-Wu failure predictions using dry and environmental properties are plotted in Figures 6.1 and 6.2 for C(F)/VE 510A and C(G)/VE510. The plots show that environmental exposure has little effect on off-axis tensile and compression strength.

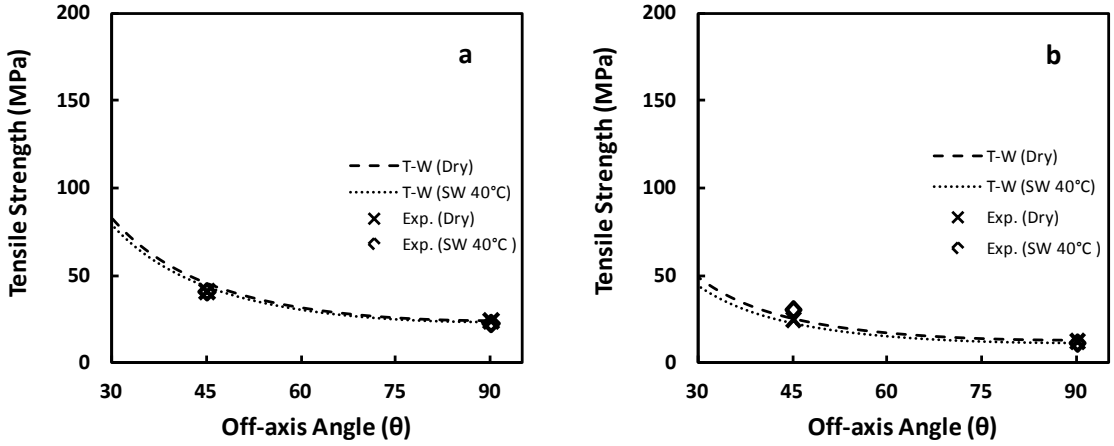

Figure 6.1: Experimental data points and Tsai-Wu tensile strength prediction for dry and SW 40°C a) C(F)/VE 510A b) C(G)/VE 510A

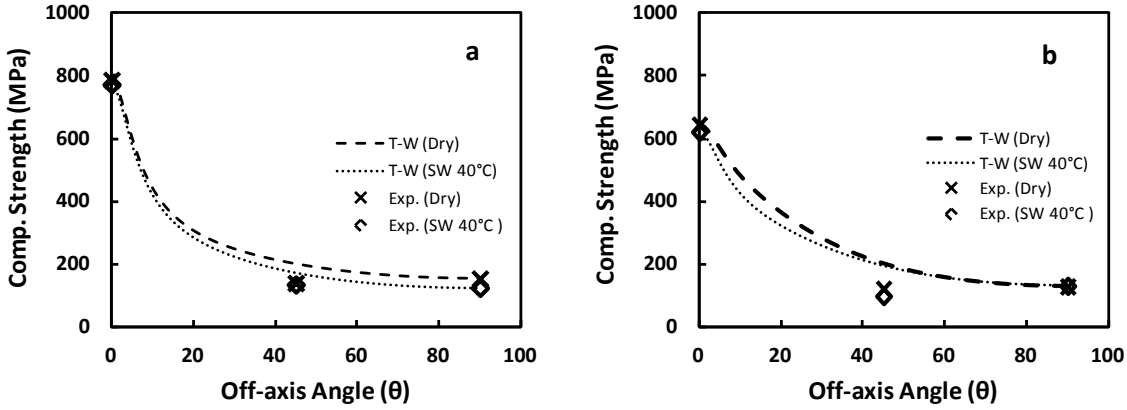

Figure 6.2: Experimental data points and Tsai-Wu compressive strength prediction for dry and SW 40°C a) C(F)/VE 510A b) C(G)/VE 510A

The following section presents a failure analysis of dry and SW40°C C(F)/VE510A and C(G)/VE510A composites in the 1-2 plane using NU and Tsai-Wu failure criterions. Figures 6.3 and 6.4 show failure envelopes (NU and Tsai-Wu) and experimental strengths data for C(F)/VE510A and C(G)/510A composites. The NU theory is better at predicting off-axis compression failure than Tsai-Wu. However, for the stress state of pure in-plane shear stress ($\sigma_2 = 0$) and in off-axis tension the NU

theory deviates substantially from experimental data while the Tsai-Wu criterion is in better agreement. The Tsai-Wu equation is defined by in-plane shear strength and as a result the envelope must pass through (S_6). The NU theory does not include the in-plane shear strength in the compression and tensile failure criterions, Equations (6.9a) and (6.9c). The NU shear curve does include (S_6). However, the shear criterion grossly overestimated the transverse tensile strength.

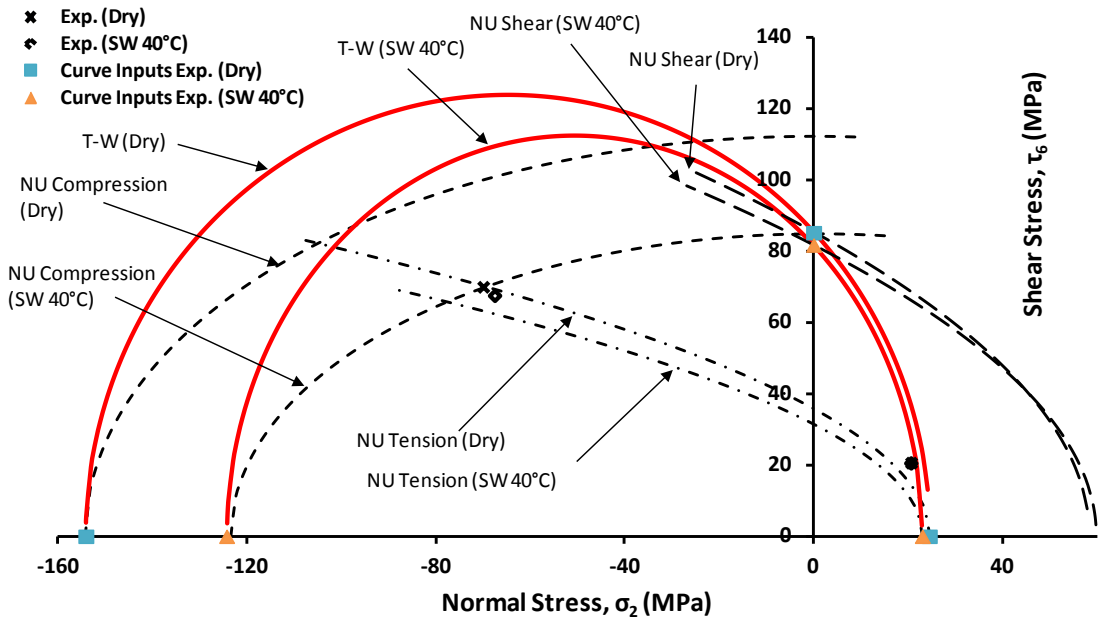

Figure 6.3: NU failure envelope transverse and shear combined stress states for C(F)/VE510A dry and SW 40°C specimens.

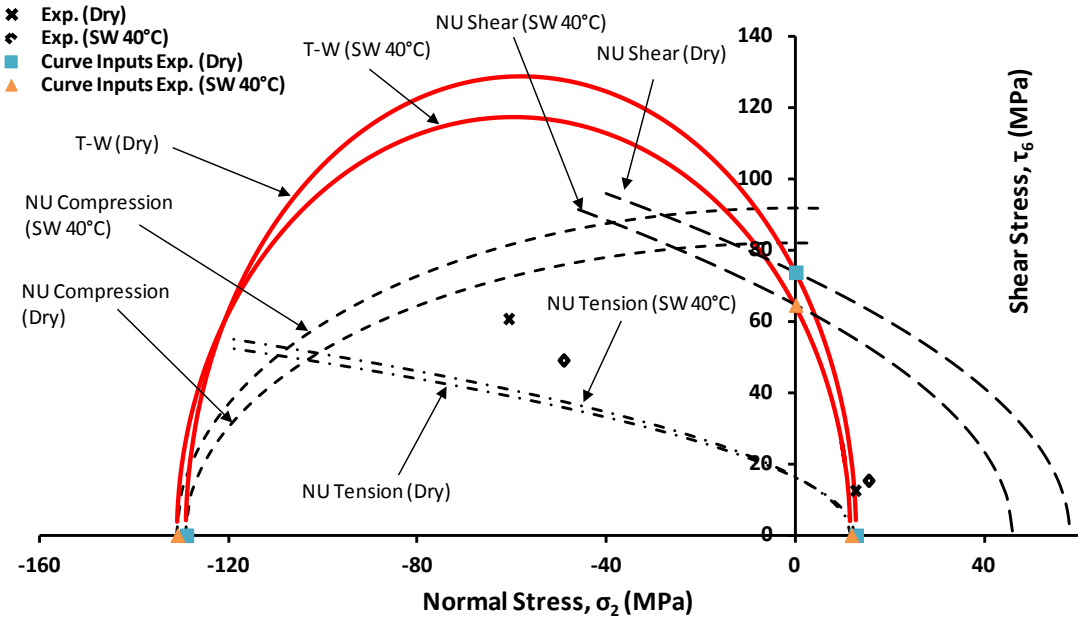

Figure 6.4: NU failure envelope transverse and shear combined stress states for C(G)/VE510A Dry and SW 40°C specimens.

7 CONCLUSIONS

Neat resins and composite specimens were exposed to marine environments until moisture content reached a point of saturation. An experimental investigation was undertaken to determine the effects of marine environmental exposure on the mechanical properties of vinylester resins (VE510A and VE8084). Neat resin specimens were tested in tension, compression and shear according to ASTM standards or verified test methods. Carbon/vinylester composites were tested to determine the effects of moisture absorption and fiber sizing on the mechanical properties. Carbon/VE510A composite specimens with F- and G-sizing were tested in tension and compression with different ply orientations as well as in-plane and interlaminar shear according to ASTM standards. Micromechanics analysis was conducted on elastic properties and failure strengths of the composites. Failure analysis was also conducted on the composites using combined stress failure criteria. This investigation revealed:

- VE8084 absorbs about twice the amount of moisture as VE510A.
- Moisture exposure increased overall ductility of both VE8084 and VE510A resins.
- The composites with F-sized fibers absorbed less moisture than the composites with G-sized fiber.

- Analysis of moisture absorption revealed that up to 90% of the moisture is accumulated at the fiber/matrix interface (wicking) of the carbon/vinylester composite.
- The composites with F-sized carbon fibers displayed less wicking than those with G-sized fibers
- Composites with F-sized fiber displayed higher strength in tension, compression and shear than those with G-sized fibers. The composites with F-sized fibers also consistently maintained higher strength after moisture exposure than composites with G-sized fibers.
- Moisture had little to no effect on longitudinal, 45° off-axis and transverse tensile properties of composites with both F- and G- sized fibers. The compression strength for the 0°, 45° off-axis and transverse compression specimens showed some reduction after moisture exposure.
- The in-plane shear (Iosipescu) and interlaminar shear (SBS) decreased after moisture absorption. Most affected were the composites with G-sized fibers.
- Micromechanics analysis provide reasonable predictions of the stiffness constants of the composites.
- The Cooper-Kelly model shows that composites with both F and G sized carbon fibers in a vinylester matrix have low fiber/matrix interface strength.
- The Tsai-Wu failure criterion applied to 45° off-axis tensile specimen provides a strength in agreement with experimental results. For the 45° off-axis compression specimens the Tsai-Wu criterion provides very unconservative strength predictions.

- The NU failure criterion fits experimental 45° off-axis compression strength data better than the Tsai-Wu failure criterion.

8 REFERENCES

[1] I. M. Daniel and O. Ishai, *Engineering Mechanics of Composite Materials*, 2nd ed. Oxford University Press, USA, 2005.

[2] J. B. Alfers and A. C. Bushey, "Down to Sea in Plastics: Practical, Light, Structure Reinforced by Fiber Glass Combines Many Good Features," vol. 1, pp. 5-10, Oct. 1952.

[3] M. O. Critchfield, T. D. Judy, and A. D. Kurzweil, "Low-cost design and fabrication of composite ship structures," *Marine Structures*, vol. 7, no. 2-5, pp. 475-494, 1994.

[4] P. Goubalt and S. Mayes, "Comparative Analysis of Metal and Composite Materials for the Primary Structures of a Patrol Craft," *Naval Engineers Journal*, vol. 108, no. 3, pp. 387-397, May 1996.

[5] R. M. Crane and J. W. Gillespie, "Intelligent Processing and Inspection of Naval Composites," *The AMPTIAC Quarterly*, vol. 7, no. 3, p. 41 to 48, 2003.

[6] D. M. Bergen and W. Needham, "Composite Materials Applications for Engineered Reduced Maintenance in the Navy's Surface Fleet (()," presented at the 2009 DoD Corrosion Conference, Washington DC, 2009.

[7] S. Marais, M. Metayer, T. Q. Nguyen, M. Labbe, and J. M. Saiter, "Diffusion and permeation of water through unsaturated polyester resins-influence of resin curing," *European Polymer Journal*, vol. 36, no. 3, pp. 453-462, Mar. 2000.

[8] A. M. Visco, N. Campo, and P. Cianciafara, “Comparison of seawater absorption properties of thermoset resins based composites,” *Composites Part A: Applied Science and Manufacturing*, vol. 42, no. 2, pp. 123-130, Feb. 2011.

[9] Y. J. Weitsman and M. Elahi, “Effects of Fluids on the Deformation, Strength and Durability of Polymeric Composites – An Overview,” in *Mechanics of Time-Dependent Materials*, vol. 4, Netherlands: Kluwer Academic Publishers, 2000, pp. 107-126.

[10] K. V. Arun, S. Basavarajappa, and B. S. Sherigara, “Damage characterisation of glass/textile fabric polymer hybrid composites in sea water environment,” *Materials & Design*, vol. 31, no. 2, pp. 930-939, Feb. 2010.

[11] W. L. Bradley and T. S. Grant, “The effect of the moisture absorption on the interfacial strength of polymeric matrix composites,” *Journal of Materials Science*, vol. 30, no. 21, pp. 5537-5542, 1995.

[12] C. L. Schutte, “Environmental durability of glass-fiber composites,” *Materials Science and Engineering: R: Reports*, vol. 13, no. 7, pp. 265-323, Nov. 1994.

[13] P. Davies, F. Pomies, and L. A. Carlsson, “Influence of Water Absorption on Transverse Tensile Properties and Shear Fracture Toughness of Glass/Polypropylene,” *Journal of Composite Materials*, vol. 30, no. 9, pp. 1004 - 1019, Jun. 1996.

[14] E. P. Gellert and D. M. Turley, “Seawater immersion ageing of glass-fibre reinforced polymer laminates for marine applications,” *Composites Part A: Applied Science and Manufacturing*, vol. 30, no. 11, pp. 1259-1265, Nov. 1999.

[15] J. L. Thomason, “The interface region in glass fibre-reinforced epoxy resin composites: 2. Water absorption, voids and the interface,” *Composites*, vol. 26, no. 7, pp. 477-485, Jul. 1995.

[16] L. L. Sobrinho, M. Ferreira, and F. L. Bastian, “The effects of water absorption on an ester vinyl resin system,” *Materials Research*, vol. 12, pp. 353-361, Sep. 2009.

[17] F. Pomies and L. A. Carlsson, “Analysis of Modulus and Strength of Dry and Wet Thermoset and Thermoplastic Composites Loaded in Transverse Tension,” *Journal of Composite Materials*, vol. 28, no. 1, pp. 22 -35, Jan. 1994.

[18] F. A. Ramirez, L. A. Carlsson, and B. A. Acha, “Evaluation of water degradation of vinylester and epoxy matrix composites by single fiber and composite tests,” *Journal of Materials Science*, vol. 43, no. 15, pp. 5230-5242.

[19] B. C. Ray, “Temperature effect during humid ageing on interfaces of glass and carbon fibers reinforced epoxy composites,” *Journal of Colloid and Interface Science*, vol. 298, no. 1, pp. 111-117, Jun. 2006.

[20] C. A. Wood and W. L. Bradley, “Determination of the Effect of Seawater on the Interfacial Strength of an Interlayer E-glass/Graphite/Epoxy Composite by In situ Observation of Transverse Cracking in an Environmental SEM,” *Composites Science and Technology*, vol. 57.

[21] Y. J. Weitsman, *Fluid Effects in Polymers and Polymeric Composites*. .

[22] R. Gopalan, R. M. V. G. K. Rao, M. V. V. Murthy, and B. Dattaguru, “Diffusion Studies on Advanced Fibre Hybrid Composites,” *Journal of Reinforced Plastics and Composites*, vol. 5, no. 1, pp. 51 -61, Jan. 1986.

[23] R. Gopalan, B. Somashekar, and B. Dattaguru, “Environmental effects on fibre—Polymer composites,” *Polymer Degradation and Stability*, vol. 24, pp. 361-371, 1989.

[24] C.-H. Shen and G. S. Springer, “Moisture Absorption and Desorption of Composite Materials,” *Journal of Composite Materials*, vol. 10, no. 1, pp. 2 -20, Jan. 1976.

[25] A. Kootsookos and A. P. Mouritz, “Seawater durability of glass- and carbon-polymer composites,” *Composites Science and Technology*, vol. 64, no. 10-11, pp. 1503-1511, Aug. 2004.

[26] F. A. Ramirez, *Evaluation of water degradation of polymer matrix composites by micromechanical and macromechanical tests*. Florida Atlantic University, 2008.

[27] Ashland DERAKANE, “DERAKANE 510A-40 Epoxy Vinyl Ester Resin.” Nov-2004.

[28] Ashland DERAKANE, “DERAKANE 8084 Epoxy Vinyl Ester Resin.” .

[29] “Torayca T700s Data Sheet.” Toray Carbon Fibers America, Inc.

[30] M. Hyer, *Stress Analysis of Fiber-Reinforced Composite Materials*, Updated. Destech Pubns Inc, 2008.

[31] F. T. Wallenberger, J. C. Waston, and H. Li, “Glass Fibers,” *ASM Handbook*, vol. 21.

[32] D. Hartman, M. E. Greenwood, and D. M. Miller, “High Strength Glass Fibers,” Owens Corning Corp., Lit-2006-111 R2 (02/2006), 2006.

[33] A. Mortensen, *Concise Encyclopedia of Composite Materials, Second Edition*, 2nd ed. Elsevier Science, 2007.

[34] M. S. Madhukar and L. T. Drzal, “Fiber-Matrix Adhesion and Its Effect on Composite Mechanical Properties: I. Inplane and Interlaminar Shear Behavior of Graphite/Epoxy Composites,” *Journal of Composite Materials*, vol. 25, no. 8, pp. 932-957, 1991.

[35] M. S. Madhukar and L. T. Drzal, “Fiber-Matrix Adhesion and Its Effect on Composite Mechanical Properties: II. Longitudinal (0) and Transverse (90) Tensile and Flexure Behavior of Graphite/Epoxy Composites,” *Journal of Composite Materials*, vol. 25, no. 8, pp. 958-991, 1991.

[36] M. S. Madhukar and L. T. Drzal, “Fiber-Matrix Adhesion and Its Effect on Composite Mechanical Properties. III. Longitudinal (0) Compressive Properties of Graphite/Epoxy Composites,” *Journal of Composite Materials*, vol. 26, no. 3, pp. 310-333, 1992.

[37] M. S. Madhukar and L. T. Drzal, “Fiber-Matrix Adhesion and Its Effect on Composite Mechanical Properties: IV. Mode I and Mode II Fracture Toughness of Graphite/Epoxy Composites,” *Journal of Composite Materials*, vol. 26, no. 7, pp. 936-968, 1992.

[38] R. E. Allred, S. P. Wesson, A. E. Hoyt, and J. W. Whitehead, “Reactive Finishes for Improving Interfacial properties in Carbon/Vinyl Ester Laminates,” in *49th intl. SAMPE Symp. and Exhib.*, Long Beach, CA, 2004.

[39] J.-B. Donnet, Ed., *Carbon Fibers*. CRC Press, 1998.

[40] J. Jang and H. Yang, “The effect of surface treatment on the performance improvement of carbon fiber/polybenzoxazine composites,” *Journal of Materials Science*, vol. 35, no. 9, pp. 2297-2303, May 2000.

[41] L. T. Drzal, P. J. Herrera-Franco, and H. Ho, “5.05 - Fiber–Matrix Interface Tests,” in *Comprehensive Composite Materials*, Oxford: Pergamon, 2000, pp. 71-111.

[42] F. Hoecker, K. Friedrich, H. Blumberg, and J. Karger-Kocsis, “Effects of fiber/matrix adhesion on off-axis mechanical response in carbon-fiber/epoxyresin composites,” *Composites Science and Technology*, vol. 54, no. 3, pp. 317-327, 1995.

[43] F. Hoecker and J. Karger-Kocsis, “Effects of the interface on the mechanical response of CF/EP microcomposites and macrocomposites,” *Composites*, vol. 25, no. 7, pp. 729-738, 1994.

[44] A. Paipetis and C. Galiotis, “Effect of fibre sizing on the stress transfer efficiency in carbon/epoxy model composites,” *Composites Part A: Applied Science and Manufacturing*, vol. 27, no. 9, pp. 755-767, 1996.

[45] M. R. Piggott, “A new model for interface failure in fibre-reinforced polymers,” *Composites Science and Technology*, vol. 55, no. 3, pp. 269-276, 1995.

[46] C. T. Herakovich, *Mechanics of Fibrous Composites*, 1st ed. Wiley, 1997.

[47] V. M. Karbhari and S. Zhang, “E-Glass/Vinylester Composites in Aqueous Environments – I: Experimental Results,” vol. 10, no. 1, pp. 19-48, 2003.

[48] V. Alvarez, A. Vazquez, and O. De La Osa, “Cyclic Water Absorption Behavior of Glass—Vinylester and Glass—Epoxy Composites,” *Journal of Composite Materials*, vol. 41, no. 10, pp. 1275 -1289, May 2007.

[49] A. N. Fraga, V. A. Alvarez, A. Vazquez, and O. de la Osa, “Relationship between Dynamic Mechanical Properties and Water Absorption of Unsaturated Polyester and

Vinyl Ester Glass Fiber Composites," *Journal of Composite Materials*, vol. 37, no. 17, pp. 1553 -1574, 2003.

[50] M. T. Shaw and W. J. MacKnight, *Introduction to Polymer Viscoelasticity, 3rd Edition*, 3rd ed. Wiley-Interscience, 2005.

[51] C.-L. Tsai, M.-C. Cheng, and S.-L. Chang, "Gradient-dependent Model for Moisture Diffusion in a Polymer Matrix Composite Laminate," *Journal of Composite Materials*, vol. 41, no. 4, pp. 419 -434, Feb. 2007.

[52] J. Zhou and J. P. Lucas, "The effects of a water environment on anomalous absorption behavior in graphite/epoxy composites," *Composites Science and Technology*, vol. 53, no. 1, pp. 57-64, 1995.

[53] S. Pavlidou, K. Krassa, and C. D. Papaspyrides, "Woven glass fabric/polyester composites: effect of interface tailoring on water absorption," *Journal of Applied Polymer Science*, vol. 98, no. 2, pp. 843-851, Oct. 2005.

[54] M. L. Costa, M. C. Rezende, and S. F. M. de Almeida, "Effect of Void Content on the Moisture Absorption in Polymeric Composites," *Polymer-Plastics Technology and Engineering*, vol. 45, pp. 691-698, Jul. 2006.

[55] C. H. Shen and G. S. Springer, "Effects of Moisture and Temperature on the Tensile Strength of Composite Materials," *Journal of Composite Materials*, vol. 11, no. 1, pp. 2-16, 1977.

[56] C.-H. Shen and G. S. Springer, "Environmental Effects on the Elastic Moduli of Composite Materials," *Journal of Composite Materials*, vol. 11, no. 3, pp. 250 -264, Jul. 1977.

[57] Y. J. Weitsman, “2.11 - Effects of Fluids on Polymeric Composites—A Review,” in *Comprehensive Composite Materials*, Oxford: Pergamon, 2000, pp. 369-401.

[58] ASTM Standard D638 -03, “Standard Test Method for Tensile Properties of Plastics.” West Conshohoncken, PA, 2003, ASTM International.

[59] A. E. Lever and J. A. Rhys, *Properties and Testing of Plastics Materials*, 3rd ed. Littlehampton Book Services Ltd, 1968.

[60] S. Turner, *Mechanical Testing of Plastics*. Newnes-Butterworth, 1973.

[61] G. C. Ives, J. A. Mead, and M. M. Riley, *Handbook of Plastics Test Methods*. Newnes-Butterworth, 1971.

[62] J. V. Schmitz, *Testing of Polymers Volume 1*. JOHN WILEY & SONS@, 1965.

[63] ASTM Standard D695 -02a, “Standard Test Method for Compressive Properties of Rigid Plastics.” West Conshohoncken, PA, 2002, ASTM International.

[64] D. E. Walrath and D. F. Adams, “The losipescu shear test as applied to composite materials,” *Experimental Mechanics*, vol. 23, no. 1, pp. 105-110, Mar. 1983.

[65] N. Iosipescu, “New Accurate Procedure for Single Shear Testing of Materials,” *Journal of Materials*, vol. 2, no. 3, pp. 537 - 566, Sep. 1967.

[66] ASTM Standard D5379 / D5379M, 2005, “Standard Test Method for Shear Properties of Composite Materials by the V-Notched Beam Method.” West Conshohoncken, PA, 2005, ASTM International.

[67] D. F. Adams, L. Carlsson, and R. B. Pipes, *Experimental Characterization of Advanced Composite Materials, Third Edition*, 3rd ed. CRC Press, 2002.

[68] J. L. Sullivan, B. G. Kao, and H. Oene, “Shear properties and a stress analysis obtained from vinyl-ester losipescu specimens,” *Experimental Mechanics*, vol. 24, no. 3, pp. 223-232, Sep. 1984.

[69] D. C. Montgomery and G. C. Runger, *Applied Statistics and Probability for Engineers*. John Wiley & Sons Inc, 1994.

[70] ASTM Standard D6641 / D6641M, 2009, “Standard Test Method for Compressive Properties of Polymer Matrix Composite Materials Using a Combined Loading Compression (CLC) Test Fixture.” West Conshohoncken, PA, 2009, ASTM International.

[71] ASTM Standard D2344 / D2344M, 2006, “Standard Test Method for Short-Beam Strength of Polymer Matrix Composite Materials and Their Laminates.” West Conshohoncken, PA, 2000, ASTM International.

[72] Y. Tang, L. Ye, D. Zhang, and S. Deng, “Characterization of transverse tensile, interlaminar shear and interlaminate fracture in CF/EP laminates with 10 wt% and 20 wt% silica nanoparticles in matrix resins,” *Composites Part A: Applied Science and Manufacturing*, no. 0.

[73] J. M. Whitney and C. E. Browning, “On short-beam shear tests for composite materials,” *Experimental Mechanics*, vol. 25, pp. 294-300, Sep. 1985.

[74] H.-yan ZHU, D.-hong LI, D.-xing ZHANG, B.-chang WU, and Y.-yong CHEN, “Influence of voids on interlaminar shear strength of carbon/epoxy fabric laminates,” *Transactions of Nonferrous Metals Society of China*, vol. 19, Supplement 2, no. 0, p. s470-s475, Sep. 2009.

[75] ASTM Standard D3039-00, “Standard Test Method for Tensile Properties of Polymer Matrix Composite Materials.” West Conshohoncken, PA, 2000, ASTM International.

[76] L. J. Hart-Smith, “5.07 - Backing-out Composite Lamina Strengths from Cross-Ply Testing,” in *Comprehensive Composite Materials*, Oxford: Pergamon, 2000, pp. 149-161.

[77] P. J. Herrera-Franco and L. T. Drzal, “Comparison of methods for the measurement of fibre/matrix adhesion in composites,” *Composites*, vol. 23, no. 1, pp. 2-27, Jan. 1992.

[78] G. A. Cooper and A. Kelly, “Role of the Interface in the Fracture of Fiber-Composite Materials,” in *Interfaces in Composites*, Committee D-30, Ed. 100 Barr Harbor Drive, PO Box C700, West Conshohocken, PA 19428-2959: ASTM International, pp. 90-90-17.

[79] I. M. Daniel, J.-J. Luo, P. M. Schubel, and B. T. Werner, “Interfiber/interlaminar failure of composites under multi-axial states of stress,” *Composites Science and Technology*, vol. 69, no. 6, pp. 764-771, May 2009.